



# **Bitlis Eren University Journal of Science and Technology**

Bitlis Eren Üniversitesi Bilim ve Teknoloji  
Dergisi

**Yıl/Year: 2022 • Cilt/Volume: 12 • Sayı/Issue: 1**

**ISSN: 2146-7706**

**Contact:**

BEU Journal of Science and Technology, Bitlis Eren Üniversitesi 13000, Merkez, Bitlis/ TÜRKİYE  
Tel: 0 (434) 222 0045

beujstd@beu.edu.tr <http://dergipark.gov.tr/beuscitech>



## Bitlis Eren University Journal of Science and Technology

<b>e-ISSN</b>	:	2146-7706
<b>Date of Issue</b>	:	June 27 2022
<b>Issue Period</b>	:	June 2022
<b>Volume</b>	:	12
<b>Issue</b>	:	1
<b>Founded</b>	:	2011
<b>Location</b>	:	Bitlis
<b>Language</b>	:	English
<b>Address</b>	:	Bitlis Eren University Journal of Science and Technology Bitlis Eren Üniversitesi 13000, Merkez, Bitlis/ TÜRKİYE
<b>e-mail</b>	:	beujstd@beu.edu.tr
<b>URL</b>	:	<a href="http://dergipark.gov.tr/beuscitech">http://dergipark.gov.tr/beuscitech</a>

# Bitlis Eren University Journal of Science and Technology

Yıl/Year: 2022 • Cilt/Volume: 12 • Sayı/Issue: 1

## Editorial Board

<b>On behalf of Bitlis Eren University Owner</b>	<b>Prof. Dr. Necmettin ELMASTAŞ</b> <i>Bitlis Eren University</i>
<b>Editor-in-Chief</b>	<b>Assoc. Prof. Dr. Kubilay TOYRAN</b> <i>Çankırı Karatekin University</i>
<b>Editorial Board</b>	<b>Prof. Dr. Mehmet Cihan AYDIN</b> <i>Bitlis Eren University</i>
	<b>Prof. Dr. Zeynep AYGÜN</b> <i>Bitlis Eren University</i>
	<b>Assoc. Prof. Dr. Murat KARAKAŞ</b> <i>Bitlis Eren University</i>
	<b>Assoc. Prof. Dr. Engin YILMAZ</b> <i>Bitlis Eren University</i>
	<b>Assoc. Prof. Dr. Musa ÇIBUK</b> <i>Bitlis Eren University</i>
	<b>Assist. Prof. Dr. Fahrettin ÖZBEY</b> <i>Bitlis Eren University</i>
	<b>Assist. Prof. Dr. Behçet KOCAMAN</b> <i>Bitlis Eren University</i>
	<b>Assist. Prof. Dr. Faruk ORAL</b> <i>Bitlis Eren University</i>
	<b>Assist. Prof. Dr. Tülay ÇEVİK SALDIRAN</b> <i>Bitlis Eren University</i>
	<b>Assist. Prof. Dr. Ramazan ERDOĞAN</b> <i>Bitlis Eren University</i>

## **Bitlis Eren University Journal of Science and Technology**

Yıl/Year: 2022 • Cilt/Volume: 12 • Sayı/Issue: 1

Bitlis Eren University Journal of Science and Technology (Bitlis Eren Univ J Sci & Technol) is an international, refereed open access electronic journal. Research results, reviews and short communications in the fields of Biology (Medicinal, Molecular and Genetics, Veterinary and Agriculture), Physics, Chemistry, Mathematics and Statistics, and also Engineering Sciences are accepted for review and publication. Papers will be published in English. Scientific quality and scientific significance are the primary criteria for publication. Articles with a suitable balance of practice and theory are preferred. Manuscripts previously published in other journals and as book sections will not be accepted.

Bitlis Eren University Journal of Science and Technology indexed in:



















- EBSCO

# Bitlis Eren University Journal of Science and Technology

Yıl/Year: 2022 • Cilt/Volume: 12 • Sayı/Issue: 1

## Articles

---

Zeynep AYGUN  , Murat AYGÜN 	1-6
<b>Electromagnetic pollution analysis of Bitlis Eren University main and vocational school campus</b>	
Kamuran SARAÇ 	7-13
<b>Synthesis and Theoretical Characterization of 4-(p-tolyl)-5-(thiophen-2-yl)-2,4-dihydro-3H-1,2,4-triazole-3-thione Using Experimental and Quantum Chemical Calculations</b>	
Ercan IŞIK  , Ali Emre ULU  , Şakir TUNÇ  , Ali KESKINER 	14-20
<b>A study on the determination of damage levels in reinforced concrete structures for different earthquakes</b>	
Ercan IŞIK 	21-26
<b>Investigation of the contribution of the reinforcement tie to the seismic behavior of reinforced-concrete columns</b>	
Emine ÇAĞDAŞ  , Aydın BÜYÜKSARAÇ  , M. Fatih IŞIK 	27-35
<b>Early intervention to risk groups with the QR code system in disasters</b>	
Muhammed TANYILDIZI 	36-42
<b>The effect of cement replacement with eggshell powder on the sorptivity index of concrete</b>	
M. Cihan AYDIN  , Elif Sevgi BIRINCIOĞLU  , Aydın BÜYÜKSARAÇ 	43-50
<b>Risk Assessment of Rockfall using GIS-Based Analytical Hierarchy Process: A Case Study of Bitlis Province</b>	
Ugur BAYRAKCI  , Seyma TULUCE DEMIRAY  , Vehpi YILDIRIM 	51-59
<b>New Soliton Solutions Arising in Some NLEEs</b>	

---

Available online at [www.dergipark.gov.tr/beuscitech](http://www.dergipark.gov.tr/beuscitech)

Journal of Science and Technology

E-ISSN 2146-7706



# Electromagnetic pollution analysis of Bitlis Eren University main and vocational school campus

Zeynep AYGUN <sup>a,\*</sup> , Murat AYGUN <sup>b</sup> <sup>a</sup>Bitlis Eren University, Vocational School of Technical Sciences, TR-13000, Bitlis, Türkiye<sup>b</sup>Bitlis Eren University, Faculty of Arts and Science, Department of Physics, TR-13000, Bitlis Türkiye

## ARTICLE INFO

### Article history:

Received 27 November 2021

Received in revised form 13 March 2022

Accepted 15 March 2022

### Keywords:

Electromagnetic pollution

Electromagnetic field

Bitlis Eren University

## ABSTRACT

In parallel with the development of technology, the increase in the number of devices emitting electromagnetic wave also increases the rate of electromagnetic pollution surrounding our environment. Determination of electromagnetic pollution level is of great importance for human health. In the present study, it was aimed to measure the electric field values of Bitlis Eren University main campus and vocational school campus in Turkey. Spectran HF60105 was used to perform the measurements at different 20 regions in different times. Based on the electric field values, the magnetic field and power density values were calculated for each location. Although, it is found that the electric field values are below the limits which are determined by international standards, those are generally higher for five regions correspond to institute, student hostel, stadium, guesthouse and engineering faculty. It can be also noted that the highest electric field value is measured as 0.201 V/m in guesthouse region on weekdays-July for UMTS. Additionally, the higher electromagnetic pollution is determined mostly in the stadium and in July measurements. The measured electric field values are generally low (<0.050 V/m) in vocational school campus.

© 2020. Turkish Journal Park Academic. All rights reserved.

## 1. Introduction

Depending on the development of industrialization and technology in the world, electric devices used in daily life are increasing day after day. Thus, all the electric devices produce electromagnetic waves based on the amount of voltage and current. Electromagnetic pollution (EMP) occurs as a result of electromagnetic waves emitted from both natural and man-made sources located around us and can be arrayed as electric current-carrying cables, radio and television transmitters and receivers, mobile phones, base stations, high voltage lines, transformers, all electrically powered devices, atmospheric discharges and sun.

The detection of EMP, whose negative effects on human health are widely discussed and researched, has been the subject of many scientific studies in Turkey as well as in the

world. High frequency EMA for a region in Italy was measured by statistical methods and measurement protocols of sources generating EMF such as power lines were determined (Paolino et al., 2001). In a study conducted in Australia, radio frequency electromagnetic energy levels emitted by base stations attracted attention (Henderson and Bangay, 2005). Benjamin and Galuccio (2001) mounted broadband measuring devices on a vehicle and made measurements between streets in order to determine the electric field strength in Brazil. Cansız and Kurt (2012) measured the EMF level in the 100 kHz-3 GHz frequency band in Diyarbakır city center with the Drive Test Method and the results were shown on the digital map. Again, environmental EMP measurements were made in the areas where the population is crowded in Ankara city center, and also in Dikmen Çaldağı and Yenimahalle Şentepe regions, where radio-television transmitters and base stations are concentrated. In these regions, electric field strength measurement was carried out

\* Corresponding author. Tel.: +90 (434) 222 00 97; fax: +90 (434) 222 91 01  
E-mail address: [zeynepyarbasi@hotmail.com](mailto:zeynepyarbasi@hotmail.com)  
ORCID : 0000-0002-2979-0283 (Z. Aygün), 0000-0002-4276-3511 (M. Aygün)

with the SRM 3000 device and isotropic probe in the frequency spectrum of 75 MHz-3 GHz (Genç, 2010). Seker et al. (1998) conducted studies on the measurement of EMP, which is constantly exposed to in the residential, workplace and hospital environment in Turkey, and compared the values obtained as a result of the measurement with the ICNIRP limit values. Ince (2007) made measurements with the EMR 300 device in the 100 kHz–3 GHz frequency region in the city center of Ankara. In this study, the total electric field strength value in the environment was measured in some regions. In the thesis study of Dilek (2014), the EMP in the Central Campus of Recep Tayyip Erdoğan University was examined. In this study, EMP measurements were made with a compact spectrum analyzer, SRM 3006, operating in the 400 MHz–6 GHz band at 21 different points in different time zones of the day. Similarly, EMF measurements were made at the Konya Selçuk University campus (Yaldız et al. 2015). The measurement results were compared with the standard values announced by ICNIRP and BTK. Karadağ et al. (2014) made an EMP analysis on campus of İnönü Unv. and evaluated the results. Keysan (2015) conducted a pollution analysis in Balıkesir city center and University campus in his thesis study. Etem and Abbasov (2016) studied EMP of the city center of Muş.

There are international standards and limits on the effects of electromagnetic radiation on human health. The International Commission for Non-Ionizing Radiation Protection (ICNIRP) is one of the organizations that set limit values for electromagnetic fields. The limit values given by this organization have been accepted by the world's leading organizations such as the World Health Organization (WHO) and the International Labor Organization (ILO). Each country has specified its own limits and for Turkey the limits are determined by ICNIRP and Republic of Turkey Information Technologies and Communication Authority (BTK).

In this study, our aim is to investigate the electromagnetic pollution, which can cause health problems like stress, headaches, insomnia, and fatigue in the short term and discomforts on the immune system or cell structure in the long term in Bitlis Eren Unv. central campus and vocational school campus. For this purpose, measurements have been taken at different regions and different times to see the dependence of pollution on population and time effect.

## 2. Illustrations

The measurements were performed by Spectran HF60105 in the range of 1MHz-9,4GHz frequency (Figure 1). It can be used effectively for the measurements of nonionizing radiation by its isotropic antenna. In the measurements made with isotropic antenna, the results can be taken in mW/cm<sup>2</sup>, W/m<sup>2</sup>, V/m, A/m units both average and maximum or minimum values. The electric field strength E (V/m), is the sum of values taken from all directions. The same measurements can also be done for magnetic field or power density. In the study, we performed our measurements in V/m unit, and the magnetic field and power density values for each E were calculated.



Figure 1. Spectran HF60105

The relation between electric field and magnetic field is given in Eq. (2.1),

$$E/H=377 \quad (2.1)$$

Power density which is also known as Poynting vector is given in Eq. (2.2), where 377 is the value of space resistance,

$$S=E.H=E^2/377 \quad (2.2)$$

With the EMP meter used in the measurements, results can be obtained in ten different frequency ranges.

1. Tetra (380 – 400 MHz)
2. ISM434 (433 – 434.8 MHz)
3. LTE800 (4G) (780 – 862 MHz)
4. ISM868 (868 – 870 MHz)
5. GSM900 (921.2 – 959.6 MHz)
6. GSM18k (1800 – 1880 MHz)
7. UMTS (3G) (2110 – 2170 MHz)
8. Wlan (2400 – 2490 MHz)
9. LTE2.6 (4G) (2500 – 2690 MHz)
0. DECT (1880 – 1900 MHz)



Figure 2. Bitlis Eren University measurement regions a) central campus and b) Vocational School campus

Before starting the measurements, 20 points were determined at regular intervals to surround the two campuses. The measurement points are shown in Figure 2. Measurements were made on weekdays and weekends, where the population density may be different, as well as in the summer period (July-2020) and the education-training period (October-2021). The recorded E values were taken by five measurements for each location and the average values were calculated.

### 3. Results and Discussion

The E limit values determined by ICNIRP and BTK for Turkey is given in Table 1 and 2. In our measurements, no values were recorded for the frequency ranges Tetra (380 – 400 MHz), ISM434 (433 – 434.8 MHz), ISM868 (868 – 870 MHz).

**Table 1.** The E limit values determined by ICNIRP and BTK.

Frequency (MHz)	Electric Field Strength (V/m)	
	ICNIRP	BTK
0.010-0.15	87	65.25
0.15-1	87	65.25
1-10	$87/f^{1/2}$	$65.25/f^{1/2}$
10-400	28	21
400-2000	$1.375f^{1/2}$	$1.03f^{1/2}$
2000-60000	61	45.75

**Table 2.** The limit values determined for GSM 900 and GSM 1800.

Frequency	900 MHz	1800 MHz
Electric field strength	41.25 V/m	58.33 V/m
Magnetic field strength	0.111 A/m	0.157 A/m
Power density	4.5 W/m <sup>2</sup>	9.0 W/m <sup>2</sup>

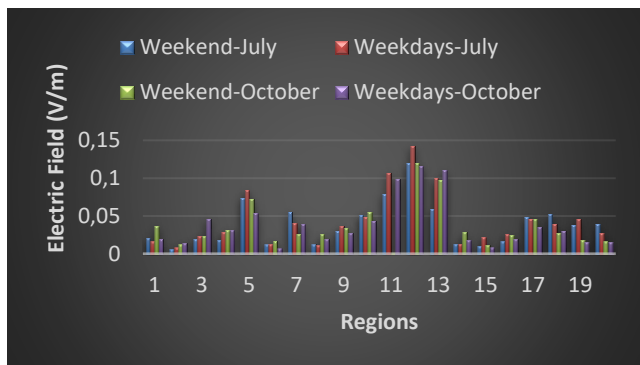


**Figure 3.** Average electric field values measured for LTE800 in all regions during the weekdays and weekends in July-2020 and October-2021.

According to the measurements taken on weekdays and weekends in July-2020 and October-2021 periods, it has been observed that the electric field values

measured in all regions are less than the upper limits determined by ICNIRP and BTK. The measured E values for each frequency range are clearly seen in Figs. 3-9. The general results are also shown in Figs. 10-12.

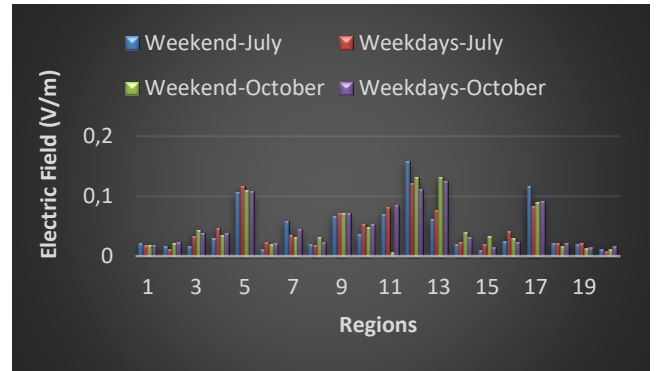


**Figure 4.** Average electric field values measured for GSM900 in all regions during the weekdays and weekends in July-2020 and October-2021.

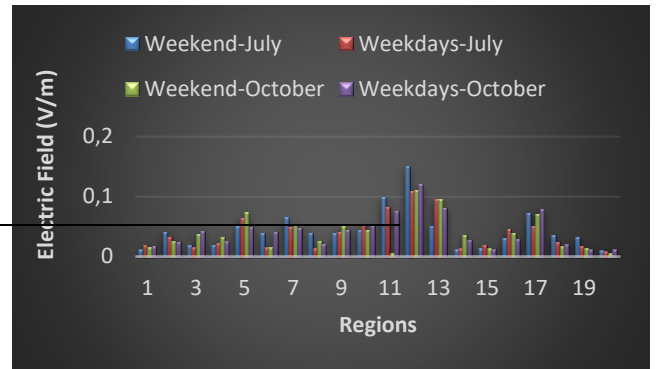


**Figure 5.** Average electric field values measured for GSM1800 in all regions during the weekdays and weekends in July-2020 and October-2021.

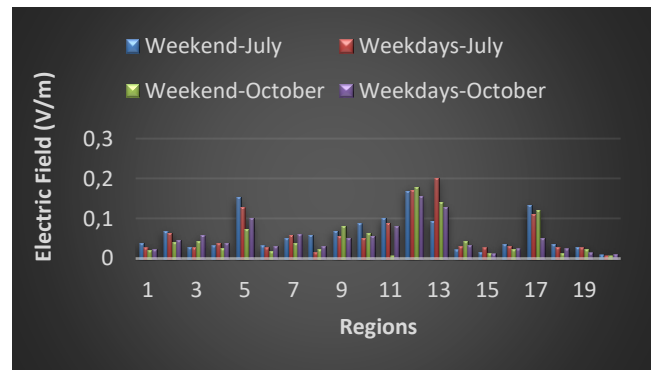


**Figure 6.** Average electric field values measured for UMTS in all regions during the weekdays and weekends in July-2020 and October-2021.



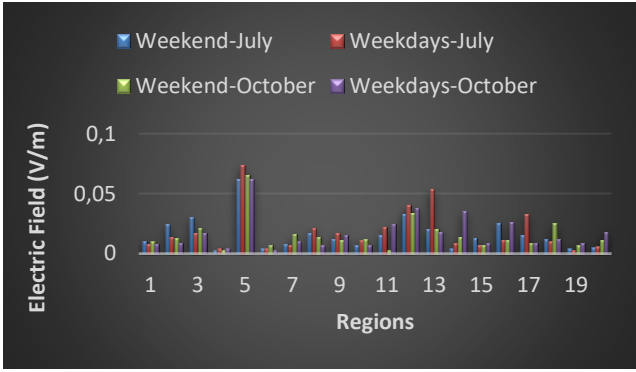


**Figure 7.** Average electric field values measured for Wlan in all regions during the weekdays and weekends in July-2020 and October-2021.

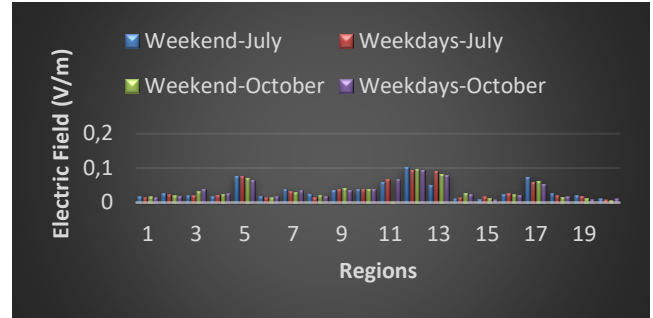


**Figure 10.** General average electric field values measured in all regions for all frequencies during the weekdays and weekends in July-2020 and October-2021.

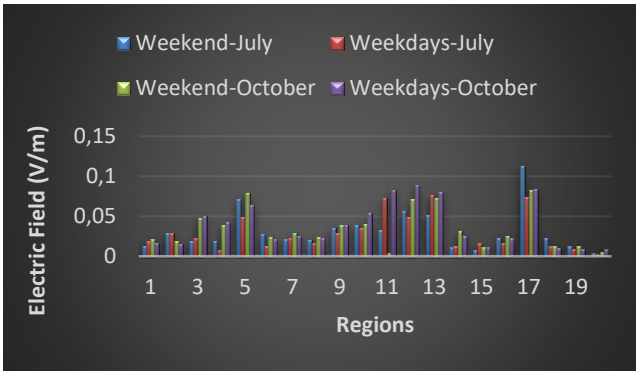


**Figure 8.** Average electric field values measured for LTE2.6 in all regions during the weekdays and weekends in July-2020 and October-2021.

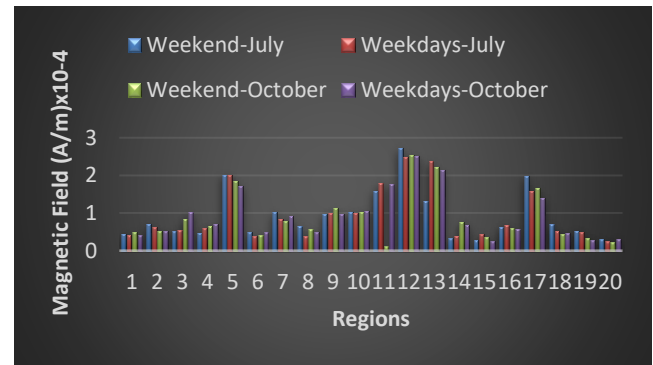


**Figure 11.** General average magnetic field values measured in all regions for all frequencies during the weekdays and weekends in July-2020 and October-2021.

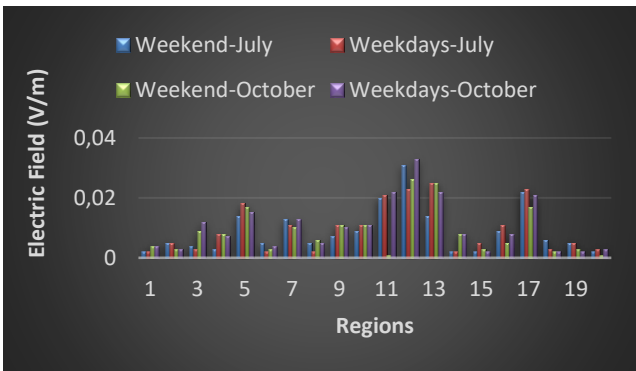


**Figure 9.** Average electric field values measured for Dect in all regions during the weekdays and weekends in July-2020 and October-2021.

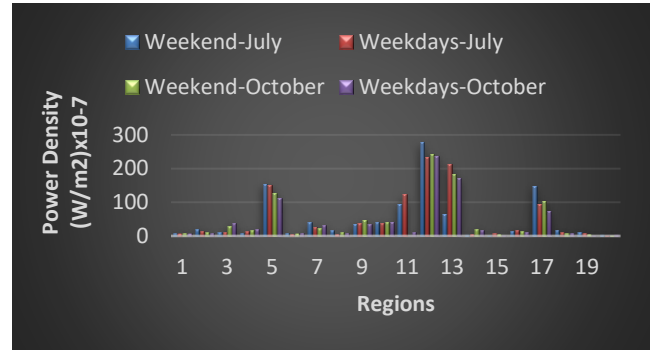


**Figure 12.** General average power density values measured in all regions for all frequencies during the weekdays and weekends in July-2020 and October-2021.

As seen from the figures, electric field values are generally higher for 5,11,12,13 and 17 regions (correspond to institute, student hostel, stadium, guesthouse and engineering faculty, respectively) than those for other regions. In weekend-July measurements, the highest E value was obtained in the 12<sup>th</sup> region for LTE800, GSM900, GSM1800 and UMTS. Location 5 had the highest E value for Wlan and location 17 had that for LTE2.6.

In weekdays-July measurements, the highest E value was obtained in the 12<sup>th</sup> region for LTE800, GSM900, GSM1800. Region 13 had the highest E value for UMTS, LTE2.6 and DECT, while region 5 had that for Wlan.

In weekend-October measurements, the highest E value was determined in the 12<sup>th</sup> region for LTE800, GSM900 (also region 13), GSM1800, UMTS and DECT. Region 17 had the highest E value for LTE2.6, while region 5 had that for Wlan.

In weekdays-October measurements, the highest E value was determined in the 12<sup>th</sup> region for LTE800, GSM1800, UMTS, LTE2.6 and DECT. Region 13 had the highest E value for GSM900, while region 5 had that for Wlan.

The highest E value for LTE800 measurements was determined in the 12<sup>th</sup> region on weekdays-July. For GSM900 measurements, the highest E value was determined on weekend-July in the 12<sup>th</sup> region. For GSM1800 measurements, the highest E value was determined on weekend-July in the 12<sup>th</sup> region. The highest E value for UMTS measurements was measured on weekdays-July in the 13<sup>th</sup> region. For Wlan measurements, the highest E value was determined on weekdays-July in the 5<sup>th</sup> region. The highest E value for LTE2.6 measurements was obtained on weekend-July in the 17<sup>th</sup> region. For DECT measurements, the highest E value was determined on weekdays-October in the 12<sup>th</sup> region.

An important point need to note is that higher values were obtained in 2020 measurements compared to the results in 2021 measurements. Since 2020 is a period when the pandemic is experienced intensely, making video calls, watching videos, transferring and sharing data, and using more electric devices on campus were intense during this period. It can be the reason obtaining this kind of result.

#### 4. Conclusions

According to the results, it can be concluded that no region exceeded the limits set by both BTK and international organizations. Therefore, it can be said that the measurement results are safe in terms of limitations. It can be seen that the highest E value was measured as 0.201 V/m in the 13<sup>th</sup> region on weekdays-July for UMTS. Among the regions, the higher EMP values were observed mostly in the 12<sup>th</sup> region. The higher EMP values were determined mostly in July measurements. The measured E values are generally low in vocational school campus. Although the obtained

EMP values are under the limit values, we can take simple precautions for our health in the long term. Electric devices must not be plugged in even if they are switched off. Electric devices should be kept as far away as possible, and we should keep short contact with devices we use constantly, such as mobile phones, computers, hair dryers, microwave ovens etc.

#### Acknowledgements

Authors acknowledge the financial support of Bitlis Eren University Scientific Research Projects Coordination Unit (BEBAP) with a project grant number 2020.005.

#### References

- Benjamin, G., Galuccio, S. 2001. Electromagnetic Environmental Measurement in Specific Populated Areas of Brazil. National Institute of Space Research Integration and Testing Laboratory, S.J.dos, Campos, Paulo, Brazil.
- Cansız, M., Kurt, M.B. 2012. Mapping of electromagnetic pollution with drive test method and evaluation of its measurement results. *Dicle Univ. Engineering Journal*, 3(2), 101-110.
- Dilek, B. 2014. Recep Tayyip Erdoğan Üniversitesi Merkez Kampüs Alanının Elektromanyetik Kirlilik Haritasının Çıkarılması. Yüksek Lisans Tezi, Fen Bilimleri Ens., Rize.
- Etem, T., Abbasov, T. 2016. Measurements Of High Frequency Electromagnetic Waves In Center Of Mus. *International Journal of Applied Mathematics, Electronics and Computers*, 95-97.
- İnce, T. 2007. Elektromanyetik Kirlilik. Yüksek Lisans Tezi, Fen Bilimleri Enstitüsü, Gazi Üniversitesi, Ankara.
- ICNIRP. 1998. Guidelines for Limiting Exposure to Time-Varying Electric, Magnetic and Electromagnetic Fields (up to 300 GHz). *Health Physics*, 74(4), 494–522.
- ICNIRP, 2009. Exposure to high frequency electromagnetic fields, biological effects and health consequences (100 kHz-300 GHz). International Commission on Non-Ionizing Radiation Protection.
- Genç, Ö. 2010. Radyo Frekanslarında Elektromanyetik Kirliliğe GSM Bantlarının Etkisinin İstatistiksel Analizi. Doktora tezi, Selçuk Üniversitesi Fen Bilimleri Enstitüsü, Konya.
- Henderson, S.I., Bangay, M.J. 2005. Survey of RF Exposure Levels from Mobile Telephone Base Stations in Australia. *Bio Electro Magnetics*, 27(1), 73-76.
- Karadağ, T., Özdemir, A.R., Abbasov, T. 2014. Longterm electromagnetic field measurements and pollution maps in a university campus. *Pamukkale Univ. Engineering Journal*, 20(8), 314-318.
- Keysan A., 2015. Balıkesir ili şehir merkezi ve Balıkesir Ün. Çalış yerleşkesinin elektromanyetik alan haritası. Yüksek lisans tezi, Fen Bilimleri Ens. Balıkesir.
- Paolino, L., Sebillio, M., Tortora, G., et al, 2001. Monitoring Electromagnetic Pollution: A GIS-Based Visual Approach. *Lecture Notes in Computer Science*, 90-101.

Seker, S., Morgül, A., Tulgar, T. M. 1998. Electromagnetic Pollution Survey in a Typical Turkish Residence, Plant and Hospital. Department of Electric-Electronics Engineering Bogaziçi University, Electrotechnical Conference, MELECON 98. İstanbul.

Yaldız, E., Seyfi, L., Nacaroglu, C. 2015. Selçuk Üniversitesi Kampüsünde (Konya) Elektromanyetik Kirlilik Haritasının Çıkarılması ve Temiz Güzergah Belirlenmesi. 1-3.



# Synthesis and Theoretical Characterization of 4-(p-tollyl)-5-(thiophen-2-yl)-2,4-dihydro-3H-1,2,4-triazole-3-thione Using Experimental and Quantum Chemical Calculations

Kamuran SARAÇ<sup>a,\*</sup>

<sup>a</sup>Bitlis Eren University, Faculty of Art and Sciences, Department of Chemistry, TR-13000, Bitlis, Türkiye

## ARTICLE INFO

### Article history:

Received 24 January 2022

Received in revised form 7 June 2022

Accepted 24 June 2022

Keywords: 4-(p-tollyl)-5-(thiophen-2-yl)-

2,4-dihydro-3H-1,2,4-triazole-3-thione

DFT

NMR

IR Spectroscopy

## ABSTRACT

The aim of the study was to synthesize 4-(p-tollyl)-5-(thiophen-2-yl)-2,4-dihydro-3H-1,2,4-triazole-3-thione and detect its experimental and the quantum chemical properties. 4-(p-tollyl)-5-(thiophen-2-yl)-2,4-dihydro-3H-1,2,4-triazole-3-thione was synthesized using by the nucleophilic substitution reaction. The synthesized title compound has been characterized both experimentally and theoretically using quantum chemical calculations and spectral techniques. The molecular geometry, vibrational frequencies, and <sup>1</sup>H and <sup>13</sup>C NMR chemical shifts of the title compound in the ground state were calculated using the density functional method (B3LYP) with the 6-311G(d, p) basis set. It was seen that the calculated infrared and nuclear magnetic resonance values were compatible with the experimental values. To determine conformational flexibility, the molecular energy profile of 4-(p-tollyl)-5-(thiophen-2-yl)-2,4-dihydro-3H-1,2,4-triazole-3-thione was obtained by DFT calculations with respect to the selected torsion angle, which was varied from 180° to +180° in steps of 20°. In addition, the HOMO- LUMO energies of this conformational structure were calculated.

© 2020. Turkish Journal Park Academic. All rights reserved.

## 1. Introduction

Triazoles are one of the most of important class of heterocyclic compounds that exhibit a broad spectrum of pharmacological activities. They have two isomer groups based on the different position of the nitrogen atoms: As 1,2,3 triazoles and 1,2,4 triazoles have a wide range of drugs as essential heterocyclic structural components anticonvulsants [1], antimalarial [2], antiproliferative [3], anticancer [4] immune-nostimulants [5] and antidiabetic [6] are biologically very important. These diverse properties of the triazole core have led researchers to develop new triazole derivatives with promising biological

activities. Biological research of 1,2,4-triazoles has been instrumental in demonstrating various pharmacological properties such as anticancer, antituberculosis. Various drugs have the triazole moiety, which highlights its importance, and recent advances by various researchers have delineated the importance of the triazole nucleus. To give a few examples of these; Beutle's study showed that various nucleoside-based triazole derivatives such as cladribine and gemcitabine, which natural nucleosides, can be used as anticancer agents [7]. Chandrasheka et al. showed that 4-isopropyl thiazole-4-phenyl-1,2,4-triazole derivative compounds exhibited strong antituberculosis activity compared to standard drugs [8]. The

\* Corresponding author. Tel.: +90 (434) 222 00 20; fax: +90 (434) 222 91 43

E-mail address: [ksarac@beu.edu.tr](mailto:ksarac@beu.edu.tr)

ORCID : 0000-0001-6684-8969 (K. Saraç)

fact that triazoles and their derivatives have such important properties causes the study of triazoles. The aim of this study is to synthesize 4-(p-tolyl)-5-(thiophen-2-yl)-2,4-dihydro-3H-1,2,4-triazole-3-thione, which is thought to be useful in at least one of these areas. It is aimed to examine experimentally and theoretically.

## 2. Materials and Methods

### 2.1. Experimental

50 ml of absolute ethyl alcohol and 10 mmol of thiophene-2-carbohydrazide were added to a 100 ml glass flask. After the reaction started, 10 mmol p-tolyl isothiocyanate was added. After about 3 hours, solid thiosemicarbazide began to form. 15 mmol potassium hydroxide was added to the solid formed and dissolution started. The reaction was stopped after six hours and the pH was brought to 3-4 with hydrochloric acid. The resulting solid was crystallized from a water-alcohol mixture. The structure of the obtained product was elucidated by spectral techniques. The reaction of the obtained compound is shown in Figure 1. Yield 68%

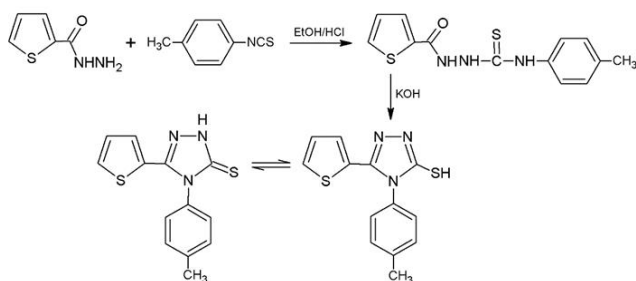


**Figure 1.** The reaction for the synthesis of 4-(p-tolyl)-5-(thiophen-2-yl)-2,4-dihydro-3H-1,2,4-triazole-3-thione.

### 2.2. Computational methods

Gaussian 09W package program and Density Functional Theory (DFT) method were used in the theoretical calculations of this study [10-11]. Energy values were obtained by using the 6-311G(d,p) basis set in the calculations. The boundary orbitals of the molecule, geometric optimization and infrared spectra were obtained by the Density Functional Theory (DFT) method. The GIAO (Gauge-Independent Atomic Orbital) [12-14] method was used to determine the NMR chemical shift values of the synthesized compound. The optimized form of

synthesized 4-(p-tolyl)-5-(thiophen-2-yl)-2,4-dihydro-3H-1,2,4-triazole-3-thione is given in Figure 2.

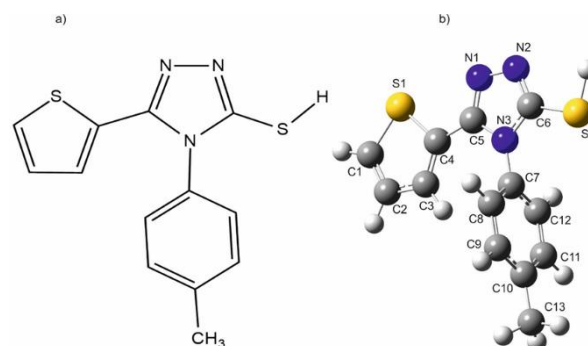


**Figure 2.** (a) Experimental form of 4-(p-tolyl)-5-(thiophen-2-yl)-2,4-dihydro-3H-1,2,4-triazole-3-thione (b) Theoretical form of 4-(p-tolyl)-5-(thiophen-2-yl)-2,4-dihydro-3H-1,2,4-triazole-3-thione.

## 3. Results and Discussion

### 3.1. Conformation Isomer

Conformation analysis is a widely used method for determining the stability of conformations resulting from possible rotations in organic compounds, investigating the stability reasons of stable conformations, and examining intramolecular interactions [15]. In the 4-(p-tolyl)-5-(thiophen-2-yl)-2,4-dihydro-3H-1,2,4-triazole-3-thione structure, the bond between the thiophene ring and the triazole ring has free rotation. Therefore, in order to observe this bond energy change by rotation, a conformation analysis at the B3LYP/6-311G(d,p) level was calculated to obtain the most stable optimized structure by rotating it around itself at 20 degree angles at each step. In Figure 3, the energy profile obtained for the molecule is given. Structures with minimum (stable) and maximum (unstable) energy were shown in the dihedral angle-energy plot. Looking at the graph, although the most unstable structures were formed at angles of approximately  $-80^\circ$  and  $+72^\circ$ , the most stable structures were obtained at  $-179^\circ$  and  $+178^\circ$  angles.

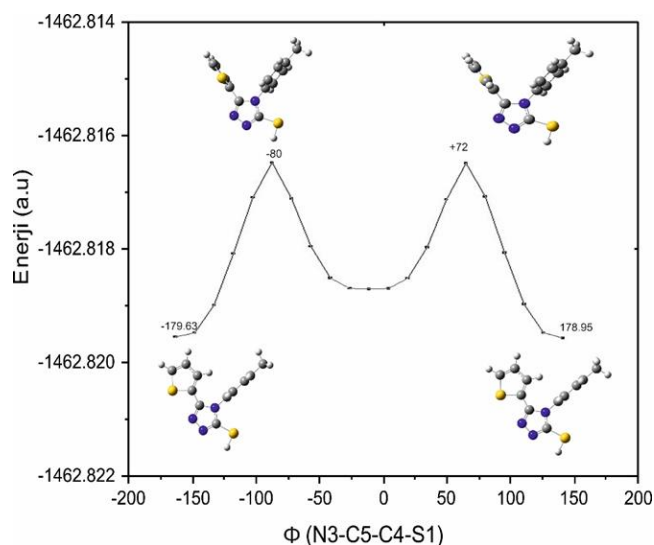


**Figure 3.** Conformation of 4-(p-tolyl)-5-(thiophen-2-yl)-2,4-dihydro-3H-1,2,4-triazole-3-thione.

### 3.2. Infrared Spectroscopy (IR)

The vibrational frequencies of 4-(p-tolyl)-5-(thiophen-2-yl)-2,4-dihydro-3H-1,2,4-triazole-3-thione were calculated theoretically and the obtained values were compared with the experimental values. When the spectra of the synthesized 4-(p-tolyl)-5-(thiophen-2-yl)-2,4-dihydro-3H-1,2,4-triazole-3-thione compound are examined, it is observed that the carboxylic acid hydrazide derivatives between 1650 and 1690  $\text{cm}^{-1}$ . It was observed that the C=O tension vibration disappeared. In addition, in 4-(p-tolyl)-5-(thiophen-2-yl)-2,4-dihydro-3H-1,2,4-triazole-3-thione compound, CH<sub>3</sub> stretch (symmetric and antisymmetric), out-of-plane There are CH bending, in-plane CH bending and aromatic CH stretching vibrations. Aromatic CH vibrational stresses are observed in the frequency range 3000-3100  $\text{cm}^{-1}$  (in the form of multiple bands). In-plane CH bending vibrations appear as sharp peaks in the 1100-1500  $\text{cm}^{-1}$  region. Out-of-plane bending vibrations are observed in the 860-1000  $\text{cm}^{-1}$  region [16-17]. The theoretically calculated CH stretching vibrations in the aromatic and thiophene ring of the compound were observed in the range of 3186-3080  $\text{cm}^{-1}$ , and experimentally in the frequency range of 3228-3063  $\text{cm}^{-1}$ . CH in-plane bending vibrations were observed at 1071 and 1288  $\text{cm}^{-1}$  experimentally at 1050 and 1250, out-of-plane bending vibrations were observed theoretically at 825 and 863  $\text{cm}^{-1}$  and experimentally at 725 and 846  $\text{cm}^{-1}$ . Other vibration values of the synthesized structure are shown in Table 1 and infrared spectrum in Figure 4.

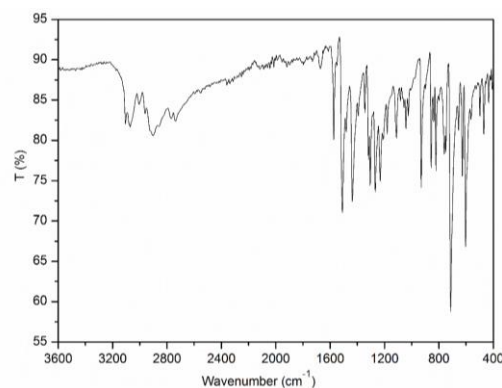


**Figure 4.** FT-IR spectrum of 4-(p-tolyl)-5-(thiophen-2-yl)-2,4-dihydro-3H-1,2,4-triazole-3-thione.

**Table 1.** Comparison of experimental and calculated vibrational frequencies of 4-(p-tolyl)-5-(thiophen-2-yl)-2,4-dihydro-3H-1,2,4-triazole-3-thione.

Symbols	Experimentally with FT-IR (cm-1)	Calculated B3LYP/6-311,G(d,p)
$\nu$ CH, Tyf	3186	3228,3210,3208
$\nu_s$ CH, Ar	3100	3063,3086,3083,3063
$\nu_{as}$ CH, Ar	3080	3062,3083
$\nu_{as}$ CH3	2970	3045,3024
$\nu$ SH	2610	2583
$\nu$ C=C, Ar	1620	1656,1613,1228
$\nu$ C=C, Tyf	1520	1548,1639,
$\nu$ C=N, Trz	1570	1565,1580,1393,1492
$\delta$ CH3	1445	1484,1417
$\delta$ CH3	1425	1482
$\delta$ CH, Ar	1050	1071,1089
$\delta$ CH, Tyf	1250	1288
$\alpha$ (Ar + CH3)	885	963
$\alpha$ CH3	890	943
$\alpha$ CH, Tyf	846	863,810
$\alpha$ CH, Ar	725	825,844

$\nu$ , strain;  $\delta$ , in-plane bending;  $\alpha$ , out-of-plane bending; s, symmetrical; ace, asymmetrical; Ar, aromatic, Tyf, Thiophene; Trz, Triazole

### 3.3. Nuclear Magnetic Resonance Spectroscopy (NMR)

The most characteristic peak of the synthesized 4-(p-tolyl)-5-(thiophen-2-yl)-2,4-dihydro-3H-1,2,4-triazole-3-thione compound was theoretically at 14.06 ppm experimentally. It is the SH/NH peak seen as singlet at 14.00 ppm. The presence of this peak is an important parameter for the formation of the compound. Next to this characteristic peak of SH/NH, hydrogens in the p-tolyl group attached to the 1,2,4-triazole ring -ortho-positions resonate theoretically at 7.20 and 7.25 ppm, experimentally at around 7.29 ppm, while protons in the -meta position resonate as a doublet, theoretically 6.60 and 6.63 ppm, and experimentally 6.73 and 6.97 ppm, it gave a doublet signal. In addition, the protons of the methyl group attached to the p-tolyl group theoretically gave a singlet signal at 1.80, 1.95 and 2.00 ppm, experimentally at 2.39 ppm. Finally, the protons in the thiophene ring can be evaluated as follows; The proton adjacent to the sulfur atom resonated in low field due to the electron negativity of the sulfur atom compared to the other protons in the ring, giving an experimental signal at 7.64 ppm theoretically at 7.41 ppm, while other protons gave an experimental signal at 7.36 ppm and theoretically at 6.90 ppm. The experimental and theoretically calculated  $^1\text{H}$  and  $^{13}\text{C}$ -NMR spectrum values of the compound are given in Table 2. In addition, the  $^1\text{H}$ -NMR and  $^{13}\text{C}$ -NMR spectra of the compound are shown in Figure 5 and Figure 6.

**Table 2.** Theoretical and experimental  $^1\text{H}$  and  $^{13}\text{C}$  isotropic chemical shifts (with respect to TMS, all values in ppm) for the title compound.

Atom	Theoretical (B3LYP) 6-311G(d,p)	Experimental(ppm) (DMSO- $d_6$ )
C1	139.2	132.9
C2	127.5	127.3
C3	129.4	128.1
C4	135.3	130.6
C5	149.0	146.5
C6	165.6	169.2
C7	134.4	130.3
C8	131.9	128.8
C9	132.5	129.2
C10	144.2	140.3
C11	132.7	129.2
C12	131.2	128.8
C13	18.3	21.3
3H(thiophene)	6.90, 6.90 and 7.41	7.36, 7.36 and 7.64
3H( $\text{CH}_3$ )	1.80, 1.95 and 2.00	2.39
4H(Ar-H)	6.60, 6.63, 7.20 and 7.25	6.73, 6.97, 7.29 and 7.29
1H(SH)	14.00	14.06

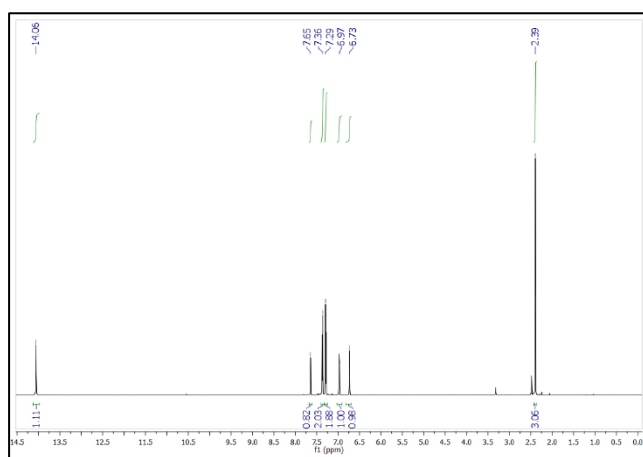


**Figure 5.**  $^1\text{H}$ -NMR spectrum of 4-(p-tolyl)-5-(thiophen-2-yl)-2,4-dihydro-3H-1,2,4-triazole-3-thione.

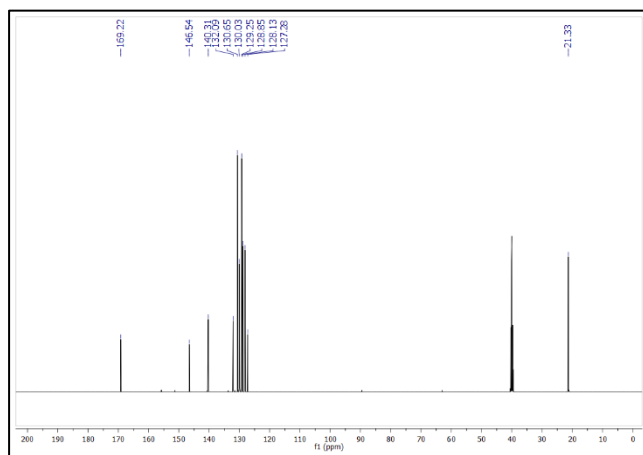


**Figure 6.**  $^{13}\text{C}$ -NMR spectrum of 4-(p-tolyl)-5-(thiophen-2-yl)-2,4-dihydro-3H-1,2,4-triazole-3-thione.

### 3.4. Frontier Molecular Orbitals (FMOs)

Boundary orbitals, the highest energy filled molecular orbital (HOMO) and the lowest energy vacant molecular orbital (LUMO), have an important place in the explanation of chemical reactions. Since most of the chemical reactions occur by gaining or losing electrons, HOMO and LUMO are effective in the chemical interactions in the structure of the molecule. Since the received electron will be placed in the LUMO orbital, the smaller the energy of this orbital, the easier it will be to take the electron. Since the given electron will be in the HOMO orbit, the higher the energy of this orbit, the greater the tendency to donate electrons. Electrons in HOMO are the first to be separated during ionization [18]. The HOMO-LUMO graph of the compound is given in Figure 7. When calculating the HOMO and LUMO energy values of the molecule, the energy difference between the ground and first excited levels is -4.626 eV. If the HOMO-LUMO of the same molecule is re-excited, the calculated energy difference is -5.837 eV. In excited and ionic molecules, the dispersion of electron density, that is, activation, will make the molecule weaker and therefore the interaction between the molecules will also weaken. This is the reason for the decrease in the energy difference between HOMO-LUMO when the molecule is excited to higher levels [19].



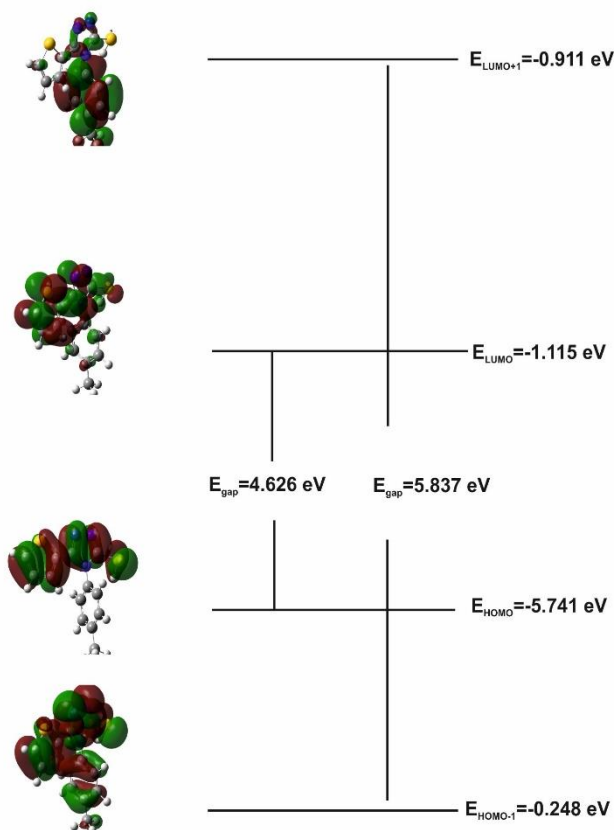


**Figure 7.** By method B3LYP/6-311G(d,p) of 4-(p-tolyl)-5-(thiophen-2-yl)-2,4-dihydro-3H-1,2,4-triazole-3-thione calculated HOMO and LUMO energies.

#### 4. Conclusions

In this work, 4-(p-tolyl)-5-(thiophen-2-yl)-2,4-dihydro-3H-1,2,4-triazole-3-thione synthesized by reaction of thiophene-2-carbohydrazide and p-tolyl isothiocyanate. Its compound structure was elucidated by characterizing it by spectroscopic methods such as FT – IR,  $^1\text{H-NMR}$  and  $^{13}\text{C-NMR}$ . In addition, quantum mechanical methods were used to obtain information about its electronic structure, and the obtained data were found to be compatible when compared with experimental methods. By calculating the conformation analysis of the compound, it was observed that the most unstable state was formed at angles of approximately  $-80^\circ$  and  $+72^\circ$ , and the most stable state was obtained at angles of  $-179^\circ$  and  $+178^\circ$ . By calculating the HOMO and LUMO energy values of the obtained structure, the energy difference between the ground state and first excited levels of the molecule is  $-4.626\text{ eV}$ . If the HOMO-LUMO of the same molecule is re-excited, the calculated energy difference was calculated as  $-5.837\text{ eV}$ , and the high

energy gaps in both cases showed that the molecule had a stable structure.

#### References

- [1] Guan, L. P., Jin, Q. H., Tian, G. R., Chai, K. Y., Quan, Z.S.2007. Synthesis of some quinoline-2 (1H)-one and 1, 2, 4-triazolo [4, 3-a] quinolin derivatives as potent anticonvulsants. *J Pharm Pharm Sci*, 10 (3): 254-62.
- [2] Gujjar, R., Marwaha, A., El Mazouni, F., White, J., White, K.L., Creason, S., Phillips, M. A. 2009. Identification of a metabolically Stable triazolopyrimidine-based dihydroorotate dehydrogenase inhibitor with antimalarial activity in mice. *Journal of medicinal chemistry*, 52(7): 1864-1872.
- [3] Mohammad, Y., Fazili, K. M., Bhat, K. A., Ara, T. 2017. Synthesis and biological evaluation of novel 3-O-tethered triazoles of diosgenin as potent antiproliferative agents. *Steroids*, 118, 1-8.
- [4] Huang, M., Deng, Z., Tian, J., Liu, T. 2017. Synthesis and biological evaluation of salinomycin triazole analogues as anticancer agents. *European journal of medicinal chemistry*, 127, 900-908.
- [5] Lee, T., Cho, M., Ko, S.Y., Youn, H. J., Baek, D. J., Cho, W. J., Kim, S.2007. Synthesis and evaluation of 1, 2, 3-triazole containing analogues of the immunostimulant  $\alpha$ -GalCer. *Journal of medicinal chemistry*, 50(3): 585-589.
- [6] Wang, G., Peng, Z., Wang, J., Li, X., Li, J. 2017. Synthesis, in vitro evaluation and molecular docking studies of novel triazine-triazole derivatives as potential  $\alpha$ -glucosidase inhibitors. *European journal of medicinal chemistry*, 125, 423-429.
- [7] Beutler, E. 1992. Cladribine (2-chlorodeoxyadenosine). *The Lancet*, 340 (8825): 952-956.
- [8] Kumar, G.S., Prasad, Y.R., Chandrashekar, S.M. 2013. Synthesis and pharmacological evaluation of novel 4-isopropylthiazole-4-phenyl-1, 2, 4-triazole derivatives as potential antimicrobial and antitubercular agents. *Medicinal Chemistry Research*, 22(2): 938-948.
- [9] Tanak, H. 2011. DFT computational modeling studies on 4-(2, 3-Dihydroxybenzylideneamino)-3-methyl-1H-1, 2, 4-triazol-5 (4H)-one. *Computational And Theoretical Chemistry*, 967(1): 93-101.
- [10] Becke, AD. 1988. Density-functional exchange-energy approximation with correct asymptotic behavior. *Physical review A*, 38(6): 3098-3100.
- [11] Beck, A. D. 1993. Density-functional thermochemistry. III. Therole of exact exchange. *J. Chem. Phys*, 98(7), 5648-5660.

- [12] Lee, C., Yang, W., & Parr, R. G. 1988. Development of the Colle Salvetti correlation-energy formula into a functional of the electron density. *Physical review B*, 37(2): 785-790.
- [13] Merrick, J. P., Moran, D., Radom, L. 2007. An evaluation of harmonic vibrational frequency scale factors. *The Journal of Physical Chemistry A*, 111(45):11683-11700.
- [14] Dodds, J. L., McWeeny, R., & Sadlej, A. J. 1977. Self-consistent perturbation theory: Generalization for perturbation-dependent non orthogonal basis set. *Molecular Physics*, 34(6): 1779-1791.
- [15] Öztürk, E., Irak, Z. T., Gümüş, S. 2019. (E)-2-((Fenilimino) metil) Fenol Molekülünün Teorik Olarak İncelenmesi. *Journal of the Institute of Science and Technology*, 9(1): 407-414.
- [16] Bellamy, L. J. 1980. Associated XH Frequencies, The Hydrogen Bond. In *The Infrared Spectra of Complex Molecules*. Springer, Dordrecht. 240-292.
- [17] Shahhosseini, L., Nateghi, M. R., SheikhSivandi, S. 2016. Electrochemical synthesis of polymer based on 4-(2-thienyl) benzenamine in aqueous solutions: Electrochemical properties, characterization and application. *Synthetic Metals*, 211, 66-74.
- [18] McNaught, A. D. 1997. *Compendium of chemical terminology* Oxford: Blackwell Science. 1669-1971.
- [19] Sakarya, H. 2015. Experimental and theoretical studies of FT-IR, FT-Raman and NMR calculations of 2, 2-ethylenedianiline molecule with the help of density function theory. Master Thesis Ahi Evran University, Institute of Science and Technology. Kırşehir.1-115

Available online at [www.dergipark.gov.tr/beuscitech](http://www.dergipark.gov.tr/beuscitech)

Journal of Science and Technology

E-ISSN 2146-7706



# A study on the determination of damage levels in reinforced concrete structures for different earthquakes

Ercan IŞIK\* , Ali Emre ULU , Şakir TUNÇ , Ali KESKINER 

Bitlis Eren University, Department of Civil Engineering, TR-13000, Bitlis, Türkiye

## ARTICLE INFO

### Article history:

Received 31 January 2022

Received in revised form 31 May 2022

Accepted 31 May 2022

### Keywords:

Damage level

RC structures

EMS-98

Earthquake

Seismic parameter

## ABSTRACT

It is important for spatial planning and urban transformation to determine and manage all the information about the buildings damages after the earthquake. In this respect, the first damage assessments should be made as quickly and practically as possible, especially immediately after the earthquake. Within the scope of this study, the reinforced-concrete structure's damage classification that given in the European Macro-Seismic Scale (EMS) was used, taking into account five different earthquakes in Turkey. Sample buildings were identified for five different degrees of damage foreseen in the EMS. In addition to the information about these earthquakes, seismic parameters were obtained for these earthquake epicenters. The peak ground acceleration values measured for all earthquakes considered in this study were compared with the currently recommended peak ground acceleration values.

© 2022. Turkish Journal Park Academic. All rights reserved.

## 1. Introduction

Earthquakes occur in seismically active regions and different levels of structural damage can occur as a result of destructive earthquakes. It is important to detect structural damage as a result of destructive earthquakes and to decide on repair and strengthening or demolition depending on the damage situation. Post-earthquake damage assessment is one of the important steps of modern disaster management. In particular, the first damage assessments to be made immediately after the earthquake should be carried out quickly. The need for rapid damage assessments is made both for the continuation of the social life after the earthquake and for deciding whether the

structures in the earthquake zone will be used immediately or whether repair and strengthening are needed (Bilgin et al., 2021; Hadzima-Nyarko et al., 2018; Tabrizikahou et al., 2021; Harirchian et al., 2021; Arslan and Korkmaz, 2007). Due to the large scale of the damage, the size of the affected area and the lack of sufficient expert personnel, damage assessments are not carried out quickly and practically. Insufficient public resources and difficult terrain conditions also negatively affect the damage assessment process (Işık et al., 2017; Doğan et al., 2021). It is necessary to act as fast as possible and to reach the maximum building in the minimum time while the damage assessment processes are being carried out (Işık et al., 2021). In this respect, the information to be collected about the damages should be as necessary. For all these reasons, the

\* Corresponding author. Tel.: +90 (434) 222 00 30; fax: +90 (434) 222 91 45

E-mail address: aeulu@beu.edu.tr

ORCID : 0000-0001-8057-065X (E. Işık), 0000-0001-7499-3891 (A. E. Ulu), 0000-0002-1711-654X (Ş. Tunç), 0000-0002-4382-0952 (A. Keskiner)

building data that will be the basis for the first damage assessments after the earthquake should be selected correctly. Damage assessment forms can be used to apply this information in the field is an easy, fast and practical way. With the help of these forms filled in the field, evaluations to be made in a more comfortable environment, a final decision can be made about the building. Damage assessments to be carried out systematically will significantly affect the loss of life and property in a possible second earthquake (Işık et al., 2021a).

In addition, the calculation of seismic ground motion parameters (acceleration, velocity, displacement) required for calculating the seismic loading conditions to which soil and engineering structures will be exposed in the future can be obtained by seismic hazard analysis (Moehle and Deirlein, 2004). Geographical location of the epicenter, earthquake acceleration, earthquake magnitude or intensity and loss of life and property are statistical data that are recorded after each earthquake and can be used afterwards.

Within the scope of this study, five different destructive earthquakes that occurred in Turkey were taken into account. These are the 1999 Düzce, 2003 Bingöl, 2011 Van, 2020 Sivrice (Elazığ) and 2020 İzmir earthquakes. Peak ground acceleration (PGA) and peak ground velocity (PGV) values for all earthquake epicenters were obtained for the last two earthquake hazard maps. These obtained values were

compared with the values measured after the earthquake. The loss of life and property caused by the magnitude of these earthquakes is stated. In the next part of the study, information on why the damage assessment forms should be used is given. By giving information about the European Macro-Seismic Scale (EMS-98), which is used for damage grading of reinforced-concrete (RC) structures, sample RC buildings were selected for damage grading for five different earthquakes. The study will contribute to this and similar studies in terms of obtaining the seismic parameters of these earthquake epicenters, as well as the use of EMS-98 for five different destructive earthquakes.

## 2. Considered Earthquakes

Seismicity is based on geological, tectonic and statistical data. Macro seismic data about the earthquake's time, central and supracentral location, source parameters and its effects are the most important parameters in determining the earthquake hazard of a region. The seismicity of a region is an indicator of a future earthquake in that region (Kramer,1996; Morell et al. 2020; Özmen and Can, 2016; Kutanis et al., 2018). Within the scope of this study, five important earthquakes in recent years, which caused significant losses for Turkey, were taken into account. The representation of these earthquakes on the map is given in Figure 1.

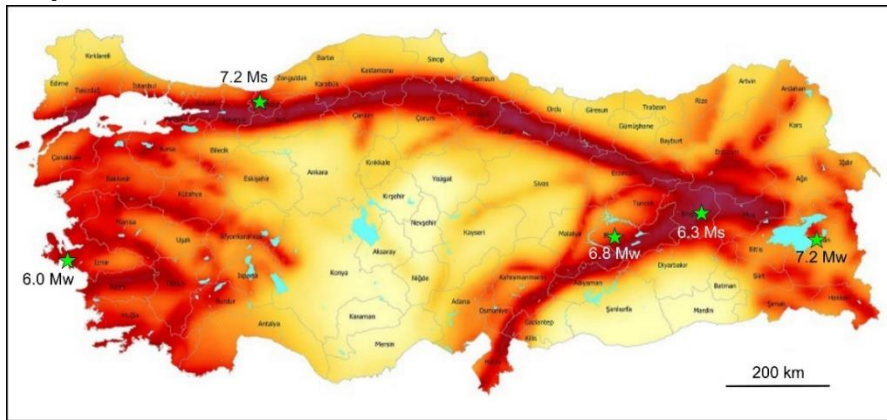


Figure 1. Earthquakes considered in the study.

The magnitude, location, and loss of life and property of these considered earthquakes are shown in Table 1. The data are

taken from the database of institutions that record important earthquake data of Turkey, such as AFAD and KOERI.

Table 1. Characteristics of the considered earthquakes.

No	Date	Lat.	Lon.	Magnitude			Loss of Life	Number of Damaged Buildings	Location
				Mb	Ms	Mw			
1	12.11.1999	40.81	31.19	6.2	7.2		763	35519	Düzce
2	01.05.2003	39.00	40.46	5.7	6.3		176	6000	Bingöl
3	23.10.2011	38.76	43.36			7.2	644	17005	Van
4	24.01.2020	38.48	39.12			6.8	41	1915	Sivrice (Elazığ)
5	30.10.2020	37.90	26.74			6.0	117	259	Seferihisar (İzmir)

In the earthquakes examined in this study, a total of 1741 lives were lost and 60698 buildings were damaged. In each earthquake, on average, 350 citizens lost their lives and 12150 buildings were damaged. This clearly demonstrates the destructiveness of these earthquakes in Turkey.

While only one ground motion level was expressed in the previous earthquake code (TSDC-2007), four different earthquake ground motion levels were expressed in the current seismic design code (Turkish Building Earthquake Code/TBEC-2018). Within the scope of this study, four different earthquake ground motion levels, 2%, 10%, 50% and 68%, were taken into account. The four different ground motion levels considered are included in the current earthquake code and are shown in Table 1.

**Table 2.** Comparison of PGA and  $S_{Ds}$  values

No	Location	TSDC-2007 Seismic Zone	TSDC-2007 PGA (g)	TBEC-2018 PGA (g)	PGA2007/PGA2019	$S_{Ds}$ 2007	$S_{Ds}$ 2018	$S_{Ds2007}/S_{Ds2018}$
1	Düzce	1	0.400	0.588	0.680	1.000	1.291	0.775
2	Bingöl	1	0.400	0.633	0.632	1.000	1.403	0.713
3	Van	2	0.300	0.399	0.752	0.750	0.844	0.889
4	Sivrice (Elazığ)	1	0.400	0.542	0.738	1.000	1.184	0.845
5	Seferihisar (İzmir)	1	0.400	0.449	0.891	1.000	0.983	1.017

The currently used code and the PGA values predicted in the map for the five earthquakes were higher than the previous ones. In the design spectral acceleration coefficients, while the current values for the four earthquake epicenters were higher, they were lower for only the İzmir earthquake.

'AFAD Turkey Acceleration Database and Analysis System' (TADAS) is used to provide a better understanding of damaging

**Table 3.** Earthquake ground motion levels (TBEC-2018)

Earthquake level	Repetition Period (year)	Probability of exceedance (in 50 years)	Description
DD-1	2475	0.02	Largest earthquake ground motion
DD-2	475	0.10	Standard design earthquake ground motion
DD-3	72	0.50	Frequent earthquake ground motion
DD-4	43	0.68	Service earthquake movement

The comparison of PGA and design spectral acceleration coefficients ( $S_{Ds}$ ) predicted for five earthquakes in the last two seismic design code is given in Table 2.

earthquake characteristics. Measured values for earthquakes were obtained using this system for all cases. These obtained values were compared with the values predicted in the last two seismic design codes and earthquake hazard maps. The comparison of the measured values with the four different ground motion levels stipulated in the current seismic design code is also given in Table 3. The values for the current code were obtained using the Turkey Earthquake Hazard Map Interactive Web Earthquake Application (TEHMIWA).

**Table 3.** Comparison of PGA values

Earthquake No	Date	Measured Values			PGA <sub>2018</sub>				PGA <sub>2007</sub>
		PGA (cm/s <sup>2</sup> )	PGV (cm/s)	PGD (cm)	DD-1	DD-2	DD-3	DD-4	DD-2
1	30.10.2020	179.31	22.53	5.16	0.825	0.449	0.175	0.126	0.400
2	24.01.2020	292.80	45.34	10.99	0.957	0.542	0.201	0.152	0.400
3	23.10.2011	178.35	26.11	5.55	0.837	0.399	0.109	0.073	0.300
4	01.05.2003	501.44	37.21	15.74	1.121	0.633	0.256	0.175	0.400
5	12.11.1999	806.98	80.16	47.79	0.996	0.588	0.211	0.123	0.400

The PGA values measured for the 2020 İzmir, 2020 Sivrice (Elazığ), 2011 Van earthquakes were lower than the values predicted in the last two maps for the design earthquake ground motion level. The PGA value measured for the 2003 Bingöl earthquake was higher than the predicted value in the previous map, but lower than the predicted value in the current map. The PGA value measured in the 1999 Düzce earthquake was greater than the PGA values predicted for the standard design earthquake ground motion level on both maps. However, it was smaller than the predicted PGA value for DD-1, which is the largest earthquake ground motion level for this earthquake base. Therefore, only Düzce earthquake was greater than the PGA value predicted for the design ground motion level in the current map, and for the other four earthquakes, it was below the predicted values for the design earthquake ground motion level.

---

### **3. Damage Rating in RC Structures**

The characteristics of earthquakes directly affect the loss of life and property. In addition, the structural characteristics of the existing building stock in the earthquake zone directly affect the loss of life and property. Obtaining accurate and timely information on structural damage will guide both the reduction of casualties and the effective implementation of

emergency rescue (Zhai and Zeng, 2017; Xian et al., 2016). In this respect, an important factor in fast and practical damage analysis based on observations is to have a detailed and accurate building inventory and comprehensive damage data (Bessason and Bjarnason, 2016). Damage information of buildings is essential for rescue, humanitarian and reconstruction operations in the disaster area. Building damages can be graded in the field using damage scales (Sharma et al., 2017).

There are many different macro seismic scales to assess and classify structural damage after an earthquake more quickly (Zanini et al., 2019; Gómez Capera, 2007). The European Macroseismic Scale (EMS-98) was developed by the European Seismological Commission (ESC), taking into account the wider damage levels, considering the security gaps in the (Mercalli-Cancani-Sieberg (MM-31 ve MM-56) and Medvedev, Sponheuer-Karnik (MSK-64 ve MSK-81) gauges (Zanini et al., 2018; Grünthal, 1998; Grünthal and Levret, 2001). Within the scope of this study, earthquake damages were determined for different earthquakes by using five different damage ratings for RC structures in the European Macro-Seismic Scale -98 (EMS-98). While determining earthquake damages, academic studies on earthquakes were taken into account. Damage grading of RC structures in EMS-98 is shown in Figure 2.



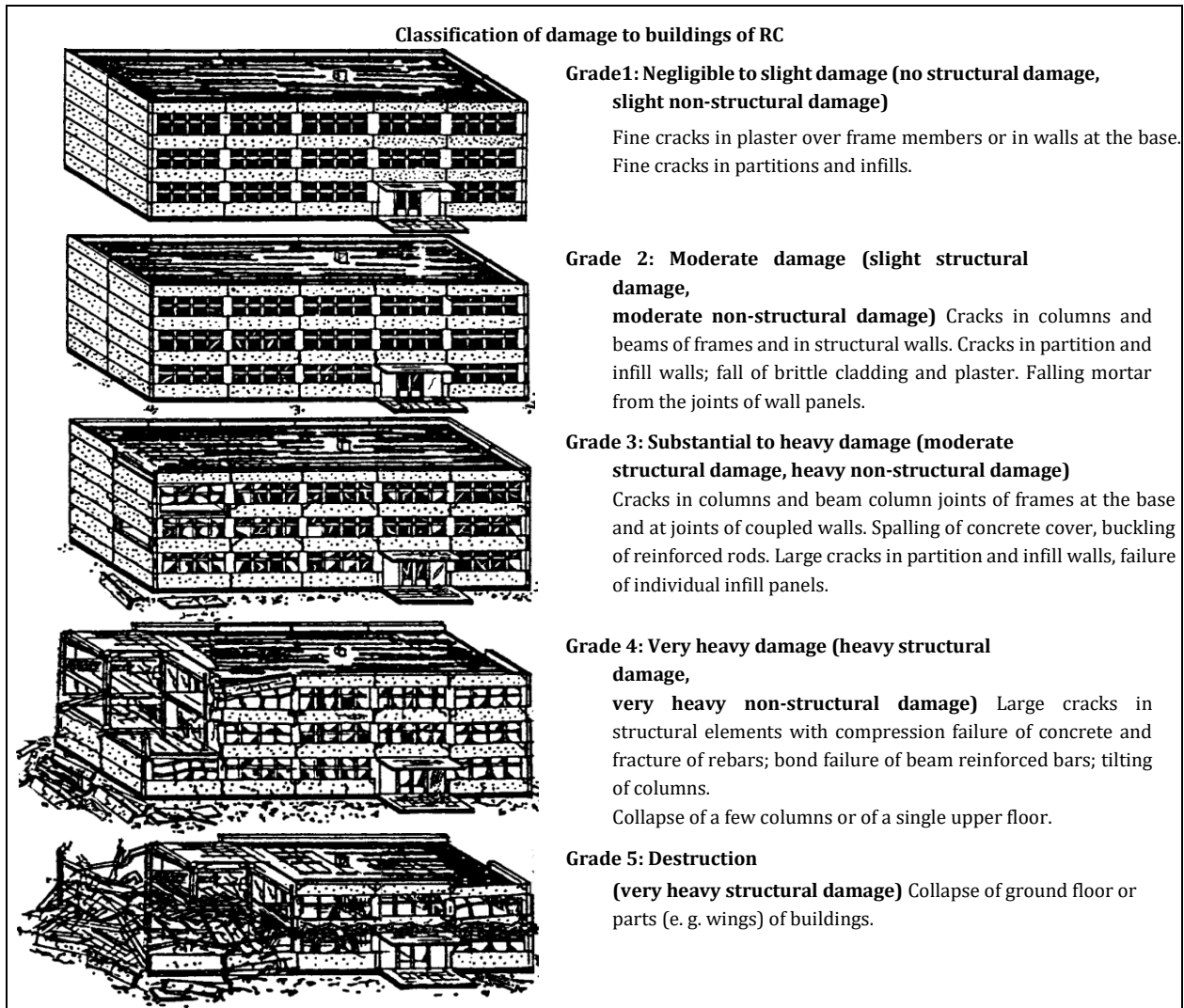


**Figure 2.** Damage grades in RC structures according to EMS-98

The visuals used in the 1st degree damage grade for the considered earthquakes are shown in Figure 3.



**Figure 3.** Negligible to slight damage for different earthquakes (Grade 1)

The moderate damage (Grade 2) for RC buildings for selected earthquakes are shown in Figure 4.



**Figure 4.** Moderate damaged RC buildings

The substantial to heavy damaged (Grade 3) RC buildings for selected earthquakes are shown in Figure 5.



**Figure 5.** The substantial to heavy damaged (Grade 3) RC buildings

Very heavy damaged buildings for selected earthquakes are shown in Figure 6.



**Figure 6.** Very heavy damaged (Grade 4) RC buildings

Destruction of some RC buildings (Grade 5) for selected earthquakes are shown in Figure 7.



**Figure 7.** Destruction of (Grade 5) RC buildings

Total collapse, soft story damage, cracks in structural system elements, infill wall damages and damages in column-beam junctions are the damages observed in the buildings studied. The reasons for such damages are that the building does not receive engineering service and that the earthquake-resistant building design principles are not taken into account both in the design and during the construction phase. In addition, poor workmanship, lack of inspection, low material strength and design errors are other factors that can increase the amount of damage. Soft/weak floors, strong beams – weak columns, short columns, irregularities in plan and vertical, which adversely affect the behavior of buildings under earthquake effects, increase the probability of damage to structures. Insufficient lateral rigidity and insufficient use of RC shear walls can negatively affect the behavior of structures under earthquake effects and increase the amount of damage. In addition, factors such as generally made similar mistakes in reinforcement processing (insufficient wrapping, insufficient or incomplete reinforcement arrangements, insufficient or incorrect clamping, etc.) affect the degree of damage.

#### 4. Conclusions

Within the scope of this study, seismic parameters were obtained for the last two earthquake hazard maps for five different earthquake locations. The predicted PGA values on these maps were compared with the PGA values measured during the earthquake. The seismic parameter values predicted on a regional basis in the previous map have been replaced by site-specific seismic parameter values. The study once again demonstrated the importance of site-specific calculation of seismic parameters. Except for the 1999 Düzce earthquake, for the other four earthquakes considered, the

design in the current map was lower than the PGA values predicted for ground motion. However, the value measured for the 1999 Düzce earthquake was lower than the value recommended for the largest ground earthquake (DD-1) for that location. In this respect, it can be stated that the current earthquake hazard map is sufficient to reveal the earthquake hazard.

In addition, damage grading of RC buildings was carried out for five different earthquakes considered in the study using EMS-98. Quick and practical determination of damage after an earthquake is a part of modern disaster management for the continuation of social life. At this point, people who will make earthquake damage assessment should first receive training on how to do damage assessments. As a result of this process, field studies will be faster and more reliable. Successful data collection often heavily depends on this preparation. Otherwise, field studies need to be renewed to collect data.

All kinds of data to be obtained as a result of any damage assessment and rating to be made after the earthquake are valuable data in terms of civil and earthquake engineering. With the help of these data, the seismicity of the region and the characteristics of the building stock, its strengths and weaknesses can be revealed. In addition, it is possible to make necessary arrangements in earthquake resistant building design principles by using these data. One of the most obvious examples that can be given to this is the concrete class. Generally, damages in RC structures are associated with low concrete strength. In this respect, while the lowest concrete class envisaged in the 1975 earthquake code in Turkey was C14, it was increased to C20 in the 2007 seismic design code and to C25 in the current seismic design code.

Damage degrees in buildings under earthquake effects generally depend on structural features. It is not possible to predict earthquakes with today's technologies. Therefore, the fact that the amount and degree of earthquake damage is much lower is related to the use of earthquake resistant building design principles both in the construction and design phases. In this context, Turkey has demonstrated its sensitivity in this regard by renewing and updating its earthquake resistant building design principles many times. At this point, the sensitivity of decision makers and practitioners in the building sector will contribute to lower earthquake damage.

#### Acknowledgements

There is nothing to declare.

#### References

- Arslan, M.H., and Korkmaz, H.H., 2007. What is to be Learned from Damage and Failure of Reinforced Concrete Structures During Recent Earthquakes in Turkey? *Engineering Failure Analysis*, 14(1), 1-22.
- Aydın, A., 2012. Van depreminde hasar gören mevcut betonarme bir binadaki hasarın, DBYBHY 2007'ye göre yapılan performans analiz sonuçları ile karşılaştırılması, Yüksek Lisans Tezi, Fen Bilimleri Enstitüsü, İstanbul.
- Bessason, B., and Bjarnason, J.Ö. 2016. Seismic Vulnerability of Low-rise Residential Buildings Based on Damage Data from Three earthquakes (Mw6. 5, 6.5 and 6.3). *Engineering Structures*, 111, 64-79.



- Bilgin, H., Shkodrani, N., Hysenlliu, M., Ozmen, H.B., Isik, E., and Harirchian, E., 2022. Damage and Performance Evaluation of Masonry Buildings Constructed in 1970s during the 2019 Albania Earthquakes. *Engineering Failure Analysis*, 131, 105824.
- DEMP, 2020. Interactive earthquake map web page for the 08.06.2020 available at <https://tdth.afad.gov.tr/>
- Dogan, G., Ecemis, A.S., Korkmaz, S.Z., Arslan, M.H., and Korkmaz, H.H., 2021. Buildings Damages after Elazığ, Turkey Earthquake on January 24, 2020. *Natural Hazards*, 1-40.
- Doğangün, A., 2004. Performance of Reinforced Concrete Buildings During the May 1, 2003 Bingöl Earthquake in Turkey. *Engineering Structures*, 26(6), 841-856.
- Emre, Ö., Herece, E., Doğan, A., Parlak, O., Özaksoy, V., Çiplak, R., and Özalp, S., 2003. Bingöl Depremi Değerlendirme Raporu. Maden Tetkik Arama Enstitüsü Rapor, (10585).
- Erdil, B., 2017, 2011 Van Depremlerinin Ardından: Tasarım ve Uygulama Farkları. 4. Uluslararası Deprem Mühendisliği ve Sismoloji Konferansı 11-13 Ekim 2017, Anadolu Üniversitesi, Eskişehir, Türkiye
- Gómez Capera A.A., Albarello, D., Gasperini, P., 2007. Aggiornamento Relazioni fra l'Intensità Macrosismica e PGA, Technical Report. Convenzione INGV-DPC 2004-2006.
- Grünthal, G., 1998. European Macroseismic Scale 1998. European Seismological Commission (ESC).
- Grünthal G., Levret A. 2001. L'échelle macrosismique européenne. Conseil de l'Europe – Cahiers du Centre Européen de Géodynamique et de Séismologie, Vol. 19. 2001.
- Hadzima-Nyarko, M., Ademovic, N., Pavic, G., and Sipos, T.K., 2018. Strengthening techniques for Masonry Structures of Cultural Heritage According to Recent Croatian Provisions. *Earthquakes and Structures*, 15(5), 473-485.
- Harirchian, E., Hosseini, S.E.A., Jadhav, K., Kumari, V., Rasulzade, S., Işık, E., and Lahmer, T. 2021. A Review on Application of Soft Computing Techniques for the Rapid Visual Safety Evaluation and Damage Classification of Existing buildings. *Journal of Building Engineering*, 102536.
- <http://www.koeri.boun.edu.tr/new/> (Accessed date: 05 January 2022)
- <https://deprem.afad.gov.tr/galeri/246572> (Accessed date:05 January 2022)
- <https://tadas.afad.gov.tr/list-event> (Accessed date: 05 January 2022)
- <https://tdth.afad.gov.tr> (accessed date:06 January 2022).
- Isik, E., Aydin, M.C., and Buyuksarac, A., 2020. 24 January 2020 Sivrice (Elazığ) Earthquake Damages and Determination of Earthquake Parameters in the Region. *Earthquakes and Structures*, 19(2), 145-156.
- Işık, E., Işık, M.F., and Bülbül, M.A., 2017. Web Based Evaluation of Earthquake Damages for Reinforced-Concrete Buildings. *Earthquakes and Structures*, 13(4), 423-432.
- Işık, E., Özdemir, M., and Karaşın, İ.B., 2018. Performance Analysis of Steel Structures with A3 Irregularities. *International Journal of Steel Structures*, 18(3), 1083-1094.
- Işık, M., Işık, E., and Harirchian, E., 2021. Application of IOS/Android Rapid Evaluation of Post-Earthquake Damages in Masonry Buildings. *Gazi Mühendislik Bilimleri Dergisi (GMBD)*, 7(1), 36-50.
- Işık, E., 2015. Hasarlı bir Betonarme Binanın Performans Puanının Hesaplanması. *International Anatolia Academic Online Journal Sciences Journal*, 3(2), 47-52.
- İMO İzmir Şubesi, 2020, İzmir Depremi Raporu.
- İnel, M., Özmen, H.B., and Çaycı, B.T., 2013. Simav and Van Depremleri (2011) Yapı Hasar Nedenlerinin Değerlendirilmesi. *Pamukkale Üniversitesi Mühendislik Bilimleri Dergisi*, 19(6), 256-265.
- Kramer, S.L., 1996. *Geotechnical earthquake engineering*. Pearson Education India.18TC005365.
- Kutanis, M., Ulutaş, H., and Işık, E., 2018. PSHA of Van Province for Performance Assessment Using Spectrally Matched Strong Ground Motion Records. *Journal of Earth System Science*, 127(7), 1-14.
- Mercalli G. 1902. Intensity scales. *Bollettino della Societa Sismologica Italiana* 8:184–91.
- Moehle, J., and Deierlein, G.G., 2004. A Framework Methodology for Performance-based Earthquake Engineering. In 13th World Conference on Earthquake Engineering (Vol. 679).
- Morell, K.D., Styron, R., Stirling, M., Griffin, J., Archuleta, R., and Onur, T., 2020. Seismic Hazard Analyses from Geologic and Geomorphic Data: Current and Future Challenges. *Tectonics*, 39(10), e20
- Özden, Ş., Akpınar, E., and Atalay, H.M., 2011. Tarihli Van Depreminde Gözlenen Yapı Hasarları. *Kocaeli Üniversitesi, Kocaeli*.
- Özmen, B., and Can, H., 2016. Ankara için Deterministik Deprem Tehlike Analizi. *Gazi Üniversitesi Mühendislik Mimarlık Fakültesi Dergisi*, 31(1).
- Şahin H., Alyamaç K.E., Durucan A.R., Demirel B., Ulaş Açıkgenç M., Bildik A.T., Durucan C., Demir T., Ulucan M., and Demirbaş N., 2020. 24 Ocak 2020 Mw 6.8 Sivrice/Elazığ Depremi Elazığ Bölgesi Yapısal Hasarlar İnceleme ve Analiz Raporu, Yapı ve Beton Uygulama ve Araştırma Merkezi, Fırat Üniversitesi, Rapor No:2020/D001, Elazığ, Türkiye.
- Sharma, R.C., Tateishi, R., Hara, K., Nguyen, H. T., Gharechelou, S., and Nguyen, L. V. 2017. Earthquake Damage Visualization (EDV) Technique for the Rapid Detection of Earthquake-Induced Damages Using SAR Data. *Sensors*, 17(2), 235.
- Tabrizikahou, A., Hadzima-Nyarko, M., Kuczma, M., and Lozančić, S., 2021. Application of Shape Memory Alloys in Retrofitting of Masonry and Heritage Structures Based on their Vulnerability Revealed in the Bam 2003 Earthquake. *Materials*, 14(16), 4480.
- TBEC-2018, 2018. Turkish Building Earthquake Code, T.C. Resmi Gazete; 30364 Ankara Turkey.
- Xian, L., He, Z., and Ou, X., 2016. Incorporation of Collapse Safety Margin into Direct Earthquake Loss Estimate. *Earthquakes and Structures*, 10(2), 429-450.
- Yakut, A., Sucuoğlu, H., Binici, B., Canbay, E., Donmez, C., İlki, A., and Ay, B.Ö., 2021. Performance of Structures in İzmir after the Samos Island Earthquake. *Bulletin of Earthquake Engineering*, 1-26.
- Zanini, M.A., Hofer, L., and Faleschini, F., 2019. Reversible Ground Motion-To-Intensity Conversion Equations Based on the EMS-98 Scale. *Engineering Structures*, 180, 310-320.
- Zhai, W., and Zeng, W., 2017. Building Damage Assessment Using a Single Post-Earthquake Polarsar Image: a Case of the 2010 Yushu Earthquake. In *IOP Conference Series: Earth and Environmental Science* (Vol. 57, No. 1, p. 012018). IOP Publishing.

Available online at [www.dergipark.gov.tr/beuscitech](http://www.dergipark.gov.tr/beuscitech)

Journal of Science and Technology

E-ISSN 2146-7706



# Investigation of the contribution of the reinforcement tie to the seismic behavior of reinforced-concrete columns

Ercan IŞIK\* 

Bitlis Eren University, Department of Civil Engineering, TR-13000, Bitlis, Türkiye

## ARTICLE INFO

### Article history:

Received 02 February 2022

Received in revised form 31 May 2022

Accepted 07 June 2022

### Keywords:

Reinforced-concrete columns

Reinforcement tie

Seismic behavior

Pushover analysis

Shear capacity

## ABSTRACT

In seismic design codes it is obligatory to use special earthquake reinforcement ties in reinforced-concrete structural columns. Lack of special earthquake reinforcement ties or any deficiency in arrangement or amount of these reinforcements can cause different levels of damage to the reinforced-concrete structural elements after the earthquake. Within the scope of this study, a total of eight different structural models were created in order to determine the effect of the reinforcement-ties on the shear capacity of reinforced-concrete columns, considering four different reinforcement-tie models and two different reinforcement materials. The period, seismic capacity and target displacement values were obtained for each structural model. In addition, demand, limit and capacity values for shear force were obtained and compared. Significant contribution to the seismic behaviour of the structure with use of reinforcement ties was observed. Material strength and the amount of reinforcement ties used significantly contributing to the seismic behaviour of the structure.

© 2022. Turkish Journal Park Academic. All rights reserved.

## 1. Introduction

Earthquakes cause different levels of destructive damages in engineering structures. The magnitude of the earthquake and structural characteristics of the building stock affect the amount of damage. In this context, determining the existing building stock characteristics before a possible earthquake is a part of modern disaster management (Shendkar et al., 2021; Işık et al., 2018; Harirchian et al., 2020; Arslan, 2010). In addition, collapsed and heavily damaged structures after the earthquake reveal the importance of earthquake resistant structure design. (Tabrizikahou et al., 2021; Bilgin et al., 2021; Harirchian et al., 2021). Particularly, the damages that occur in reinforced-concrete (RC) structures, which constitute a large part of the existing building stock, add a special importance to

the studies on the earthquake performance of such structures (Doğan et al., 2021; Büyüksaraç et al., 2021 Hadzima-Nyarko and Šipoš, 2017).

Reinforced-concrete structural system that constitutes a large part of the existing building stock is preferred due to its properties. RC is a composite building material formed by the combination of two different materials namely reinforcement and concrete. In RC structures, insufficient reinforcement and concrete properties significantly affect the behavior of the structure under the influence of earthquakes (İnel et al., 2008; Işık et al., 2021; Arslan ve Korkmaz, 2007). The deficiencies of the transverse and longitudinal reinforcements are one of the causes of structural damage in RC structures as a result of destructive earthquakes. Reinforcement defects can increase the degree of damage in structures especially in vertical load-

\* Corresponding author. Tel.: +90 (434) 222 00 30; fax: +90 (434) 222 91 45  
E-mail address: [eisik@beu.edu.tr](mailto:eisik@beu.edu.tr)  
ORCID : 0000-0001-8057-065X (E. Işık)

bearing elements such as columns and shear walls. Choosing the placement and numbers of the transverse and longitudinal reinforcements to be used in the columns in accordance with the relevant regulations and standards and placing them as in the project during the construction phase are important in fulfilling the functions expected from the reinforcements. Reinforcement arrangement details in columns, shear walls, beams, slabs and foundation elements that make up RC frames directly affect the strength, ductility and rigidity of RC structure (Stepinac et al., 2021; Yakut et al., 2021; Işık, 2014; Doğangün, 2004; Çelebi et al., 2013; Işık et al., 2020; Erdil, 2017; Tapan et al., 2013; Pekgokgoz and Avcil, 2021). Many studies have been carried out to determine the effect of transverse and longitudinal reinforcements on structural properties of RC columns.

Çolakoğlu (2020) investigated the effect of transverse reinforcement spacing change, which is an important effect that determines the earthquake performance of RC column, on its trans linear behavior. Taşkın and Okay (2019) investigated the effect of transverse reinforcement type on column behavior in their study. Merter and Uçar (2015) investigated the effects of longitudinal reinforcement ratio, transverse reinforcement pitch spacing and axial load on the energy consumption and cross-section energy consumption of reinforced concrete sections under monotonic loading in nonlinear behavior. İnel et al., (2007) investigated the seismic performance of mid-height RC buildings with different story numbers, as well as the transverse reinforcement spacing, as well as different parameters. On the other hand, Meral (2018) investigated the effects of parameters such as axial load, concrete compressive strength, longitudinal reinforcement ratio, longitudinal reinforcement yield strength, transverse reinforcement spacing, transverse reinforcement diameter, transverse reinforcement yield strength and volumetric ratio of transverse reinforcement on the curvature ductility of column sections. İnel et al., (2008), while determining the behavior of fourteen RC buildings under earthquake effects, also took into account the variation of transverse reinforcement spacing, along with other variables. Foroughi et al., (2020) investigated the effect of material model, axial load and transverse reinforcement ratio on the behavior of RC columns in their study. Aydemir et al., (2009) derived analytical relations for realistic and practical calculation of  $M_p$  in rectangular reinforced concrete columns. Hasgöl et al., (2016) tested four RC cantilever column elements with low concrete strength and insufficient transverse reinforcement in their study.

One or more of the effects such as bending, shear, torsion may cause damage to the columns at the same time. If there is not enough transverse reinforcement at the joints and in the column enclosing area, the core concrete is easily crushed and fractured, the longitudinal column reinforcements are buckled. One of the reinforcements used in the columns is the reinforcement ties that keep the opposing reinforcements or rows of reinforcements at the same distance by connecting them to each other. These ties are used in RC shear walls and columns, which are vertical load-bearing elements. In addition to ensuring that both longitudinal and transverse reinforcements work together by clamping each other, it also works as a distance protector between the reinforcements. Especially in seismic design codes, it is called special

earthquake reinforcement tie and its use is important. The crossties can clamp the reinforcements together and prevent the reinforcements from moving under the effect of concrete casting and earthquake. It can prevent the buckling of the transverse reinforcements as well as helping to the transverse reinforcements that meet the shear force in the vertical structural elements. Reinforcement ties can be seen as a type of transverse reinforcement and can contribute to the fulfillment of the functions of these reinforcements. These ties can also be used to maintain the cover spacing. When all these features are taken into consideration, the reinforcement ties used properly will increase the strength and ductility of the columns. The diameter and spacing of special earthquake reinforcement ties are the same as the diameter and spacing of stirrups. The reinforcement ties must be applied separately at both ends so as to wrap the longitudinal reinforcements and outer stirrups. Stirrups and reinforcement ties are applied by being firmly attached to the longitudinal reinforcements so that they do not slip from their places while concrete is poured.

Although the contribution of reinforcement ties to the earthquake behavior of the building is known, there is limited number of experimental and analytical studies that investigated the effect of reinforcement ties on seismic behaviour of RC structural elements. Within the scope of this study, the contribution of different reinforcement ties arrangements to the seismic behavior of the structure was analytically determined using eigenvalue and pushover analysis. In this context, a total of eight different structural models were created. For each model, limit values for shear force, demand, capacity and limit values, as well as period, seismic capacity, target displacement values were obtained.

## 2. Structural Analysis

A 7-storey RC building was chosen as an example in order to demonstrate the cross-ties effect. The floor plan of the selected RC building is shown in Figure 1. Analyzes were performed using Seismostruct software (Seismosoft, 2022).

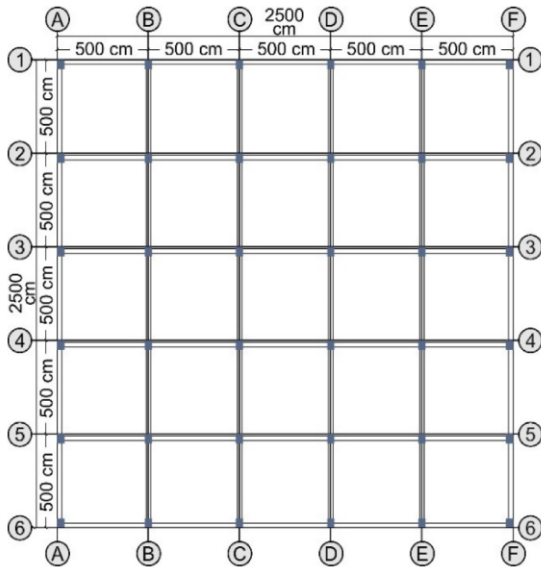


Figure 1. Floor plan of the RC building selected as an example

The 2 and 3 dimensional structural models of the RC building chosen as an example and the representation of the applied loads are given in Figure 2.

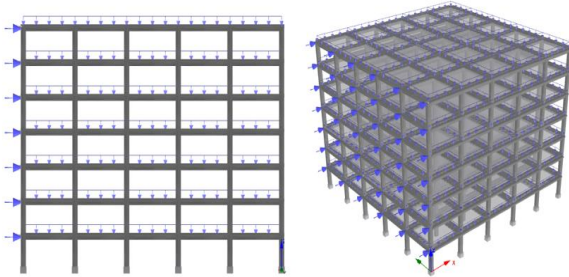


Figure 2. 2 and 3 dimensional structural models and applied loads of the RC structure analyzed

The material and dimensional properties of the structure as well as the parameters used in the series of the analysis are shown in Table 1.

Table 1. Analysis input values considered for the sample RC structure


Parameter	Value
Concrete grade	C25
Reinforcement grade	S220 and S420
Beams	250*600mm
Height of floor	120 mm
Cover thickness	25 mm
Columns	400*500mm
Longitudinal Reinforcement	Corners 4Φ20 Top bottom side 4Φ16 Left right side 4Φ16

Transverse reinforcement	Φ10/100
Steel material Model	Menegotto-Pinto
Concrete material model	Mander et al. nonlinear
Constraint type	Rigid diaphragm
Incremental load	2,38 kN
Permanent Load	5 kN/m
Target Displacement	0.42m
PGA	0.654g
Ground Type	C
Importance Class	II
Damping	5%

Structural models used to consider the effect of reinforcement ties are shown in Table 2. While creating the models, two different types of reinforcement (S220 and S420), were taken into account. In addition, four different types of cross-ties were chosen as the other variable as shown in Table 2.

Table 2. Considered cross-sections and their description

Model No	Section	Material	Description
Model I		S220	Double
Model II		S420	Double
Model III		S220	Single
Model IV		S420	Single
Model V		S220	None
Model VI		S420	None
Model VII		S220	Diamond

Model VIII		S420	Diamond
------------	---	------	---------

In the structural analysis, the limit states given in Eurocode-8 (Part 3) and used worldwide were taken into consideration for damage estimation. Three performance limit states, namely Near Collapse (NC), Significant Damage (SD) and Damage Limitation (DL) were obtained for all structural models respectively. The period, base shear capacity and performance limit states values obtained as a result of the structural analysis are given in Table 3 for S220; and in Table 4 for S420 reinforcement.

**Table 3.** Comparison of the analysis results for S220

Model No	Period (s)	Base Shear (kN)	DL (m)	SD (m)	NC (m)
Model I	0.699	6758.33	0.222	0.284	0.492
Model III	0.699	6752.07	0.221	0.283	0.491
Model V	0.699	6733.28	0.220	0.283	0.49
Model VII	0.699	6767.02	0.222	0.284	0.493

**Table 4.** Comparison of the analysis results for S420

Model No	Period (s)	Base Shear (kN)	DL (m)	SD (m)	NC (m)
Model I	0.699	9550.29	0.238	0.305	0.529
Model III	0.699	9508.26	0.237	0.304	0.527
Model V	0.699	9437.49	0.236	0.303	0.525
Model VII	0.699	9593.55	0.238	0.305	0.529

The load factor continued until the 51st step in all models, except for Model 5 (S220 without reinforcement ties). In Model 5, after 29<sup>th</sup> load step, the phase was terminated and the entire load could not be applied. There was no change in the natural vibration period of the structure due to the presence and different arrangements of reinforcement-ties. With the increase of reinforcement ties in cross-section, there was an increase, in seismic capacity for both S220 and S420. The reinforcement ties were found to be more effective in Model VII and Model VIII. The least effect was obtained for Model V and Model VI, which are models with no reinforcement ties. The grade of the reinforcement ties has caused significant changes in the performance of the columns and structure. The change in the transverse and longitudinal reinforcement materials grades used in all columns caused very significant changes in the seismic capacity. From this point of view, use of S420 and equivalent reinforcements contributed approximately 50% in the base shear. The target displacement values decreased with the decrease in the amount of reinforcement ties for both reinforcement grades.

The main purpose of performance-based engineering, is to determine the performance of structure at different limit states. This can be accomplished efficiently in SeismoStruct software through the definition of Performance Criteria. The

comparison of the demand and limit values obtained for Column 111 and Column 163 located on the ground story as a result of the structural analysis is given as an example in Table 5. PR means performance ratio.

**Table 5.** The comparison of demand and limit shear values

Model	Col 111			Col 163		
	Demand	Limit	PR	Demand	Limit	PR
Model I	174.01	381.3	0.456	221.02	449.47	0.492
Model II	217.51	558.2	0.390	321.92	690.51	0.466
Model III	165.91	317.5	0.522	202.14	379.50	0.533
Model IV	220.45	444.38	0.496	304.92	565.94	0.539
Model V	150.93	245.43	0.615	176.59	306.15	0.577
Model VI	237.48	354.71	0.670	257.58	430.36	0.599
Model VII	168.42	497.06	0.339	236.10	579.54	0.407
Model VIII	214.48	791.72	0.271	342.58	940.41	0.364

Shear capacity of the columns were determined using code-based check in the software used was used. The main difference between the Code-based Checks and the Performance Criteria is that the latter are checks against the 'expected' values of the response quantities, whereas the former follow the conservative assessment methodologies as defined by the corresponding Codes and Standards (Antoniou and Pinto, 2003). The shear capacity of the Sections module was calculated using the expression of EC8-Part 3. The comparison of demand and capacity shear values is given in Table 6.

**Table 6.** The comparison of demand and capacity shear values

Model	Col 111			Col 163		
	Demand	Capacity	PR	Demand	Capacity	PR
Model I	174.01	255.07	0.682	221.05	313.67	0.705
Model II	217.51	361.38	0.602	321.86	475.71	0.677
Model III	165.91	211.33	0.785	202.14	265.92	0.760
Model IV	220.45	287.31	0.767	304.93	392.31	0.777
Model V	150.93	162.75	0.927	176.59	215.29	0.820
Model VI	237.48	233.91	1.015	257.58	299.36	0.860
Model VII	168.42	329.56	0.511	236.10	400.59	0.589
Model VIII	214.48	514.46	0.417	342.58	642.98	0.533

In Model 6, shear capacity has been exceeded in a total of four columns. On the other hand, in Model 5, since the analysis could not be completed shear capacity values were not obtained. For all other structural models, no shear force capacity is exceeded.

The shear capacity of each column increased significantly with increasing number of reinforcement ties in the cross section. The lowest shear capacities were obtained for Model V and Model VI, in which no reinforcement ties were used, while the highest values were obtained for Model VII and Model VIII, in which diamond type reinforcement ties were used.

The nonlinear behavior of the structures is assessed based on the material strains implemented in the SeismoStruct (2022). For this, purpose strains were respectively taken as  $-0.0035$ ,  $-0.008$ , and  $+0.10$ , for spalling of cover concrete (crush\_unc), crushing of core concrete (crush\_conf), and fracture of steel (fracture). The number of elements exceeding these strain limit states for the 36 columns on the ground floor in all structural models are given in Table 7. Only one column fracture was observed in Model 5, in which is no reinforcement ties were used. With increasing the usage of reinforcement ties, the number of damaged elements were decreased.

**Table 7.** The comparison of material strain

Model No	Number of columns is ground story		
	Crush-conf	Fracture	Crush-unc
Model I	36/36	0/36	36/36
Model II	30/36	0/36	36/36
Model III	36/36	0/36	36/36
Model IV	30/36	0/36	36/36
Model V	36/36	1/36	36/36
Model VI	36/36	0/36	36/36
Model VII	30/36	0/36	36/36
Model VIII	30/36	0/36	36/36

## 5. Results and Conclusions

It is possible to ensure that the structure exhibits ductile behavior in order to minimize the level of damage of the structures in possible earthquakes, if the structural elements have sufficient and necessary strength at the same time. Use of reinforcement ties in reinforced concrete columns provides important contributions to the ductility and strength properties of RC structural elements. The transverse and longitudinal reinforcements used in RC columns directly affect the seismic behavior of the structures. The amount of reinforcement ties to be used provides significant positive contributions. However, providing this contribution in practice will only be possible if it is made in accordance with the reinforcement arrangement and placement rules.

In the current seismic design codes used in Turkey, stirrups are used in all earthquake zones, in columns of all RC systems with normal ductility level, column-beam junction areas, shear end zones and beam wrapping zones are 'special earthquake stirrups', and reinforcement ties are 'special earthquake reinforcement tie'. will be arranged. The diameter and spacing of special earthquake reinforcement ties will be the same as the diameter and spacing of stirrups. The reinforcement ties will definitely wrap the longitudinal reinforcements at both ends. The operations to be carried out in accordance with this and

similar equipment regulation rules are important for the fulfillment of the functions expected from the equipment.

## References

- Antoniou, S.; Pinho, R. SeismoStruct–Seismic Analysis Program by Seismosoft; Technical User Manuel; SeismoStruct: Pavia, Italy, 2003
- Arslan, M.H., Korkmaz, H.H. 2007. What is to be learned from damage and failure of reinforced concrete structures during recent earthquakes in Turkey?. *Engineering Failure Analysis*, 14(1), 1-22.
- Arslan, M.H., 2010. An evaluation of effective design parameters on earthquake performance of RC buildings using neural networks. *Engineering Structures*, 32(7), 1888-1898.
- Aydemir, C., Zorbozan, M., Alacali, S.N. 2009. Dikdörtgen kesitli betonarme kolonların Mp moment kapasitelerinin belirlenmesi. *Teknik Dergi*, 20(96), 4545-4565.
- Bilgin, H., Shkodrani, N., Hysenlliu, M., Ozmen, H.B., Isik, E., Harirchian, E. 2022. Damage and performance evaluation of masonry buildings constructed in 1970s during the 2019 Albania earthquakes. *Engineering Failure Analysis*, 131, 105824.
- Büyüksaraç, A., Isik, E., Harirchian, E. 2021. A case study for determination of seismic risk priorities in Van (Eastern Turkey). *Earthquake and Structures*, 20(4), 445-455.
- Çelebi, E., Aktas, M., Çağlar, N., Özocak, A., Kutanis, M., Mert, N., Özcan, Z. 2013. October 23, 2011, Turkey/Van–Ercis earthquake: structural damages in the residential buildings. *Natural Hazards*, 65(3), 2287-2310.
- Çolakoğlu, H.E. 2020. Betonarme kolonların deprem performansında enine donatı aralığı etkisinin sayısal olarak incelenmesi. *Adıyaman Üniversitesi Mühendislik Bilimleri Dergisi*, 7(12), 1-13.
- Dogan, G., Ecemis, A.S., Korkmaz, S.Z., Arslan, M. H., Korkmaz, H.H. 2021. Buildings Damages after Elazığ, Turkey Earthquake on January 24, 2020. *Natural Hazards*, 1-40.
- Doğangün, A. 2004. Performance of reinforced concrete buildings during the May 1, 2003, Bingöl Earthquake in Turkey. *Engineering Structures*, 26(6), 841-856.
- EN 1998-3 (2005). Eurocode-8: Design of Structures for Earthquake Resistance-Part 3: Assessment and Retrofitting of Buildings; European Committee for Standardization: Bruxelles, Belgium, 2005.
- Erdil, B. 2017. Why RC buildings failed in the 2011 Van, Turkey, earthquakes: construction versus design practices. *Journal of Performance of Constructed Facilities*, 31(3), 04016110.
- Foroughi, S., Jamal, R., Yüksel, B. 2020. Sargı donatısı ve eksenel yük seviyesinin betonarme kolonların eğrilik süneklik ile etkin kesit rijitliğe etkisi. *El-Cezeri Journal of Science and Engineering*, 7(3), 1309-1319.

- Hadzima-Nyarko, M., Kalman Šipoš, T. 2017. Insights from existing earthquake loss assessment research in Croatia. *Earthquakes and structures*, 13(4), 365-375.
- Harirchian, E., Hosseini, S. E. A., Jadhav, K., Kumari, V., Rasulzade, S., Işık, E., ... & Lahmer, T. 2021. A review on application of soft computing techniques for the rapid visual safety evaluation and damage classification of existing buildings. *Journal of Building Engineering*, 102536.
- Harirchian, E., Lahmer, T., Buddhiraju, S., Mohammad, K., Mosavi, A. 2020. Earthquake safety assessment of buildings through rapid visual screening. *Buildings*, 10(3), 51.
- Hasgöl, U., Yavaş, A., Türker, K., Terzi, M., Birol, T. 2016. DBYBHY-2007'de tanımlanan hasar kriterlerinin betonarme kolon elemanlar için incelenmesi. *Uludağ University Journal of the Faculty of Engineering*, 21(2), 499-514.
- Inel, M., Ozmen, H. B., Bilgin, H. 2008. Re-evaluation of building damage during recent earthquakes in Turkey. *Engineering Structures*, 30(2), 412-427.
- İnel, M., Bilgin, H., Özmen, H.B. 2007. Orta Yükseklikteki Betonarme Binaların Deprem Performanslarının Afet Yönetmeliğine Göre Tayini. *Pamukkale Üniversitesi Mühendislik Bilimleri Dergisi*, 13(1), 81-89.
- İnel, M., Bilgin, H., Özmen, H.B. 2008. Orta yükseklikli betonarme binaların Türkiye'de yaşanan son depremlerdeki performansı. *Teknik Dergi*, 19(91), 4319-4331.
- Işık, E., Harirchian, E., Bilgin, H., Jadhav, K. 2021. The effect of material strength and discontinuity in RC structures according to different site-specific design spectra. *Res. Eng. Struct. Mater*, 7, 413-430.
- Işık, E. 2014. The effects of 23.10. 2011 Van earthquake on near-field and damaged on structures. *International Anatolia Academic Online Journal, Scientific Science*, 2(2), 10-25.
- Işık, M. F., Işık, E., Bülbül, M.A. 2018. Application of iOS/Android based assessment and monitoring system for building inventory under seismic impact. *Gradevinar*, 70 (12), 1043-1056
- Isik, E., Aydin, M. C., Buyuksarac, A. 2020. 24 January 2020 Sivrice (Elazığ) earthquake damages and determination of earthquake parameters in the region. *Earthquakes and Structures*, 19(2), 145-156.
- Işık, E., Karaşin, İ. B., Demirci, A., and Büyüksaraç, A., 2020. Seismic risk priorities of site and mid-rise RC buildings in Turkey. *Challenge*, 6(4), 191-203.
- Meral, E. 2018. Yapısal Parametrelerin Betonarme Kolonların Eğrilik Sünekliğine Etkileri. *Osmaniye Korkut Ata Üniversitesi Fen Bilimleri Enstitüsü Dergisi*, 1(1), 28-43.
- Merter, O., Uçar, T. 2015. Betonarme kesitlerin doğrusal elastik ötesi davranışında tüketilen enerjiye boyuna donatı oranının, enine donatı aralığının ve eksenel yükün etkisi. *Niğde Ömer Halisdemir Üniversitesi Mühendislik Bilimleri Dergisi*, 4(1), 21-39.
- Pekgokgoz, R.K., Avcil, F. 2021. Effect of steel fibres on reinforced concrete beam-column joints under reversed cyclic loading. *Građevinar*, 73 (12), 1185-1194
- Seismosoft. *SeismoStruct 2022—A Computer Program for Static and Dynamic Nonlinear Analysis of Framed Structures*. 2022. Available online: <http://www.seismosoft.com>
- Shendkar, M. R., Kumar, R. P., Mandal, S., Maiti, P. R., Kontoni, D.P.N. 2021. Seismic risk assessment of reinforced concrete buildings in Koyana-Warna region through EDRI method. *Innovative Infrastructure Solutions*, 6(3), 1-25.
- Stepinac, M., Lourenço, P. B., Atalić, J., Kišiček, T., Uroš, M., Baniček, M., Novak, M.Š. 2021. Damage classification of residential buildings in historical downtown after the ML5. 5 earthquake in Zagreb, Croatia in 2020. *International Journal of Disaster Risk Reduction*, 56, 102140.
- Tabrizikahou, A., Hadzima-Nyarko, M., Kuczma, M., Lozančić, S. 2021. Application of shape memory alloys in retrofitting of masonry and heritage structures based on their vulnerability revealed in the Bam 2003 earthquake. *Materials*, 14(16), 4480.
- Tapan, M., Comert, M., Demir, C., Sayan, Y., Orakcal, K., İlki, A. 2013. Failures of structures during the October 23, 2011, Tabanlı (Van) and November 9, 2011 Edremit (Van) earthquakes in Turkey. *Engineering Failure Analysis*, 34, 606-628.
- Taşkın, M., Okay, F. 2019. Sargilama tipinin deprem yüklerine maruz kalan kolonların davranışına etkisinin sayısal olarak modellenmesi. *Mühendislik Bilimleri ve Tasarım Dergisi*, 7(1), 205-210.
- Yakut, A., Sucuoğlu, H., Binici, B., Canbay, E., Donmez, C., İlki, A., ... & Ay, B.Ö. 2021. Performance of structures in İzmir after the Samos Island earthquake. *Bulletin of Earthquake Engineering*, 1-26.



Available online at [www.dergipark.gov.tr/beuscitech](http://www.dergipark.gov.tr/beuscitech)

Journal of Science and Technology

E-ISSN 2146-7706



# Early intervention to risk groups with the QR code system in disasters

Emine ÇAĞDAŞ<sup>a</sup> , Aydın BÜYÜKSARAÇ<sup>\*b</sup> , M. Fatih IŞIK<sup>c</sup> 

<sup>a</sup> Bitlis Eren University, Graduate Education Institute, TR-13000, Bitlis, Türkiye

<sup>b</sup> Çanakkale Onsekiz Mart University, Çan Vocational School, TR-17400, Çanakkale, Türkiye

<sup>c</sup> Hitit University, Department of Electric and Electronic Engineering, TR-19030, Çorum, Türkiye

## ARTICLE INFO

### Article history:

Received 13 February 2022

Received in revised form 16 May 2022

Accepted 30 May 2022

### Keywords:

Disaster

Risk Groups

Data

Health

## ABSTRACT

While disasters are situations in which people cannot cope with their own capacities, it is impossible for risk groups that need the care of others not to be affected by it. Our country is frequently exposed to disasters due to its geopolitical position, irregular population growth, being a developing country, increased industrialization, insufficient infrastructure, and many other reasons. It is very important that disadvantaged community members who need help are easily accessible and identifiable at the time of disaster. The main purpose of this study is to provide the fastest, most accurate and reliable information to the elderly living alone, to children who lost their parents during the event, to women, to those who cannot do the work they need to do on their own in their personal or social life due to any deficiencies, to those who have their own disease and who have been harmed by disasters. In this study, the risk groups that will be affected by disasters were determined and the data of the people created as an example were transferred to the data matrix system. First of all, individuals in risk groups (disabled, chronic patients, elderly, children and women) were determined and then a data matrix was created on the website.

© 2018. Turkish Journal Park Academic. All rights reserved.

## 1. Introduction

Undoubtedly, disasters have been one of the biggest problems faced by mankind throughout history (Ekinci et al., 2020). Throughout history, the definition of disaster has varied in research due to different perceptions (Başegmez, 2017). A disaster is defined as a situation that causes damage, destruction, human losses after an event, and requires external assistance to a large extent by exceeding the capacity to cope

with their own means according to the World Health Organization (WHO) (Öztaş, 2019).

Disaster and Emergency Management Presidency (AFAD-DEMP) has defined disaster as a crisis situation that causes loss of life and property by stopping or interrupting normal life activities and requiring urgent intervention (Karabulut and Bekler, 2019). According to the International Federation of Red Cross and Red Crescent Societies (IFRC), disasters are catastrophic that seriously disrupt the functioning of society and cause material, economic and irreversible vital losses that the society cannot overcome by using its own resources

\* Corresponding author. Tel.: 05053870502

E-mail address: [absarac@comu.edu.tr](mailto:absarac@comu.edu.tr)

ORCID: 0000-0002-0962-1263 (E. Çağdaş), 0000-0002-4279-4158 (A. Büyüksaraç), 0000-0003-3064-7131 (M.F. Işık)



(Özkazanç, 2015). Many definitions of disaster can be found in the literature review apart from the definitions given. The common feature of all these definitions is that they exceed the coping capacity and cause great loss of life and property. The magnitude of the disaster experienced is determined by the injury and loss of life, that is, it is associated with the result rather than the type of disaster experienced (Altun, 2018).

It has been determined as the main goal to provide early intervention to disadvantaged groups, to reach losses and to prevent post-disaster abuses, by combining personal information with the data matrix application, to provide ease of access to this information in extraordinary situations in this study.

### 1.1. Vulnerability

It is defined as needing the help of another person to fulfill their vital functions, being in a situation that prevents bilateral communication, being unable to protect oneself from attacks, bad behavior and abuses (Taştan and Aydınöğlü, 2015). While the capacity of individuals to cope with the dangers and risks of disasters is different from each other, this situation becomes more complicated for individuals with age, gender, physical and mental disabilities. Babies and children, women, the elderly and people with disabilities are more vulnerable than other individuals. This leads to a decrease in the survivability capacity in emergencies and disasters (Sheikhbardsiri et al., 2017). Some characteristics of individuals cause them to be exposed to abuses more easily and to wear out. Age, gender, physical and mental status are some of them. The elderly and children are more easily abused and abused because they need the help of others. Considering that the elderly and children do not have the ability to make decisions causes the autonomy of these people to be ignored. Being a woman causes the person to be harmed, abused and hurt more easily. Especially women in pregnancy are more affected by disasters. People with a health status, physical or mental disability, and terminal illness are more likely to be affected by disasters than normal individuals (URL-1).

Within the scope of the Sendai Framework, it was stated that the states that are members of the United Nations should take measures in accordance with the universal values for the reduction of disaster risks, but that would meet the national and local needs, and suggestions were made to carry out studies to reduce the disaster risks. People with private health care needs have the highest morbidity and mortality rates during disasters. To give an example, after the Great East Japan earthquake of 2011, it has been proven because of the research that the disaster-related death rate of disabled people is 4 times higher when compared to other members of the society. After the tsunami that occurred due to the 2004 Indian Ocean earthquake, it was determined that 700 people with physical disabilities lost their lives in the Andomon Islands because they could not evacuate to high and safe areas (Tün et al., 2019). In a study conducted by Buluş Kırıkkaya and Gerdan (2018), the problems faced by the disabled people were examined, and while the participants of 30 people stated that they were

prepared for disaster and had an idea under normal conditions, they showed that they did not have a clear idea when they were disabled or have a disabled relative.

## 2. Materials and Method

In this study, a data matrix identification system was designed to be integrated into risk groups in order to provide early intervention in case of a disaster, to reach losses and to prevent post-disaster abuses. First of all, a group definition was made in five different categories that were targeted for the application. Infant-children, women, chronic patients, the disabled and the elderly are considered as risk groups within the scope of the study.

### 2.1. Infant-Child

A baby is a creature that starts with birth and lives within the next 24 months. Child covers the period from 3 years to 11 years (URL-2). Studies on the location of disaster victims in our country are very new. According to unofficial figures after the 17 August 1999 earthquake, it is said that more than 300 people disappeared and these losses may have fallen into the hands of organs, prostitution and drug mafia or illegal traders (URL-3). After the Varto earthquake that took place on August 19, 1966, 40 children were left orphaned, and they waited for an intervention and a helping hand with the wounds they received from various parts (Büyüksaraç and Bektaş, 2017).

After the civil war in Syria, 28266 children died and 4469 children were arrested. It is not known what happened to the arrested children. It is stated that the number of children who lost their lives due to torture is 176. As a result of the 2004 Indian Ocean tsunami, nearly 4400 children lost both their mother and father. Due to the drought in Africa, thousands of children have been orphaned and death rates have increased. It is stated that 42% of Palestinian children living under Israeli siege are exposed to more than one disability. Due to the civil war in Syria, living in an unhealthy camp environment and being fed with water and food, children have faced the risk of many diseases. A significant increase has been observed in the number of children with disabilities, especially with the use of chemical weapons in wars. To give an example, while there were 300,000 disabled children in Afghanistan before the long war, this number increased to 867,100 between 2005 and 2006 due to the war and landmines (Kutluoğlu and Karayel, 2019). Security is one of the most common problems in war zones. The lack of security of life as a result of conflicts and bombardments, living in constant fear of death, causes individuals to migrate to different countries. Most of the refugees who try to immigrate to different countries become targets of malicious people such as human trafficking, organ mafia. Women and children are most affected by this condition. When the research is examined, approximately 1.2 million children are subject to human trafficking every year (Kutluoğlu and Karayel, 2019).

Nearly 500,000 children living under siege in Syria do not have access to regular humanitarian aid and basic services. In 2013, thousands of people died as a result of the civil war in South Sudan, 60 children and adults were stuffed into containers and strangled. Many deaths and destructions have occurred as a result of Hurricane Matthew, and 90 thousand children under the age of 5 are still waiting for humanitarian aid in need (URL-4).

Children are disproportionately affected by all types of disasters compared to adults. The fragile, needy and weak structures of children increase the rate of being affected by disasters as disaster victims. Limoncu and Atmaca (2018), who showed that children are more affected by disasters than adults, according to their study, 48% of school-age children are affected by disasters on average, while 52% are severely or very seriously affected. In 2011, approximately 66 million children are affected by disasters in the world every year (Mudavanhu et al., 2015). After the hurricane caused by monsoon rains in India, 300 children/adolescents were affected by the disaster, and it was determined that 200 children/adolescents had at least one psychosocial problem related to the disaster. Based on these results, it was stated in the published report that 66.7% of children/adolescents were affected by the disaster after the Uttarakhand disaster and this value was quite high (Anaelraj et al., 2016). Between 2002 and 2012, 31,012 babies died in Japan and 1450 in Tohoku. The Great East Japan Earthquake and Tsunami (GEJET) appears to have a greater impact on post neonatal deaths than neonatal deaths (Toshiro et al., 2019). Toshiro et al. (2018) examined the deaths of children under the age of 10 years after 2008-2014 and after the 2011 great earthquake in Japan, and it was found that the mortality rate among children younger than 10 years old was 6.4 times higher than the rate before and after 2011 during the 2011 disaster period. According to the data obtained from UNICEF, within 10 years, 2 million children died, 6 million children were injured, 12 million children were displaced from their homes, and nearly 10 million children were exposed to post-traumatic stress disorder (Gözübüyük et al., 2015).

## 2.2. Women

Female individuals who have completed their development and completed the age of 18 are called women (URL-5). Disasters do not affect people equally, the impact of disasters on women's lives is different from other groups of a community. After disasters, women's fundamental rights to health and safety are violated. After the 2010 Haiti earthquake, sexual assault victimization of 660 women was investigated and it was determined that 31.06% of them were exposed to sexual assault (Cenat et al., 2019). In a study conducted by researchers from the London School of Economics and Essex universities, 21 years of disaster data from 141 countries were evaluated, and as a result, it was determined that women died more than men in disasters (URL-6). The gender gap has also emerged in a number of disasters, including the tsunami in

Asia. The victimization of men and women after disasters such as Hurricane Mitch, Hurricane Katrina and other types of storms in the Americas, European heat waves and cyclones in South Asia was compared. It has been observed that women are more at risk than men (Asghari, 2018). It has been reported that 644 people lost their lives in the earthquakes that took place in Van on October 23 and November 9, 2011, and the majority of those who lost their lives were women who were caught while doing work at home during the earthquake. On the other hand, after the Van earthquake, female suicide rates were found to be high in and around Van (TTB, 2012). It has been reported that after the earthquake, women in tent cities experienced situations that limited their freedom of life and movement (going to toilets and showers due to fear of being abused) (URL-7). After the 2004 Indian Ocean tsunami, the death rate of women was found to be four times higher than that of men. It was determined that male death rate of female deaths after flood and cyclone in Bangladesh Gorky in 1991 was 14:1, while female deaths were 55% in the earthquake that occurred in Nepal in 2015, the death rate of other citizens was 45% (Hemachandra et al., 2018).

Disasters affect girls and boys, women, the elderly, and the disabled in different ways and in severity. Therefore, their responses to disasters differ from other individuals. Women are more affected by disasters than men due to the role of motherhood, poverty, low level of education, and gender roles imposed on them. Women have been exposed to various difficulties because of their gender. The problems arising from the gender inequality of women and their examples are given below.

Behaviours of women arising from their upbringing, acquired skills, being affected by gender role, for example, women's lack of swimming or climbing skills, protecting their children and households due to the responsibilities imposed on them, taking active attitudes depending on their decision to move them to another place in case of disaster, situations such as the difficulties experienced by the clothes caused the victimization of women to be more in disasters.

In crisis and disaster situations, there are difficulties due to the difficult and limited access to reproductive health services. Obstetrics, pregnancy, and puerperal care are needed for many reasons, for which we can increase their access to gynecological and reproductive health services. After a disaster, the number of women who give birth prematurely, those whose birth is approaching, and women who need birth control services are increasing due to the fear of the disaster.

Post-disaster nutrition, infections and infectious diseases are increasing. The fact that toilets and bathrooms are outside the

camp after the disaster creates difficulties in use (Dündar et al., 2018). The use of dirty water due to insufficient water has led to an increase in diseases and loss of life (Coşkun, 2018). Trafficking in women increases after disasters and wars. In Turkey, 99% of human trafficking for sexual exploitation is women. Different forms of human trafficking are also encountered, such as forced marriage, burdening the entire household, begging, and adoption (Boz and Şengün, 2017). According to the latest estimates, the number of women traded in earthquake regions has been close to 20,000 (Coşkun, 2018).

### 2.3. Chronic patients

Insidious and progressive deviation in physiological functions is defined as health problems that do not improve throughout life, have a complex course, and affect the lives of individuals who require constant care (Akpınar and Ceran, 2019). The number of chronic diseases in our country is constantly increasing. There is no definitive treatment for these diseases. Only symptomatic or reliever treatments are applied. Diabetes, asthma, cancer, AIDS, blood pressure, migraine, COPD, allergies, ulcers, heart diseases, anemia are the most common types of chronic diseases (Dülger, 2003). The first four causes of death in 1980 in Turkey were heart diseases, perinatal, pneumonia, and cancer (URL-8). The reason why chronic patients are handled in disasters is the increase in the victimization rate due to the increase in problems in accessing this type of treatment or the need for medication and special medical equipment after a possible earthquake (Uğur et al., 2014).

### 2.4. Elderly

In the definition accepted by the World Health Organization, it covers individuals who are chronologically 65 years and older (Beğner and Yavuzer, 2012). It turned out that 70% of those who died after Hurricane Katrina in New Orleans were elderly. After the Mis hurricane, 200 elderly people were abandoned by their caregivers, and after this disaster, the chronic disease picture worsened due to the inability of more than 200,000 elderly to use the drugs for diseases such as diabetes and asthma. The majority of the 465 people who died during the Chicago heat wave in 1995 were over the age of 75 (Gibson and Hayunga, 2006). Labra et al. (2018), examined the factors that cause an increased risk of death during a heat wave for people aged 65 and over, pointing out that there are factors such as living alone, social isolation, inadequate air conditioning systems, living in the upper floors of apartments, and other housing features. In order to evaluate the post-disaster situation of the elderly, HelpAge International interviewed 300 elderly women and men, some of the elderly stated that they were indifferent to them and their opinions were not taken into account in case of disasters and emergencies, and some reported that they did not receive adequate humanitarian aid. Half of the interviewed

elderly reported feeling anxious and hopeless (Labra et al., 2018). A nationwide telephone interview survey was conducted with 1648 elderly people in the USA in 2005 by AARP and Harris Interactive, approximately 13% of elderly people aged 50 and over stated that they would not be able to evacuate from their homes in case of natural disasters without help, 46% stated that they needed help from outsiders, 67% stated that they needed help from outside. of them stated that they could evacuate on their own (Figure 1). It is also seen in the graph in Figure 1 that these rates are higher for the elderly over 75 years old, except for evacuation without needing the help of someone else, especially when they need help from outsiders (URL-9).

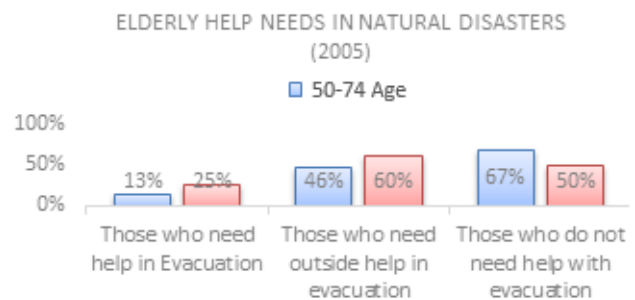


**Figure 1.** Telephone interview survey of 1,648 seniors nationwide in the USA by AARP and Harris Interactive (URL-9).

Advancing age is a very strong risk factor for having more than one chronic disease. About 80% of older people have at least one chronic condition, such as heart disease, diabetes, or stroke. All disasters disproportionately affect older adults, especially those who are chronically disease. Among the reasons for being particularly vulnerable during and after disasters are physical disabilities, decreased sensory awareness, adaptation problems, chronic health conditions, and economic constraints that prevent adequate preparation and adaptability in social disasters. In the survey conducted by Harris Interactive survey in 2005, it was concluded that half of the 13 million elderly people aged 50 and over in the United States would seek help from someone other than themselves after a disaster (URL-10).

### 2.5. Disabled people

In the most general terms of the United Nations, it has been defined as the inability of normal individuals to fulfil their vital functions as a result of genetic or later deficiencies in their personal or social lives (Koca, 2010). The definition made by the United Nations General Assembly for the disabled is the inability of healthy individuals to do the things that they need to do in their personal or social life without the need for the help of another person, because of any congenital or acquired deficiencies (Koca, 2010).

According to the results of the 2002 disability research conducted by the Turkish Statistical Institute and the Administration for the Disabled, 12.29% of the total population has at least one disability (Sarı and Aktar, 2017). Out of a total of 8 million 431 thousand 937 disabled citizens, 9.7% consists of chronic diseases, 1.25% orthopedic, 0.38% language and speech, 0.48% mental, 0.37% hearing, 0.6% visually impaired citizens (URL-11). The most common types of disability.

**Visually impaired:** They are individuals with complete or partial vision loss or impairment in one or both eyes (Pascolina and Mariotti, 2012). As a result of the survey conducted in 39 countries, it was revealed that there are 285 million visually impaired people, 39 million of whom are blind (URL-12).

**Hearing impairment:** They are people who have completely or partially lost their hearing (URL-13). The inability of a person with language and speech disabilities to pronounce the sounds they make properly and fluently, and those with impaired speech speed and voice.

**Orthopedic disability:** They are people who have lost their physical abilities to varying degrees due to disorders in the skeletal, muscular and nervous systems for any reason, and who have difficulty in performing their daily life activities and therefore need the help of another person (Yumuşak, 2014).

**Mental disability:** They are individuals who differ by about two standard deviations in mental function and need special and supportive training (URL-13).

**Chronic illness:** They are diseases that have long-lasting and continuous treatments in any part of the body (URL-13).

## 2.6. Quick Response (QR) Code

information, blood transfusion tracking and blood group information will be accessed quickly. In the study of Taiwanese researchers, the transfer of prescription information between hospitals and pharmacies to a computerized environment was provided to identify patients with data matrix (Uzun and Bilgin, 2016; Işık et al., 2018; Işık et al., 2020).

In order to apply QR code within the scope of the study, parametric information for the risk group members consisting of 42 people selected from the province of Bitlis was transferred to the database in the electronic environment, and a data matrix application was carried out to be used on smart phones and tablets in order to evaluate and monitor this transferred information. This system provided data matrix-based medical identification and identification of disaster

A type of matrix barcode, or two-dimensional bar, was originally designed for the automotive industry in Japan. Recently, the QR Code system has become popular. It has more storage capacity than standard UPC barcodes due to its fast readability. The code consists of a black module (square dots) arranged on a square grid on a white background (Masalha and Hirzallah, 2014). QR code were used in many different fields (Işık et al., 2019; Işık et al. 2018). It was first used in the pharmaceutical industry in Turkey (URL-3). The features that make the QR code widely used can be listed as follows.

- 360° readability,
  - High speed feature,
  - Expanded data capacity (depending on symbol size and information type)
  - Support of different types of information (binary, numeric, alpha-numeric, Kanji / Kana)
  - Resistance to non-linear appearance (eg due to uneven surfaces)
  - High level of standardization (eg AIM, JIS, JAMA, ISO and IEC)
  - Error checking and correction algorithm (Reed-Solomon) (Canadi et al., 2010),
  - It has the ability to store large amounts of data in a small area without accessing the database to support information distribution and detection (Warasart and Kuacharoen, 2012).
- QR codes are widely used for processing patient data in the Asia-Pacific regions. Various hospital supports were developed in Brenmoor, United Kingdom, and QR codes were placed on blood bag labels. Data matrix is used in accordance with the patient safety policy at Adden brooke hospital in Cambridge. Thanks to the QR code integrated into the wristband, personal

victim identification information. A unique medical system data matrix tag is assigned to each selected member. Thus, easy access to information such as personal information, disease history, regularly used drugs, and disability will be ensured. The QR code can be integrated into portable items such as the collar tag of the shirt, the tag with the washing instructions of the clothes, the necklace or the ID card.

The age, gender, diagnosis of the disease, drugs used, blood type, disability status, surgery information and allergic reaction information of the risk groups in question are shown in Table 1. Some information on the table, such as the drugs she/he used, allergies and disabilities, were hidden due to the privacy policy and were only given as Yes/No.

**Table 1.** Sample parametric data of individuals in the risk group for which QR code will be applied.

Risk Group	Sample No	Gender (F/M)	Age	Disease	Drugs Used (Yes/No)	Blood Type	Disability/Allergy (Yes/No)	Surgery undergone
Elderly	1	F	71	diabetes mellitus	Yes	A Rh(+)	No	Yes
	2	F	68	atherosclerosis eye pressure	Yes	O Rh(+)	Yes	No
	3	M	66	KOAH	Yes	AB Rh(-)	Yes	No
	4	M	65	Primary hypertension, diabetes	Yes	B Rh(+)	No	No
	5	F	90	Myalgia, hypertension	Yes	A Rh(-)	No	Yes
Infant-Child	1	F	4	Asthma	Yes	A Rh(+)	Yes	Yes
	2	M	6	type-2 diabetes	Yes	A Rh(+)	No	Yes
	3	F	5	Epilepsy	Yes	O Rh (+)	No	No
	4	F	5	dystonia	Yes	O Rh (+)	No	No
	5	M	6	Epilepsy	Yes	A Rh (+)	Yes	No
Females	1	F	34	Ankylosing spondylitis	Yes	AB Rh (+)	Yes	No
	2	F	41	Antivertigo	Yes	A Rh (-)	No	No
	3	F	33	Granilamatös mastit	Yes	A Rh (+)	Yes	Yes
	4	F	48	infertility	Yes	AB Rh (+)	Yes	No
	5	F	52	Hepatitis-B	Yes	O Rh (+)	Yes	No
Cronic Patients	1	M	49	Cardiac insufficiency	Yes	AB Rh(-)	Yes	Yes
	2	F	29	Gastritis	Yes	A Rh(+)	Yes	Yes
	3	F	31	Hemophilia	Yes	O Rh(-)	Yes	No
	4	M	29	Hypertension	Yes	AB Rh(+)		No
	5	F	52	chronic anemia	Yes	B Rh(+)		No
Disabled	1	F	35	multiple sclerosis	Yes	A Rh(+)	Yes	No
	2	M	12	Down Syndrome	Yes	AB Rh(-)	No	No

### 3. Results

In this study, it was determined as the main goal to provide easy access to this information in extraordinary situations by combining personal information with the data matrix application, which will provide early intervention to disadvantaged groups, reach losses and prevent post-disaster abuses. First of all, risk group members were defined. The members of this group were examined under 5 categories: infant-child, female, chronically ill, disabled and elderly. A total of 42 people were interviewed, 10 people from the elderly, women, children and chronic patient categories, and 2 people from the disabled group. A small sample group was created by selecting 2 people from each category among the 42 people interviewed and integrating them with the data matrix on a website where parametric information of 10 people in total

was created. As in the image in Figure 2, information such as age, gender, disease information, medications used, allergy status, blood group, etc., which will enable early intervention, is provided to this created web area. Thus, an individual data matrix identity was created. The QR codes on these IDs were read by mobile phones and access to the information of individuals was provided. DataMatrix necklace, shirt collar tag, top clothes can also be integrated into the places where the washing instructions are located. The places where the QR Code label will be integrated have been chosen to ensure easy access for the user, and to prevent it from being used by other people in order to eliminate abuse.

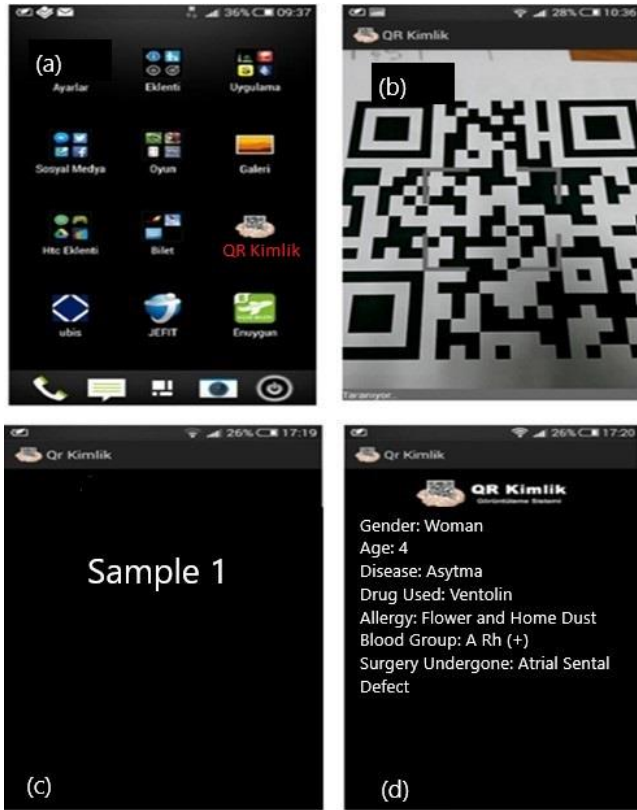


**Figure 2.** (a) QR ID web application, (b) QR code generated, (c) Person identification and (d) Contact information

#### 4. Conclusions

Disasters cause permanent damage and destruction in the region where they occurred throughout history. Today, the number of people affected by extraordinary situations is increasing day by day. For this reason, various studies are carried out to reduce the loss of life, to reach the losses early and to reduce the vulnerability. The degree of victimization experienced in disaster situations is not equal for all people. Risk group members are more affected by this condition than normal people. With the application of the QR code identification system developed due to these grievances, it will be easier to identify risk groups in disasters and if necessary, treatments will be made on time. This will save more human lives.

The database created by this method will be stored in a specified web area and can be kept as a very important and necessary source of information in terms of providing easy access to the information of the segments of the society, which is defined as a risk group for a region or community. However, this system, which was applied to a small group in the province of Bitlis, can be used throughout the country, providing the opportunity to help more people. DataMatrix created based on

the database can be carried by people in different ways. For this purpose, different applications are included in the study, and it is suggested by us that it can be used as embroidered on the collar tag on the clothes or necklace/tag, etc., in the application to be made for Bitlis.

#### Acknowledgements

This article was produced from Emine Çağdaş's master's thesis.

#### References

- Akpınar, N.B., Ceran, M.A., 2019. Kronik Hastalıklar ve Rehabilitasyon Hemşireliği. Adnan Menderes Üniversitesi Sağlık Bilimleri Dergisi, 3(2), 140-152.
- Altun, F., 2018. Afetlerin Ekonomik ve Sosyal Etkileri: Türkiye Üzerinden Bir Değerlendirme. Sabahattin Zaim Üniversitesi, Sosyal Çalışma Dergisi, 2, 1-15.
- Anaelraj, D., Naveen Kumar, C., Somanathan, R., Chandran, D., Bangalore, R.N., Math, S.B., 2016. Uttarakhand Disaster 2013: Experienced by Children and Adolescents. The Indian Journal of Pediatrics, 28, 316-321.
- Asghari, B.A., 2018. Explore are the Role of Women in Disasters: Propose Suggestion for Women Involvement in Disasters with Focus on Health Sector. PhD Dissertation, Hacettepe University Graduate School of Social Sciences Department of Health Management, Ankara.
- Başeğmez, D., 2017. Hastanelerde Afet Yönetimine İlişkin Mevcut Durumun Değerlendirilmesi. Yüksek Lisans Tezi, Okan Üniversitesi, Sağlık Bilimleri Enstitüsü, İstanbul.
- Beğler, T., Yavuzer, H., 2012. Yaşlılık ve Yaşlılık Epidemiyolojisi. İstanbul Üniversitesi Cerrahpaşa Tıp Fakültesi İç Hastalıkları Anabilim Dalı Geriatri Bilim Dalı, 25, 1-3.
- Boz, F.Ç., Şengün, H., 2017. Afet ve Kalkınma İlişkisinde Kadın. Women in the Relationship Between Disaster and Ekonomik Development. Bayburt Üniversitesi, International Journal of Social Science, 59, 359-374.
- Buluş Kırıkkaya, E., Gerdan, S., 2018. Engelli ve Engelli Adayı Bireylerin Bir Afet Anında Nasıl Davranacaklarına İlişkin Görüşleri. Dirençlilik Dergisi, 2(2), 123-129.
- Büyüksaraç, A., Bektaş, Ö., 2017. Varto Depremi 19 Ağustos 1966. Çantay Yayıncılık. İstanbul.
- Canadi, M., Höpken, W., Fuchs, M., 2010. Application of QR Codes in Online Travel Distribution. 137-148 in Proceedings of the International Conference in Lugano. Information and Communication Technologies in Tourism, Switzerland.
- Cenat, J.M., Smith, K., Morse, C., Derivois, D., 2019. Sexual Victimization, PTSD, Depression and Social Support Among Women Survivors of the 2010 Earthquake in Haiti: A Moderated Moderation Model. Psychological Medicine, 1-12.
- Coşkun, E., 2018. İnsan/Kadın Ticaret ve Toplumsal Cinsiyet Eşitliği: Türkiye'de İnsan/Kadın Ticareti İle Mücadelenin Mevcut Durum Analizi: Normatif Politik Yapı. Ceid Yayınları, Ankara.
- Dülger, A., 2003. Kronik Hastalıklar. Platform Yayıncılık. İstanbul.

- Dündar, O., Adal Dündar, R., Özölcer İ.H., Aksoy, B., 2018. Afet Ve Acil Durumlarında Su İhtiyacının Belirlenmesi ve Yönetimi. 2nd International Symposium. 04-06 Mayıs 2018, Sakarya, 962-974.
- Ekinci, R., Büyüksaraç, A., Ekinci, Y. L., Işık, E., 2020. Bitlis ilinin doğal afet çeşitliliğinin değerlendirilmesi. Doğal Afetler ve Çevre Dergisi, 6(1), 1-11.
- Gibson, M.J., Hayunga, M., 2006. We Can Do Better: Lessons Learned for Protecting Older Persons in Disasters, AARP, 14-15.
- Gözübüyük, A.A., Duras, E., Dağ, H., Arıca, V., 2015. Olağanüstü Durumlarda Çocuk Sağlığı. Journal of Clinical and Experimental Investigations, 6(3), 324-330.
- Hemachandra, K., Amaratunga, D., Haigh, R., 2018. Role of Women in Disaster Risk Governance. ICBR, 1187-1194.
- Işık, E., Antep, B., Büyüksaraç, A., Işık, M.F., 2019. Observation of behavior of the Ahlat Gravestones (TURKEY) at seismic risk and their recognition by QR code. Structural Engineering and Mechanics, An Int'l Journal, 72(5), 643-652.
- Işık, M. F., Işık, E., Bülbül, M.A., 2018. Application of iOS/Android based assessment and monitoring system for building inventory under seismic impact. Gradjevinar, 70(12), 1043-1056.
- Karabulut D, Bekler T, 2019. Doğal Afetlerin Çocuklar ve Ergenler Üzerindeki Etkileri. Doğal Afetler ve Çevre Dergisi, 5(2), 368-376.
- Koca, C., 2010. Engelsiz Şehir Planlaması Bilgilendirme Raporu, Dünya Engelliler Vakfı, İstanbul, p.1-35.
- Kutluoğlu Karayel AH, 2019. Savaş Mağdurları Yetimler. İnsamer Yayıncılık. İstanbul.
- Labra, O., Maltais, D., Lacroix, G.G., 2018. Medium-Term Health of Seniors Following Exposure to a Natural Disaster. A Journal of Medical Care Organization, Provision and Financing, 55, 1-11.
- Limoncu, S., Atmaca, A.H., 2018. Çocuk Merkezli Afet Yönetimi. Megaron, 13(1), 132-143.
- Masalha, F., Hirzallah, N., 2014. A Students Attendance System Using QR Code. International Journal of Advanced Computer Science and Applications, 5(3), 75-79.
- Mudavanhu, C., Manyena, S.B., Collins, A.E., Bango, P., Mavhura, E., Manatso, D., 2015. Taking Children's Voices in Disaster Risk Reduction a Step Forward. International Journal of Disaster Risk Science. 6(3), 267-281.
- Öztaş S, 2019. Afet Yönetiminde Afet Sonrası İyileştirme Çalışmaları için Çözüm Yaklaşımları. Doktora Tezi, Atatürk Üniversitesi Fen Bilimleri Enstitüsü, Erzurum.
- Özkazanç S, 2015. Sosyal, Mekansal ve Ekonomik Boyutlarıyla Afetlerde Konutları. 3.Türkiye Deprem Mühendisliği ve Sismoloji Konferansı, 14-16 Ekim 2015, İzmir, s:1
- Pascolina, D., Mariotti, S.P., 2012. Global Estimates of Visual Impairment. Biritish Journal of Ophtalmology, 96, 614-618.
- Taştan, B., Aydınoglu, A.Ç., 2015. Çoklu Afet Risk Yönetiminde Tehlike ve Zarar Görebilirlik Belirlenmesi için Gereksinim Analizi. Marmara Coğrafya Dergisi, 31, 366-397.
- Sarı, O.T., Aktar, E., 2017. Deprem Sonrası Yapılan/Yapılacak Binalarda Engelli ve Yaşlılara Dönük Düzenlemelere İlişkin Uygulayıcıların Görüşleri: Van İli Örneği. İnsan ve Toplum Bilimleri Araştırmaları Dergisi, 1(6), 482-499.
- Sheikhbardsiri, H., Yarmohammadian, M.H., Rezaei, F., Maracy, M.R., 2017. Rehabilitation of Vulnerable Groups in Emergencies and Disasters: A Systematic Review. World J Emerg Med, 8(4),253-263.
- Toshiro, A., Yoshida, H., Okamoto, E., 2019. Infant, Neonatal and Post neonatal Mortality Trends in a Disaster Region and in Japan, 2002-2012: a Multi-Attribute Compositional Study. BMC Public Health, 19.1085.
- Toshiro, A., Sakisaka, K., Okamoto, K., Yashida, H., 2018. Differences in Infant and Chil Mortality Before and After the Great East Japan Earthquake and Tsunami: A Large Population-Based Ecological Study. BMJ Open, 8(11), 1-11.
- Tün, M., Pekkan, E., Kurt, O., Uygucgil, H., 2019. Engelli Bireylere Erişim Çözümlerinde CBS ve Ağ Analiz Yöntemlerinin Kullanımı; Eskişehir Örneği. ESTÜDAM Halk Sağlığı Dergisi, 4(2), 88-104.
- Türk Tabipler Birliği, 2012. Deprem Birinci Yılında Van ve Erciş Raporu. P. 1-34.
- Uğur, C., Güzelkaya, D., Gürbüz, Z., 2014. Afet Odaklı Sosyal Hasar Görebilirlik Analizine İlişkin Veri Toplama Amaçlı Anket İşi, Sonuç Raporu, İstanbul, 1-122.
- URL-1. [https://acikders.ankara.edu.tr/pluginfile.php/7795/mod\\_resoruce/content/0/14.%20HaftaTOPLUMDA%20R%C4%B0SK%20GRUPLARI%28%20%C4%B0NC%C4%B0NEB%C4%B0L%C4%B0R%20GRUPLAR%29.pdf](https://acikders.ankara.edu.tr/pluginfile.php/7795/mod_resoruce/content/0/14.%20HaftaTOPLUMDA%20R%C4%B0SK%20GRUPLARI%28%20%C4%B0NC%C4%B0NEB%C4%B0L%C4%B0R%20GRUPLAR%29.pdf) Toplumda Risk Grupları (date of access: 09.09.2018).
- URL-2. <https://www.cadempsikoloji.com/blog/posts/cocuk-gelisim-donemleri> (date of access: 24.05.2018).
- URL-3. <https://arsiv.ntv.com.tr/mews/24431.asp.deprem-kayıplarına-ulaşamadı> (date of access: 30.07.2018).
- URL-4. <https://www.bbc.com/turkce/haberler-dunya-38262319> (date of access: 07.07.2019).
- URL-5. <https://onedio.com/haber/hala-anlamayanlar-icin-13-adimda-neden-bayan-degil-kadin-demeliyiz--742855> (date of access: 11.09.2019).
- URL-6. <https://www.sivildusun.net>. Mavi Kalem 'Afet ve Acil Durumlarda Kadın Çalıştayından Notlar'. (date of access: 20.11.2019).
- URL-7. <https://slideplayer.biz.tr/slide/13629718/> Geçici barınma koşullarında kadınları desteklemeye yönelik öneriler ve Van Depremi Örneğinde Karşılaşılan Zorluklar, Zeynep Bengü (date of access: 10.10.2019).
- URL-8. <http://www.https://slideplayer.biz.tr/slide/3217693/Kronik-Hastalıklar-Epidemiyolojisi>. (date of access: 13.10.2019).
- URL-9. <https://www.aarp.org/elderly-search/info-2005/AARP-and-Harris-Interactive-telephone-interview-survey-with-1,648-elderly-people-in-the-US-including-the-country> (date of access: 05.06.2019).
- URL-10. <https://cdc.gov/aging/pdf/disaster-planning-goal.pdf>. CDC's Disaster Planning Goal; Protect Vulnerable Older Adults (date of access: 27.08.2019).
- URL-11. <https://idealsosyalhizmet.com/engelli-bireylerin-toplumsal-hayatta-yasadiklari-zorluklar-ve-engelsiz-yarinlar-icin-cozum-onerileri/>(date of access: 10.08. 2019).
- URL-12. [http://manavgatram.meb.k12.tr/meb\\_iys\\_dosyalar/07/12/970601/dosyalar/2016\\_02/24091119\\_tmeblten.pdf?CHK=8101fcb00e2644ffc34b44bba239d03a](http://manavgatram.meb.k12.tr/meb_iys_dosyalar/07/12/970601/dosyalar/2016_02/24091119_tmeblten.pdf?CHK=8101fcb00e2644ffc34b44bba239d03a) (date of access: 21.08. 2018).

URL-13. [http://bergamaram.meb.k12.tr/meb\\_iys\\_dosyalar/35/04/964487/dosyalar/2016\\_06/14102042\\_33ortopedikengellibireyler.pdf](http://bergamaram.meb.k12.tr/meb_iys_dosyalar/35/04/964487/dosyalar/2016_06/14102042_33ortopedikengellibireyler.pdf) (date of access: 09.09.2019).

URL-14. <http://www.taniozelegitim.com.tr/zihinsel-engelliler-tanimi-ve-ozellikleri/> (date of access: 06.07. 2019).

Uzun, V., Bilgin, S., 2016. Evaluation and Implementation of QR Code Identity Tag System for Healthcare in Turkey. SpringerPlus, 5, 14-54.

Warasart M, Kuacharoen P, 2012. Paper-Based Document Authentication Using Digital Signature and QR Code.4TH International Conference on Computer Engineering and Technology, 2012, Tayland, p. 1-5.

Yumuşak, M., 2014. Engelli Bireylerin ve Ailelerinin Toplumsal Hayatta Yaşadıkları Zorluklar Araştırma Raporu. Çözüm Araştırma eğitim ve Danışmanlık LTD.ŞTİ, Şanlıurfa.



Available online at [www.dergipark.gov.tr/beuscitech](http://www.dergipark.gov.tr/beuscitech)

Journal of Science and Technology

E-ISSN 2146-7706



# The effect of cement replacement with eggshell powder on the sorptivity index of concrete

Muhammed TANYILDIZI <sup>a,\*</sup> 

<sup>a</sup> Bitlis Eren University, Department of Civil Engineering, TR-13000, Bitlis, Türkiye

## ARTICLE INFO

### Article history:

Received 22 February 2022

Received in revised form 31 May 2022

Accepted 07 June 2022

### Keywords:

Concrete

Cement

Permeability

Eggshell Powder

Sorptivity

Capillary Water Absorption

## ABSTRACT

Most concrete structures undergo severe durability issues throughout their service of life. The transition and movement of water through concrete structures is one of the main issues in the aspect of durability. The main aim of this study is to investigate the effect of cement replacement in various ratios with eggshell powder on the sorptivity (capillarity water absorption) capacity of concrete. Eggshell is a bio-waste material obtained from bakers, restaurants, and patisseries. Disposing of this waste material in landfills results in health hazards and causes environmental pollution. The use of eggshell powder in concrete, which is the most used and essential building material after water all over the world, is a beneficial way both minimize the detrimental effects of this waste on living health and the environment and also ensure the sustainability of the materials in concrete. In this paper, five different eggshell powder substitutions as 0%, 5%, 10%, 15%, 20% were employed in experimental analyses. The sorptivity index of concretes was measured at the end of each 5, 10, 15, 30, 45, and 60 minutes. The test results indicated that the sorptivity namely capillary water absorption decreased with up to a level of 5% replacement and increased with the other replacement ratios including 10%, 15%, and 20% when compared with the control concrete's result. This is attributed to the ESP may act as a better inert filler when replaced with cement up to a level of 5% to reduce the capillary pore, increase the compactness of concrete microstructure, impermeability and restrain the transition of water in the concrete structure.

© 2022. Turkish Journal Park Academic. All rights reserved.

## 1. Introduction

Concrete is the most used and essential construction material after water all over the world (Güneyisi et al., 2014; Umar et al., 2021; Mermerdaş et al., 2021). Most concrete structures undergo a variety of durability problems within their service of life (Yücel et al., 2020; Kurtoğlu et al., 2018). One of the most important parameters of concrete in the aspect of durability is permeability. The higher impermeable microstructure means higher strength and durable concrete. It is expected to be relatively impervious of concretes when durable concrete is targeted. The impermeable property of concrete is very important for structures including dams, water storage, concrete pipes, and highways (Sümer, 1994). One of the most important factors that affect the durability of concrete is the

transfer of liquids within the concrete structure. The water transferability of concrete determines its durability and strength throughout its service of life. As we know today, concrete with low water permeability shows better strength and durability properties and has a higher resistance to chemical attack. (Ramezani pour et al., 2011). In concrete structures, the penetration and accumulation of water may cause some undesirable physical and chemical problems. These problems generally are resulted from freezing-thawing cycles of water causing disruptive pressure and cracking, harmful chemical ions (Chloride, Sulphate) diffusions into the structure of concrete by water resulting in the corrosion of reinforcing steel, high humidity by water accumulation affecting the thermal comfort, etc. If the penetration and transition of water into the concrete structure is not prevented, the concrete structure will likely be damaged and its useful life

\* Corresponding author. Tel.: +90 434 222 0000-3612

E-mail address: [mtanyildizi@beu.edu.tr](mailto:mtanyildizi@beu.edu.tr)

ORCID: 0000-0002-8507-2825 (M. Tanyıldızı)

will be shortened (Lu et al., 2020; Hong et al., 2020; Karasin et al., 2022).

In projects where long service life is desired, the concrete void structure should be kept under control as the durability of concrete is highly related to its void structure (Türk and Demirhan, 2017). The interaction of potentially detrimental substances with concrete could be a trigger for its deterioration process. The permeability properties of concrete depend on both the void ratio and whether the spaces are interconnected or not. And, as the void ratio and the interconnection of them with each other increase, the penetration and transfer of detrimental substances and water into the concrete structure get easier. Therefore, the concrete gets damaged easier and its durability decreases (Tokyay and Erdoğan, 2011). For the reasons mentioned above, the water permeability of concretes should be examined and it becomes more of an issue to get necessary precautions in the design phase of concrete.

Three main procedures command the water transition in cementitious structures. These are capillary absorption, diffusion, and penetration. Penetration can occur only in the condition that the material is in a fully saturated environment. Almost most materials are in a partially saturated environment, and the water transport is generally generated by diffusion and capillary absorption. Diffusion is the movement of ions because of a concentration gradient while, sorptivity occurs with the transfer and movement of water through capillary action in short-term exposure to in partially dry concrete (Castro et al., 2011). In extended words, sorptivity is the absorption of water by tiny pores in cement-based composites with surface interaction and provides a measure of permeability, microstructure, and durability. In very tiny pores, the water rise by the effect of capillarity. The low capillary water absorption means impermeable and durable concrete (Al-Goody, et al., 2015).

In the literature review, some studies have been encountered to evaluate the sorptivity of concrete mixtures. Al-Goody et al. (2015) conducted a study to investigate the effect of nano-silica and fly ash utilization on the sorptivity index of self-compacting concrete. In their study, four different self-compacted concrete were designed and in all concrete series, the nano-silica was incorporated into concrete with replacement levels of 0, 2, 4 and 6%. Firstly, self-compacted concrete mixtures were cast without fly-ash, whereas the other second, third and fourth concrete mixtures were produced at substitution levels of fly ash in 25, 50, and 75%, respectively. The sorptivity coefficients were measured for each series at the end of 28 and 90 days. They concluded that the increase in the nano-silica content resulted in a systematic decrease in the sorptivity index. However, the increase in fly ash content until the 50% replacement level decreased the sorptivity index. Bozkurt and Yazıcıoğlu (2010) performed an experimental study to look into the effect of incorporation of pozzolanic materials and curing regimes on the capillary water absorption properties of light-weight concrete. Three different concrete

mixtures were designed in experimental program: one was control concrete mixture including no pozzolanic material, the last one was including 20% of fly ash (FA) and the last one is including 10% of silica fume (SF) as a replacement for the cement by weight. Both mixtures include pumice as lightweight aggregate. The specimens were cured in three different conditions: standard 20 °C water, sealed and air-cured for 28 days. The test results indicated that the silica fume introduced concrete gave lower sorptivity coefficient values regardless of curing conditions and concrete age when compared with control and concrete including fly ash. Liu et al. (2022) investigated the effect of fly ash, limestone, calcined clay, and curing age on the resistance to water penetration of seawater and sea-sand concrete. They reported that the low water to binder ratio with increasing curing age improved the water resistance. Also, they gave the information that increasing the water-resistance of concretes with fly ash, limestone and calcined clay content. Tanyıldızı (2022) performed a study to investigate the effect of cement replacement with waste ceramic powder on the capillary water absorption capacity of concrete mixtures. In this regard, cement was replaced with waste ceramic powder in proportions of 0%, 10%, 20% and 30%, and it was concluded from the study that the capillary water absorption namely permeability decreased with a replacement ratio of 10%. However, after 10% substitution rate, capillary water absorption increased with 20% and 30% substitution rates. Tosun and Şahin (2015) searched the capillary water absorption of concrete containing recycled coarse aggregate which was obtained from structural waste. In the experiment, the coarse aggregate was replaced with recycled aggregate in levels of 0%, 15%, 30%, 45%, and 60%. The capillary water absorption test was performed in the period of 1, 4, 9, 16, 25, 36, 49, and 60 minutes. They concluded that the capillary water absorption decreased with the increasing the recycled aggregate replacement level.

This study focuses on investigations of the effect of replacing cement with eggshell powder which is a bio-waste material obtained from bakeries, restaurants, poultry farms, and patisseries (Hamada et al., 2020) on the sorptivity index (capillary water absorption) of concrete. Utilization of these types of wastes in concrete as cement substitute material has been used for years and seems a beneficial way both reducing carbon dioxide emissions to the ecosystem in the production of cement and minimizing the cost of concrete. Also, the possible threat of waste to the environment and living health may be impeded by recycling way. At this juncture in this study, the cement was substituted with eggshell powder at replacement levels of 0%, 5%, 10%, 15%, and 20%. In total, 15 cubic specimens with 50 mm cubic size including the control concrete mixture were cast (three specimens for each replacement level) at constant water-to-binder ratio of 0.30. Concrete test specimens were cured in the water as fully immersed for 28 days and dried in an oven at 100±5 °C till they reached the constant mass after completing the water curing process. Then, specimens were put in sorptivity test

mechanism and removed at the end of the time of 5, 10, 15, 30, 45, and 60 minutes to calculate absorbed water quantity by weighing at the accuracy of 0.01 g. The sorptivity index of each concrete specimen was determined and the test results were evaluated for each replacement level. Also, the relationship between water absorption and sorptivity for all periods was investigated by regression analysis. It was noticed that the sorptivity coefficient decreased with the 5% replacement ratio with eggshell powder and increased with the other replacement ratios compared with control concrete. Also, a strong relationship between water absorption by mass and sorptivity of concrete was revealed by regression analysis. The results showed that the usage of eggshell powder up to a level of 5% as a cement substitute can improve the impermeability of namely the durability of concrete mixtures.

## 2. Experimental Program

### 2.1. Materials

In this study, Portland cement of CEM I 42.5 R was supplied from the cement factory of Yurtçim from Muş (Yurtçim, 2021). The eggshell was obtained from the bakers, restaurants, and patisseries as bio-waste. The cleaning process of eggshells was applied before drying by an electrical oven at 120 °C for 24 hours to dry the surface and make grinding easier. After the cleaning and drying process, the eggshell was ground in cement particle size approx. 90 µ by grinder machine as seen in Fig. 1.

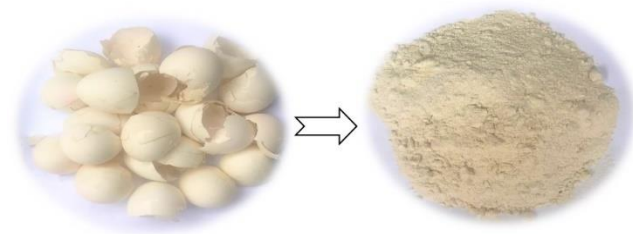


Figure 1. Eggshell powder.

The chemical and physical properties of cement and eggshell powder are presented in Table 1. The aggregate used in this study is crushed limestone with a specific gravity is 2.61 g/cm<sup>3</sup>. The material used as a superplasticizer is polycarboxylic ether-based and named Master Glenium 128 supplied from BASF Chemistry Industry with a density of 1.061–1.101 kg/lt to obtain fluidity and decrease the cement content in the concrete mixture (BASF, 2021).

Table 1 Physical properties and chemical compositions of Portland cement and eggshell powder

Analysis Report	Cement	Eggshell Powder
SiO <sub>2</sub> (%)	24.18	0.59
Al <sub>2</sub> O <sub>3</sub> (%)	6.57	0.15
Fe <sub>2</sub> O <sub>3</sub> (%)	4,5	0.04
CaO (%)	56.05	51.40
MgO (%)	1.33	0.54
SO <sub>3</sub> (%)	2.80	0.81
K <sub>2</sub> O (%)	1.22	0.09

Na <sub>2</sub> O (%)	0.34	0.44
Cl (%)	0.0071	0.09
Ignition Loss (%)	4.50	45.85
Specific gravity (g/cm <sup>3</sup> )	2.95	2.77
Specific surface (cm <sup>2</sup> /g)	4600	2950

### 2.2. Mixture Design

All mixtures were cast in constant binder amount with a 0.30 water to binder ratio. The cement was substituted with eggshell powder (ESP) at levels of 0%, 5%, 10%, 15%, and 20% by weight. The mold size of the sorptivity test was 50 mm cubic. Table 2 summarizes the concrete mixture ratios employed in this study. The abbreviations used for concrete mixtures containing ESP at levels of 0%, 5%, 10%, 15% and 30% are CC, E5, E10, E15 and E20.

Table 2 Mixture composition of concrete mixtures (kg/m<sup>3</sup>)

Materials	CC	E5	E10	E15	E20
Cement	450	427.5	400	382.5	360
ESP	-	22.5	50	67.5	90
Water	135	135	135	135	135
Superplasticizer	4.50	4.50	4.50	4.50	4.50
0-4 mm Aggregate	836	836	836	836	836
4-8 mm Aggregate	409	409	409	409	409
8-16 mm Aggregate	534	534	534	534	534

### 2.2. Test Procedure

#### Sorptivity (Capillary water absorption)

The sorptivity is the absorption of water by way of tiny pores in cement-based composites with surface interaction and provides a measure of microstructure and durability. In very tiny pores, the water rises by the effect of capillarity. A capillary water absorption test was performed to determine the sorptivity coefficient of concrete specimens based on the standard of TS EN 13057 and ASTM C1585-04. However, some technical points such as test durations are deviated from the standards. The test was conducted on a total of 15 cubes (three specimens for each concrete mixture) with 50 mm sides after 28 days of water curing. The test specimens were dried in an oven at 100±5 °C till they reached the constant mass after completing the curing process. The sides of the cubes are covered with paraffin to obstruct water suction of them from the sides of the cubes. Then, specimens were removed at the end of the time of 5, 10, 15, 30, 45, and 60 minutes from the test mechanism and weighed at the accuracy of 0,01 g. The sorptivity index or coefficient of each concrete specimen was calculated following Eq. (1) and the test results were evaluated for each replacement level.

$$S = (Q/A) / \sqrt{t} \tag{1}$$

where;

S is the sorptivity (cm/s<sup>1/2</sup>)

Q is the volume of the water absorbed (cm<sup>3</sup>)

A is the surface area in contact with water ( $cm^2$ )

t is the time (s).

Then, the square root of the elapsed time versus Q/A was plotted and the sorptivity index (capillary water absorption coefficient) was determined from the slope of the linear relationship of the best fit line. Fig. 2 shows how to interact the surface of concrete specimens with water during the capillary water absorption test.

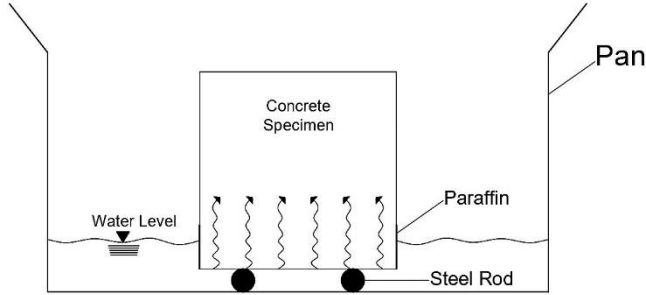


Figure 2. Detail of sorptivity test.

### 3. Results and Discussion

The sorptivity index was measured at a defined time for each concrete mixture at the end of the capillary water absorption test. Fig. 3 presents the sorptivity test results of the concrete mixtures at the end of the 5 minutes. The sorptivity index values vary between 2.05 and 2.71  $kg/(m^2.h^{0.5})$  measured at the end of 5 min. The results indicated that the sorptivity index values decreased with incorporating 5% eggshell powder but increased by the contents of 10, 15, and 20% eggshell powder compared to control concrete mixture. Replacing cement with eggshell powder at a level of 5% decreased the sorptivity index for the 5 min-interval by about 5.5%. However, in substitution levels of 10, 15, and 20%, the sorptivity index increased about 6.45, 12.0, and 24.9% compared to control concrete respectively (as seen in Fig. 3).

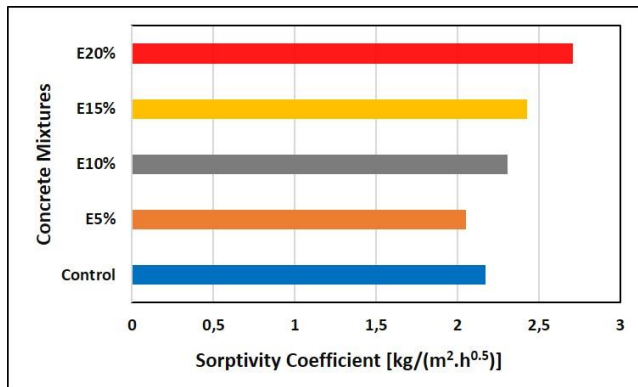


Figure 3. Sorptivity coefficients of concretes at 5 minutes.

At the end of the time of 10 min. the high and low sorptivity index value was measured as 1,52 and 2,35  $kg/(m^2.h^{0.5})$  for mixtures of again E5 and E10 respectively. For the time interval of 10 min., the sorptivity index decreased by 14.6% but increased by 5.6, 18.0, and 32.0% for the E10, E15, and E20 mix. respectively as given in Fig. 4.

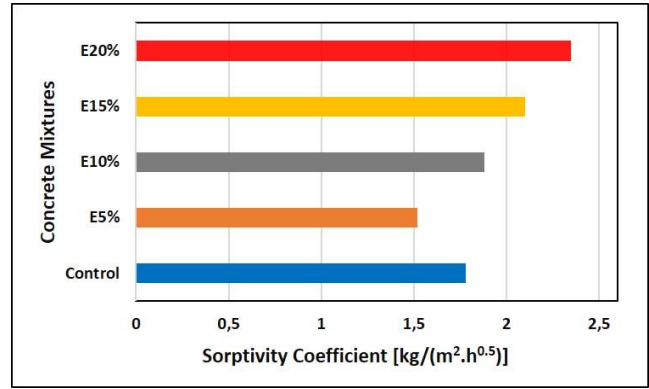


Figure 4. Sorptivity coefficients of concretes at 10 minutes.

After 15-min. water exposure interaction, the sorptivity index values were determined as 1.47, 1.23, 1.57, 1.87, and 2.02  $kg/(m^2.h^{0.5})$  for CC, E5, E10, E15, and E20 respectively. The sorptivity index decreased by 16.3% for the E5 mixture, but increased by 6.8, 27.2, and 37.4% for E10, E15, and E20 mixtures respectively presented as in Fig. 5. After 30 min. water exposure, the sorptivity index values were determined as 1.04, 0.88, 1.18, 1.51 and 1.73  $kg/(m^2.h^{0.5})$  for mixtures CC, E5, E10, E15 and E20 respectively. The sorptivity index decreased by 15.4% for the E5 mixture, but increased 13.5, 45.2 and 66.4% for the E10, E15, and E20 mixtures respectively respectively (as seen in Fig. 6).

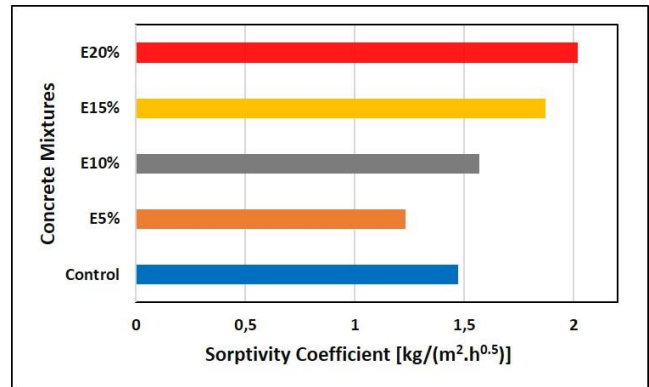


Figure 5. Sorptivity coefficients of concretes at 15 minutes.

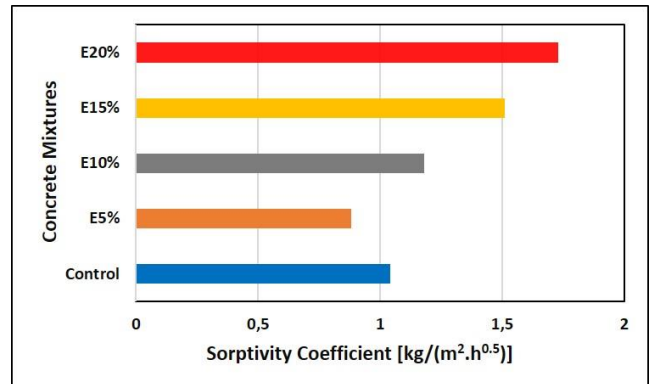


Figure 6. Sorptivity coefficients of concretes at 30 minutes.

The sorptivity index were determined as 0.93, 0.71, 1.09, 1.37 and 1.51  $kg/(m^2.h^{0.5})$  at the end of 45 min. for the CC, E5, E10, E15, and E20 mixtures respectively. The sorptivity index decreased by 23.7% for the E5 mixture but increased 17.2, 47.3

and 62,4% for the E10, E15, and E20 mixtures respectively as demonstrated in Fig. 7.

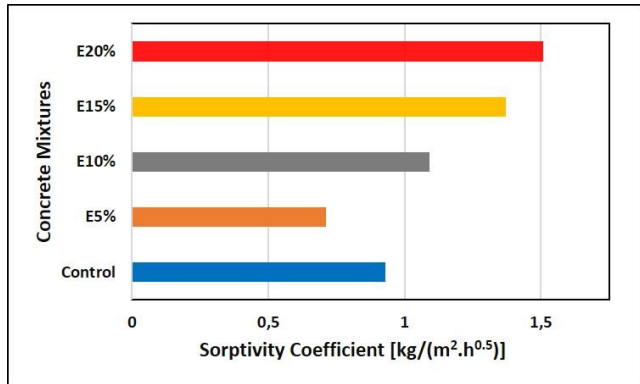


Figure 7. Sorptivity coefficients of concretes at 45 minutes.

After 60-min water exposure, the sorptivity index shaped as 0.82, 0.64, 1.01, 1.22 and 1,43 kg/(m<sup>2</sup>.h<sup>0.5</sup>) for CC, E5, E10, E15 and E20 mixtures, respectively. For the 5% content of eggshell powder, the sorptivity decreased by 22%. The sorptivity increased at the other replacement levels by 23.2%, 48,8%, and 74,4% for E10, E15, and E20 mixtures respectively when compared with the control concrete (CC) mixture as given in Fig. 8.

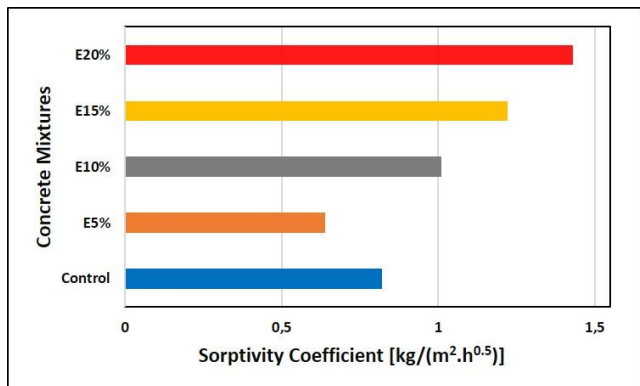


Figure 8. Sorptivity coefficients of concretes at 60 minutes.

When analyzing all sorptivity index results, it can be concluded that the replacement of cement with eggshell powder at a level of 5% increased the compactness of concrete, resulting in increased resistance against the transfer and absorption of water through the concrete microstructure. However, after a substitution ratio of 5% including 10%, 15%, and %20, it is observed that the sorptivity index enhanced, resulting in an increase in water absorption by capillary suction. All sorptivity index results for each concrete mixture are summarized in Fig. 10 for all time intervals. It is clearly seen from Fig. 10 that capillary water absorption decreases with 5% eggshell powder content but after that substitution ratio with 10%, 15% and 20%, capillary water absorption increases systematically for all time exposure.

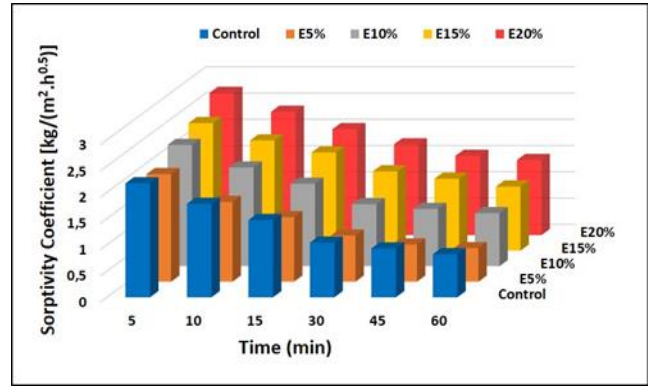


Figure 9. Summarization of Sorptivity coefficients of concretes for all time intervals.

A regression analysis was performed to correlate the water absorption by mass of concrete specimens totally immersed in water for 28 days and sorptivity index for all time intervals conducted in the study. The analyses results were presented in Fig. 10. The coefficient of determination (R<sup>2</sup>) indicates the reliability of the relationship, which is the highest value when this reliability level is equal to 1. When all regression analyzes were examined for each time period, it was seen that there was a strong relationship between the mixture's water absorption and sorptivity index. The highest determination coefficient was measured as 0,9942 for 5 min. sorptivity test and quadratic polynomial regression equation of it was given in Eq. (2):

$$S = 0,0829w^2 - 1,7017w + 10,792 \tag{2}$$

where;

S= Sorptivity

W= Water absorption by mass (%) as immersed in water

The 28-days water absorption can be determined by 5 min sorptivity test with a reliability of 99,42% using this polynomial regression equation.

#### 4. Conclusions

The sorptivity of concrete mixtures was affected by the eggshell powder content. Incorporating eggshell powder content at a level of 5% in concrete resulted in a decrease in the sorptivity index of concrete which was attributed to the improvement in compactness of the microstructure of concrete and reduction in pore sizes or volume of voids. Apart from 5%, replacement levels of 10%, 15%, and 20% were also analyzed in this study, it could be concluded that the increase in sorptivity index namely an increase in capillary water absorption capacity were observed at these replacement levels. This is likely due to occurrence of weak microstructure after the 5% replacement ratio, resulting in more water absorption and transfer of water through the microstructure of concrete. From the overall test results, it could be concluded that a 5% eggshell powder substitution rate could act as a better filler to increase the compactness and impermeability of the concrete structure, reduce the capillary void and inhibit water transfer from the concrete microstructure. Utilization of eggshell powder to improve the durability of concrete by limiting water absorption through surface interactions is a good way to minimize the harmful impact of such wastes on the



and also to minimize cement production, which is responsible for the majority of greenhouse gas emissions. In further researches, it should be taken into account that other waste materials such as rusk husk ash, corncob ash, waste slate dust should be included in the process and evaluated scientifically, as well as waste eggshell powder.

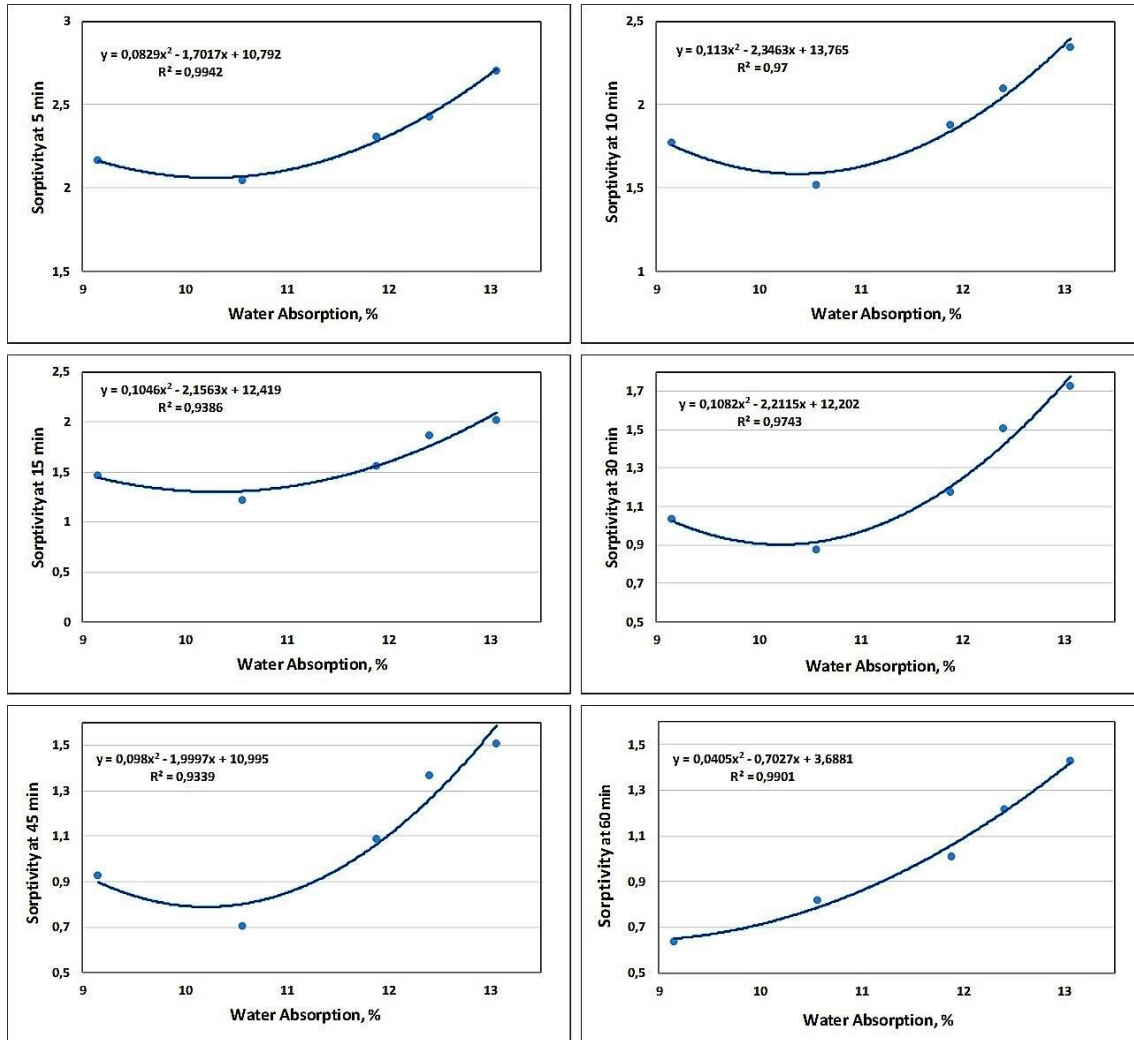


Figure 10. The relationship between water absorption by mass and sorptivity for all period

## References

Al-Goody, Asraa., Güneyisi, Erhan., Gesoğlu, Mehmet., İpek, Süleyman., 2015. Sorptivity index of self-compacting concretes with nano-silica and fly-ash. The 2<sup>nd</sup> International Conference of Buildings, Construction and Environmental Engineering (BCEE2-2015), 119-124.

ASTM C 1585-04: Standard Test Method for Measurement of Rate of Absorption of Water by Hydraulic- Cement Concretes. ASTM International, USA.

BASF: We create chemistry, Available at: <https://www.basf.com/tr/tr.html> [Accessed Date: 04.11.2022].

Bozkurt, N, Yazıcıoğlu, S., 2010. Strength and capillary water absorption of lightweight concrete under different curing conditions. CSIR.

Castro, Javier., Bentz, Dale., Weiss, Jason., 2011. Effect of sample conditioning on the water absorption of concrete. Cement and Concrete Composites, 33, 805-813. <https://doi.org/10.1016/j.cemconcomp.2011.05.007>.

Chong, B.W., Othman, R., Jaya, R.P., Hasan, M.R.M., Sandu, A.V., Nabialek, M., Jez, B., Pietrusiewicz, P., Kwiatkowski, D., Postawa, P., Abdullah, M.M.A.B., 2021. Design of Experiment on Concrete Mechanical Properties Prediction: A Critical Review. Materials, 14.

Güneyisi, E., Gesoğlu, M., Akoi, A.O.M., Mermerdas, K., 2014. Combined effect of steel fiber and metakaolin incorporation on mechanical properties of concrete. Composite Part B: Engineering, 56, 83-91. <https://doi.org/10.1016/j.compositesb.2013.08.002>.

Hamada, H.M., Tayeh, B.A., Al-Attar, A., Yahaya, F.M., Muthusamy, K., Humada, A.M., 2020. The present state of the use of eggshell powder in concrete: A review. Journal of Building Engineering, 32.

Hong, Shuxian., Yao, Wanqiong., Guo, Bangwen., Lin, Chen., Biqin, Dong., Li, Weiwen., Hou, Dongshuai., Xing, Feng., 2020. Water distribution characteristics in cement paste with capillary absorption. Construction and Building Materials, 240. <https://doi.org/10.1016/j.conbuildmat.2019.117767>.

Karasin, H., Hadzima-Nyarko, M., Işık, E., Doğruyol, M., Karasin, I.B., Czarnek, S., 2022. The Effect of Basalt Aggregates and Mineral

- Admixtures on the Mechanical Properties of Concrete Exposed to Sulphate Attacks. *Materials*, 15(4), 1581. <https://doi.org/10.3390/ma15041581>.
- Kurtoğlu, A.E., Hussein, A.K., Gülşan, M.E., Altan, M.F., Çevik, A., 2018. Mechanical Investigation and Durability of HDPE-confined SCC columns Exposed to Severe Environment. *KSCE Journal of Civil Engineering*, 22(12) 5046-505.
- Liu, Jun., Liu, Jiaying., Fan, Xu., Jin, Hesong., Zhu, Jhua., Huang, Zhenyu., Xing, Feng., Sui, Tongbu., 2022. Investigation on water sorptivity and micro properties of concrete: Effect of supplementary cementitious materials, seawater, sea-sand and water-binder ratio. *Journal of Building Engineering*, <https://doi.org/10.1016/j.jobe.2022.104153>.
- Lu, Jiang., Wang, Ke., Qu, Ming-Liang., 2020. Experimental determination on the capillary water absorption coefficient of porous building materials: A comparison between the intermittent and continuous absorption tests. *Journal of Building Engineering*, 28. <https://doi.org/10.1016/j.jobe.2019.101091>.
- Mermerdaş, K., İpek, S., Anwer, A. M., Ekmen, Ş., Özen, M., 2021. Durability performance of fibrous high-performance cementitious composites under sulfuric acid attack. 21(147). <https://doi.org/10.1007/s43452-021-00298-0>.
- Oyedutun, T.D.T., 2018. X-ray fluorescence (XRF) in the investigation of the composition of earth materials: a review and an overview. *Geology, Ecology, and Landscapes*, 2(2), 148-154.
- Ramazenian, A.A., Pilvar, A., Mahdikhani, Mahdi., Moodi, Faramarz., 2011. Practical evaluation of relationship between concrete resistivity, water penetration, rapid chloride penetration and compressive strength. *Construction and Building Materials*, 25, 2472-2479. <https://doi.org/10.1016/j.conbuildmat.2010.11.069>.
- Sümer, M., 1994. Variation of the Capillarity and Permeability of Mortars with Water-Cement Ratio. *İMO Teknik Dergi*, 743-753.
- Tanyıldızı, M., 2022. Capillarity of concrete incorporating waste ceramic powder. *Muş Alparslan University Journal of Science*, 10(1), 925-930. <https://doi.org/10.18586/msufbd.1078690>.
- Tokay, M., Erdoğan, K., 2011. "Cürufklar ve Cürufllu Çimentolar", TÇMB/AR-GE/Y97-2, Ankara.
- Tosun, Yeşim., Şahin, Remzi., 2015. Compressive Strength and Capillary Water Absorption of Concrete Containing Recycled Aggregate. *International Journal of Structural and Construction Engineering*, 9(8).
- TSE 13057, 2002. Products and systems for the protection and repair of concrete structures - Test methods -Determination of resistance of capillary absorption. Turkish Standards Institution, TSE, Ankara, Turkey.
- Türk, K., Demirhan, S., 2017. Effect of limestone powder on the rheological, mechanical and durability properties of ECC. *European Journal of Environmental and Civil Engineering*. 21(9), 1151-1170. <https://doi.org/10.1080/19648189.2016.1150902>.
- Umar, T., Tahir, A., Egbu, Charles., Honnurvali, M.S., Saidani, M., Al-Bayati, A.J., 2021. Developing a sustainable concrete using ceramic waste powder. In *Collaboration and Integration in Construction, Engineering, Management and Technology*, 157-162.
- Yurt Çimento, Available at: <https://yurtcimento.csglobal.com.tr/> [Accessed Date: 02.11.2021]
- Yücel, H.E., Öz, H.Ö., Güneş, M., 2020. The Effects of Acidic and Basic Pumice on Physico-Mechanical and Durability Properties of Self-Compacting Concretes. *Green Building & Construction Economics*, 1(1), 21-36. DOI: <https://doi.org/10.37256/gbce.112020591>.



Available online at [www.dergipark.gov.tr/beuscitech](http://www.dergipark.gov.tr/beuscitech)

Journal of Science and Technology

E-ISSN 2146-7706



# Risk Assessment of Rockfall using GIS-Based Analytical Hierarchy Process: A Case Study of Bitlis Province

M. Cihan AYDIN <sup>a,\*</sup> , Elif Sevgi BIRINCIOĞLU <sup>b</sup> , Aydın BÜYÜKSARAÇ <sup>c</sup> 

<sup>a,b</sup> Bitlis Eren University, Department of Civil Engineering, TR-13000, Bitlis Turkey

<sup>c</sup> Çanakkale Onsekiz Mart University, Çanakkale Turkey

## ARTICLE INFO

### Article history:

Received 15 March 2022

Received in revised form 22 March 2022

Accepted 16 May 2022

### Keywords:

Rockfall

Analytical Hierarchy Method

Geographic Information Systems

Risk Assessment

Bitlis Province

## ABSTRACT

Rockfall is one of the important natural disasters that can result in death, although it does not occur very often. Bitlis province in Turkey is frequently exposed to serious rockfall events due to its rugged-mountainous structure and harsh climatic conditions. Rockfall risk rely on many hazard factors such as slope, lithology, soil, elevation, precipitation, vulnerability factors i.e., land use and population. The Analytical Hierarchy process (AHP) is a highly skilled approach for risk assessment studies involving multiple decision-making criteria. In this study, the rockfall risk assessment of the province of Bitlis, which was chosen as the study area, was performed using AHP, and discussed. Geographic Information System (GIS) were used to visualize the results maps. The study concluded that the rockfall risks were mostly concentrated in the mountainous and rugged southwest and partially southeast areas, including the city and district centers. Except for the foothills of the volcanic mountains, the northern parts of the study area were generally considered as risk-free. The risk zones obtained from the study are relatively consistent with the results of a previous limited study.

© 2020. Turkish Journal Park Academic. All rights reserved.

## 1. Introduction

Rockfall is an important natural disaster that occurs in sensitive and steep rocky areas on earth and can result in death. While the rockfall mechanism is generally studied with theoretical deterministic approaches, the risk assessment is performed with spatial and statistical methods. One of the most effective methods of multi-parameter decision-making processes is Analytical Hierarchy Process (AHP). Combining AHP with GIS techniques capable of spatial analysis offers a powerful hybrid approach to risk assessment. Some remarkable studies in the literature on rockfalls are summarized as follows.

In the literature many different methods were used for assessments of the landslide and rockfall hazard. Deparis et al.

(2007) performed a case study to assess the rock fall using ground radar measurements, because the stability of a potentially unstable rock mass is highly sensitive to the continuity of the joints cutting it. Guzzetti et al. (2002) developed a three-dimensional simulation program that generates simple maps useful to assess rockfall hazard, using GIS technology to manipulate existing thematic information available in digital format. The raster maps obtained from the program have some features such as the number of rockfall trajectories calculated in each grid cell, maximum velocity and maximum height. Marzorati et al. (2002) presented a statistical approach to analyze landslides and rockfalls induced by the 1997 earthquake in the Umbria and Marche region of Italy. All the data collected in the study were digitized and located with the aid of Geographic Information System. After that they performed a multiple regression analysis to determine the

\*Corresponding author. Tel.: +90 434 222 00 00

E-mail address: [mcaydin@gmail.com](mailto:mcaydin@gmail.com)

ORCID: 0000-0002-5477-1033 (M.C. Aydın), 0000-0002-4317-9392 (E.S. Birincioglu), 0000-0002-4279-4158 (A. Büyüksaraç)

relationships between seismic factors and rock fall data. Ali et al. (2021) focused on the Besham-Chilas region of Pakistan, where rockfalls and debris flow frequently triggered by heavy rains. They used remote sensing-based techniques to identify potential hazardous sites and rated potential rockfall by using modified Pierson's rockfall hazard rating system (RHRS). One of the areas at risk of rockfalls is busy highways. Steep cutting slopes in natural ground created during road construction are the main cause of rockfall hazard. In the lawsuit filed over the fatal rockfall incident on the British Columbia highway in 1982, the Supreme Court of Canada decided that the authorities could easily foresee the risks that may occur and the accident could be prevented. This event demonstrated the importance of risk assessment on highways (Bunce et al. 1997). In another study, Budetta et al. (2016) applied a quantitative risk analysis to a busy road in southern Italy using the rockfall risk management method. Giani et al. (2004) proposed a methodology for the evaluation of the features of the motion of blocks detaching from a steep rock wall and traveling down the slope below, using real scale rockfall tests with two slopes having different morphology and lithology. The effect of the evaluated parameters on the prediction of the rockfall trajectory was investigated using dimensional numerical models. Katz et al. (2011) assessed the rockfall hazard along a rail corridor in Israel, using an inventory of historical information on past rockfall events, field surveys supported by interpretation of aerial photographs, and digital rockfall modeling. Li and Lan (2015) presented a short review on the probabilistic approaches widely used for modeling of rockfall trajectories. Based on a probabilistic approach, Canal and Akin (2016) investigated slope stability of high and steep sedimentary rock cut slope along highway in Adicevaz-Bitlis (Turkey) where possible rockfall events occur. Avtia (2016) carried out a rockfall assessment using the GIS-based AHP, taking into account some physical characteristics of the rock criteria. The author integrated the GIS hazard maps and AHP to categorize the rockfall risk. Shirzadi et al. (2017) analyzed the rockfall susceptibility of a region in Iran using three different methods together with the AHP. Some criteria affecting on the rock falls including slope angle, aspect, curvature, elevation, distance to road, distance to fault, lithology and land use were considered in their study.

The literature review presents many reasons and approaches to investigate the rockfall hazard assessment. Many criteria are considered to be sensitive to rockfall hazard in multivariate decision-making processes such as earthquake, precipitation, slope, lithology, land use. In this study, rockfall risk assessment was carried out within the borders of Bitlis province in Turkey using GIS-based AHP.

## 2. Study Area

The concept of landslide is defined as the downward movement of rock, rubble and soil materials or their mixtures with the effect of gravity (AFAD, 2020). Considering the landslide/rockfall data in Turkey, it is seen that most of them are rockfalls, slides and flows. Black Sea, Eastern Anatolia and Central Anatolia regions are the areas where landslides are frequently seen in Turkey due to the mountainous/rough and eroded surface of the earth. Bitlis province, which has a rugged and mountainous structure, is located in the Eastern Anatolia Region of Turkey. As seen on the map in Fig. 1, 412 landslide/rockfall events were reported in the study area (Bitlis) between 1950 and 2019. This rate is above the national average. Approximately 90% of the study area is mountainous, while the remaining 10% consists of plateaus and plains. The height of the important mountain, known as Nemrut Mountain, which is also a volcano in Bitlis, exceeds 3,000 m. There were 2956 rockfall events in Turkey in 2008, corresponding to 10% of the disasters that occurred in the country. Rockfalls account for 7% of the total number of people affected by disasters (Gökçe et al. 2008). Bitlis is one of the riskiest provinces in Turkey in terms of rockfalls. There were 67 rockfall events in Bitlis province between 1965 and 2010 (Ekinçi et al. 2020). Bitlis province is exposed to significant rockfall events due to its unfavorable geological and morphological features. The mountainous and steeply sloping nature of the study area increases the hazard and risk of rockfall. In addition, especially in mountainous areas such as the Bitlis-Diyarbakır highway along the Bitlis stream, the cut slopes for highways are another important cause of rockfall events. Another important factor in rockfall is seismic movements. According to Isik et al. (2012), the study area is in an active seismic region and earthquake risks for this region continue. Excessive precipitation and freeze-thaw events in the cold winter months are also factors that trigger rockfalls. The region is an area with microclimatic features that receives the most snowfall in Turkey (Aydin et al. 2015).

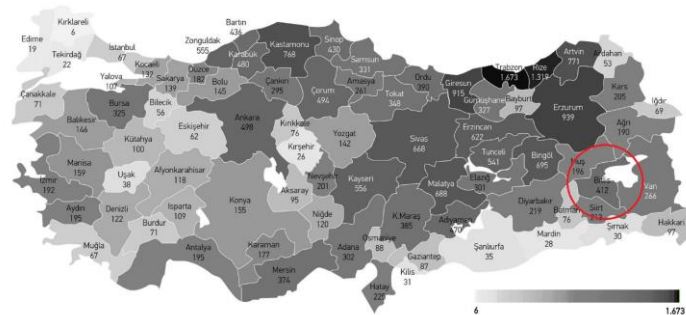


Fig. 1. Location of study area and rockfall/landslide events in Turkey between 1950 and 2019 (AFAD, 2019)

### 3. Results and Discussion

#### 3.1. Rockfall Risk Assessment

The Analytical Hierarchy Process (AHP) used in this study is the most widely used and tested method among the Multi-Criteria Decision-Making Methods (MCDM). Saaty (1980), inspired by Myers and Alpert (1968), developed this method. AHP is a flexible mathematical model that considers the priorities of events and evaluates both quantitative and qualitative criteria in decision-making problems (Dağdeviren et al. 2004). The method consists of decision stages where values are assigned and alternative values are determined according to the criteria chosen to manage the decision-making process. As the first step in AHP, hierarchical structure and comparison matrix are described. After that, the comparison matrix is converted into a priorities vector and the compliance rate is determined based on the random index values (Can, 2019). In Fig. 2, Wang et al. (2008) shows the schema of the three-level hierarchical structure for a MCDM problem. In this schema, while the top level represents the decision goal, the lower level the criteria, and the lower levels, if any, represent the lower alternatives. The lowest level contains decision options. For the consistency of pairwise comparison, the number of criteria and each criterion should be defined correctly. AHP can be used with many criteria according to their common characteristics. Once the hierarchical structure is established, the importance levels of the criteria are determined mutually. In the pairwise comparison between the criteria, the importance intensity of the criteria is scored between 1 and 9 in consultation with the decision makers, as in Table 1 (Wang et al. 2008).

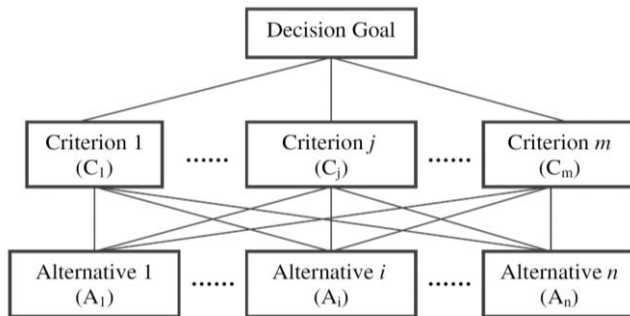


Fig. 2. Schema of three-level hierarchical structure for a MCDM problem (Wang et al. 2008)

Table 1. Importance intensities for pairwise comparison in AHP (Wang et al. 2008; Saaty, 1990)

Importance intensity (Scores)	Definition
1	Equal importance
3	Moderate importance of one over another
5	Strong importance of one over another
7	Very strong importance of one over another
9	Extreme importance of one over another
2, 4, 6, 8	Intermediate values
Reciprocals	Reciprocals for inverse comparison

The normalized matrix is obtained by dividing each element of the comparison matrix by the sum of the columns. The average of each row of the normalized matrix yields the weight vector. The product of the comparison matrix and the weight vector gives the following priorities matrix.

$$[AW_i] = [A][W_i] \quad (1)$$

The maximum eigenvalue ( $\lambda_{max}$ ) is obtained by the following equation:

$$\lambda_{max} = \frac{1}{n} \sum_{i=1}^n \frac{AW_i}{W_i} \quad (2)$$

where, n is criteria number, A is the pairwise comparison matrix, W is the weight vector. This method for determining the weight vector is called the principal right eigenvector method (EM) (Saaty, 1980). It is recommended that the pairwise comparison matrix A have an acceptable consistency that can be checked by the following consistency ratio (CR) (Wang et al. 2008):

$$CI = \frac{(\lambda_{max} - n)}{(n - 1)} \quad (3)$$

$$CR = \frac{CI}{RI} \quad (4)$$

In which, the CI is the consistency index, RI is the random inconsistency index taken from Table 2.

Table 2. RI values according to numbers of criteria (n = 1 - 10) (Saaty, 1990)

n	1	2	3	4	5	6	7	8	9	10
R	0.0	0.0	0.5	0.9	1.1	1.2	1.3	1.4	1.4	1.4
I	0	0	8	0	2	4	2	1	5	9

For  $CR < 0.10$ , the comparison matrix has acceptable consistency; otherwise, the decision-making process is repeated until consistency is achieved.  $CR = 0.00$  means the best value for consistency (Saaty, 1990; Subramanian and Ramanathan, 2012).

Based on the expert's opinion according to the scaling in Table 1, the pairwise comparison matrix in Table 3 was obtained. After obtaining the normalization matrix in Table 4 by dividing the scores in Table 3 by the sum of the related column, the weights vector of the criteria were determined by taking the average of the rows. The parameters of AHP were calculated as  $\lambda_{max} = 9.702$ ,  $RI = 1.45$  from Table 2,  $CI = 0.088$  and  $CR = 0.06$ . The consistency ratio  $CR = 6\% < 10\%$  which indicates consistency of the comparison matrix. As a result, the weights were determined as 29% slope, 22% lithology, 16% the soil, %10 precipitation, 5% distance to stream, 6% elevation, 7% aspect, 3% land use and 2% population.

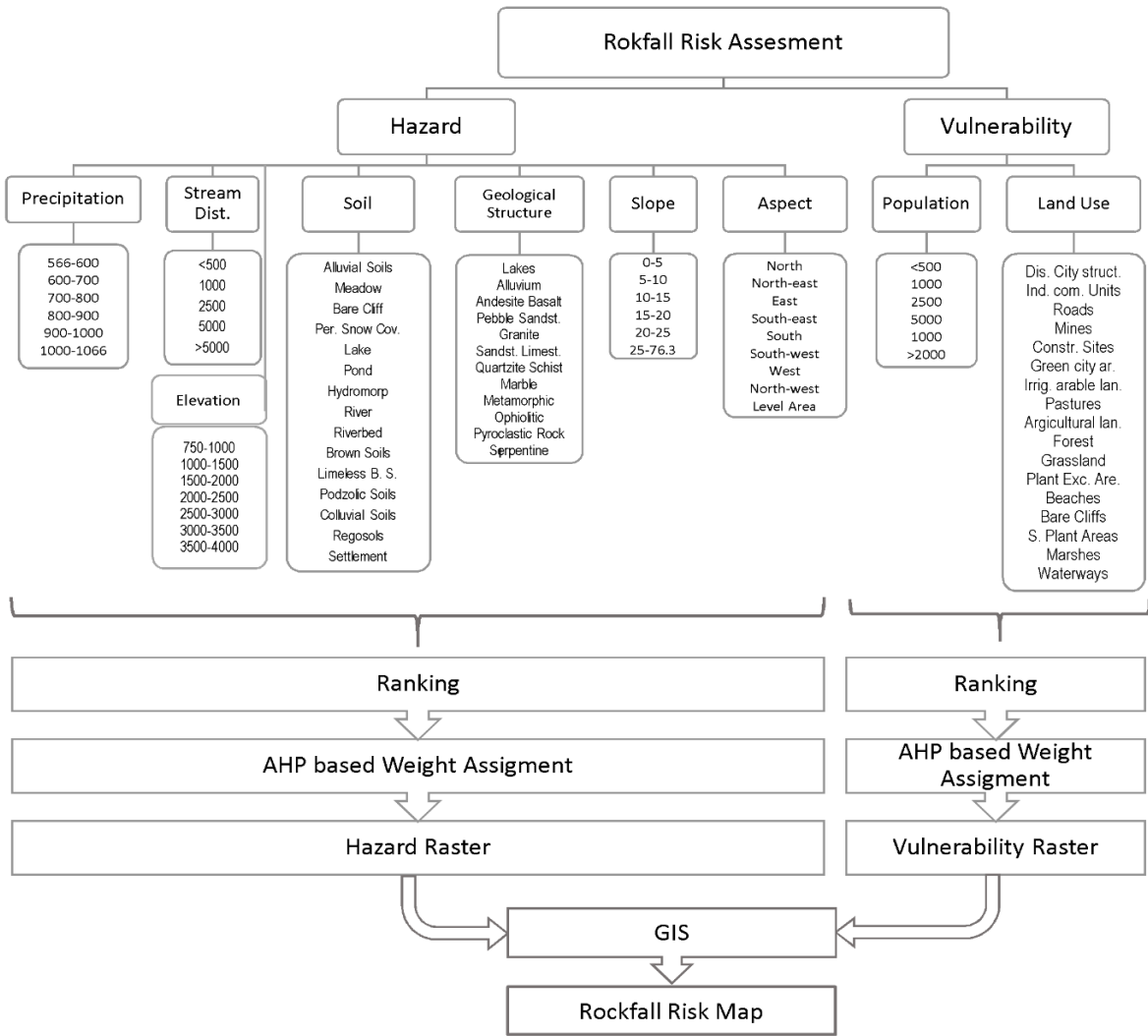


Fig. 3. Flow-chart of the GIS-based AHP for rockfall risk assessment

Table 3. The pairwise comparison matrix for flood risk of the region

Matrix A	Slope	Lithology	Soil	Precipitation	Dist. to stream	Elevation	Aspect	Land use	Population
Slope	1	2	3	3	4	5	7	7	9
Lithology	1/2	1	3	3	4	5	3	7	9
Soil	1/3	1/3	1	4	5	3	3	4	8
Precipitation	1/3	1/3	1/4	1	5	2	2	3	5
Distance to stream	1/4	1/4	1/5	1/5	1	1/2	1/3	2	5
Elevation	1/5	1/5	1/3	1/2	2	1	1/2	3	3
Aspect	1/7	1/3	1/3	1/2	3	2	1	3	2
Land use	1/7	1/7	1/4	1/3	1/2	1/3	1/3	1	2
Population	1/9	1/9	1/8	1/5	1/5	1/3	1/2	1/2	1
TOTAL	3.01	4.70	8.49	12.73	24.70	19.17	17.67	30.50	44.00

**Table 4.** Determination of weight vector from the normalization matrix

Matrix A	Slope	Lith.	Soil	Precip.	Distance to stream	Elevation	Aspect	Land use	Popul.	Wi
Slope	0.332	0.425	0.353	0.236	0.162	0.261	0.396	0.230	0.205	<b>0.289</b>
Lithology	0.166	0.213	0.353	0.236	0.162	0.261	0.170	0.230	0.205	<b>0.222</b>
Soil	0.111	0.071	0.118	0.314	0.202	0.157	0.170	0.131	0.182	<b>0.162</b>
Precipitation	0.111	0.071	0.029	0.079	0.202	0.104	0.113	0.098	0.114	<b>0.102</b>
Distance to stream	0.083	0.053	0.024	0.016	0.040	0.026	0.019	0.066	0.114	<b>0.049</b>
Elevation	0.066	0.043	0.039	0.039	0.081	0.052	0.028	0.098	0.068	<b>0.057</b>
Aspect	0.047	0.071	0.039	0.039	0.121	0.104	0.057	0.098	0.045	<b>0.069</b>
Land use	0.047	0.030	0.029	0.026	0.020	0.017	0.019	0.033	0.045	<b>0.030</b>
Population	0.037	0.024	0.015	0.016	0.008	0.017	0.028	0.016	0.023	<b>0.020</b>

### 3.2. Spatial Analysis

Using the obtained scoring and weights, raster maps of each criterion were obtained with the ArcGIS program as in Fig. 4. The projection system of all criteria was transformed into a common projection system through ArcToolbox - Projections and Transformations - Raster Project. After, the raster data was reclassified by means of ArcToolbox -3D Analyst Tools - Raster - Reclass, the data was converted into vector data via Conversion Tools - From Raster - Raster to Polygon. Then, vector data was integrated with Data Management Tools - Generalization - Dissolve. Scoring inputs was defined in the attribute table of each criterion through Data Management Tools- Fields - Add Field tool.

In Fig. 4, scoring maps of nine criterion in Fig. 3 are given by taking the expert opinions or decision makers. In the lithology map in Fig. 3, the geological structures sensitive to the rockfall were scored low, while loose structures sensitive to rockfall such as alluvial, conglomerate, sandstone, serpentine were scored high. On the slope map, higher slopes are more susceptible to rockfall and lower slopes are scored low. In the elevation map, considering that rockfall will not pose a hazard in high elevation sections and rocks falling from high areas will pose a hazard at lower elevations; high areas were scored low, and low-elevation sections were scored high. Since the effect of slope versus elevation is dominant in the pairwise comparison matrix, the risk of rockfall is reduced on low plains. The sections exposed to more freeze-thaw events in the aspect map were considered more sensitive to rockfall events than the south facades. On the soil map, loose soil structures that can be susceptible to rockfalls, especially in rough terrain, were highly scored on the map. Since the steep slopes close to the rivers are always risky areas in terms of rockfalls due to the erosion effect of the river, the regions close to the stream are rated with high scores on the distance to stream map. Areas with high precipitation were selected as more dangerous in terms of rockfall due to the erosive and freeze-thaw effect of precipitation, as seen precipitation map. Also, land use and

population maps were scored according to their vulnerability to rockfall.

Based on the raster maps in Fig. 4 and the criteria of weights obtained from the AHP, the final map for the rockfall presented in Fig. 5 was obtained using the GIS technique. According to this map, especially the steep slopes of the rugged southwest regions are high risk for rockfall. The effect of steeply sloping river valleys in the region is clearly seen in the risk assessment. It can be said that another reason for the high risk in these areas is the concentration of precipitation in these areas. In addition, the southeast region is partially under the influence of medium-high risk. Except for the foothills of Mount Nemrut and Suphan, the northern parts of the study area are generally considered as risk-free. Göksu and Leventeli (2008) also investigated potential rockfall hazard of the Bitlis province using remote sensing. For this, first digital elevation model of the area was created by using GIS, then potential rockfall risks was mapped considering only the slope and digital elevation model (DEM) as in Fig. 6. The high-risk regions in Figs. 5 and 6 match each other; however, the risk map in this study (Fig. 5) provides much more detail thanks to AHP with multiple decision criteria.

In the southern part of Bitlis, which is located on the thrust zone, the rocks lose their primitive position and contain many discontinuities as seen in Fig. 7. The rockfalls hazard is high due to the cracks especially in formations dominated by limestones with a large amount of discontinuity at high slopes and by the deformation and disintegration of the schist, calcite and volcano-sedimentary rocks below. In addition, filled discontinuities in ophiolite and serpentinite masses in this region can trigger rockfalls (Göksu and Leventeli, 2008). Filling of the discontinuities and cracks in rock masses with precipitation waters and freeze-thaw events are other important factors inducing rockfalls. Dissolution of basalt columns and prismatic ignimbrites that form steep slopes in the study area also poses significant risks in terms of rockfalls (see right photos in Fig. 7a-d).



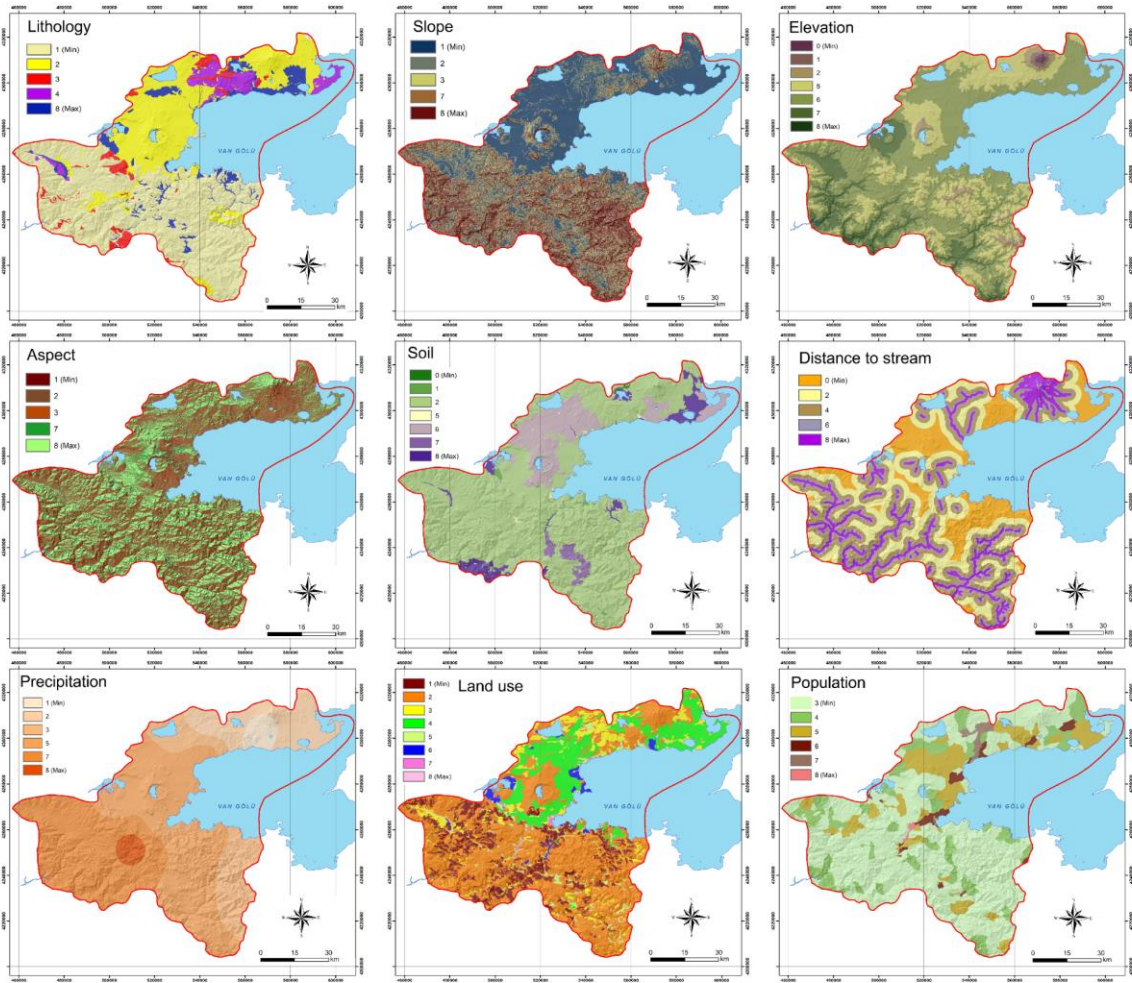


Fig. 4. Raster maps of the criteria

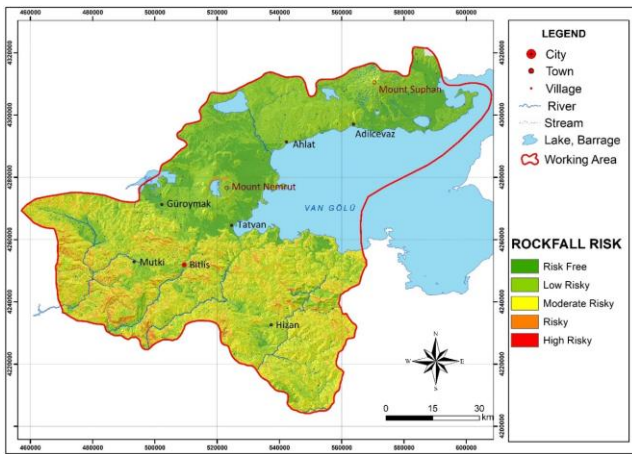


Fig. 5. Rockfall risk map of the study area in this study based on AHP

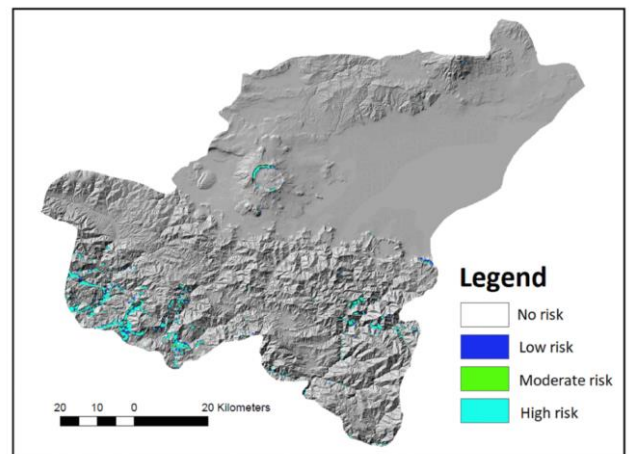


Fig. 6. Rockfall sensitivity map based on slopes and DEM (Goksu, 2017)



**Fig. 7.** Some photos of different lithological structures at risk of rockfall in the study area (a) and (b) cracked and decomposed ignimbrites, (c) Basalt columns, (d) prismatic ignimbrites

#### 4. Conclusions

As a result of the rockfall risk assessment of the province of Bitlis; it was observed that the risk is high in areas with steep slopes, lithologically affected by meteorological events such as precipitation and freeze-thaw, where land use is intense or sparse and with loose soil characteristics, with high population density and with heavy precipitation is high. Rockfall risks were mostly concentrated in the mountainous and rugged southwest and partially southeast areas, including the city and district centers such as Bitlis center, Mutki and Hizan. Except for the foothills of Nemrut and Suphan mounts, the northern parts of the study area were generally considered as risk-free. The risk zones obtained from the study are relatively consistent with a limited study done before. In general, regions with mountainous steep slopes and discontinuous rock structures were considered as areas susceptible to high rockfalls. Heavy precipitation, river valleys with steep slopes are other important factors affecting rockfall. In this study, it has also been shown that GIS-based AHP is a very successful approach in risk assessments involving multiple decision variables such as rockfalls problems. The results of this study showed that a more consistent risk definition could be made with a holistic and multi-parameter assessment in a large settlement.

#### Acknowledgement

This study has been derived from a part of E. Sevgi Birincioglu's (2021) master thesis.

#### References

- AFAD, 2019. Overview of 2019 and natural event statistics within the scope of disaster management, T.R. Ministry of Interior, Disaster and Emergency Management Presidency, [www.afad.gov.tr](http://www.afad.gov.tr). Access Date: 26.01.2022.
- Ali, S., Haider, R., Abbas, W., Basharat, M., and Reicherter, K., 2021. Empirical assessment of rockfall and debris flow risk along the Karakoram Highway, Pakistan. *Natural Hazards*, 106: 2437-2460 <https://doi.org/10.1007/s11069-021-04549-4>
- Avutia, D.J., 2016. Rock fall risk with analytical hierarchy process. *Proceedings of the First Southern African Geotechnical Conference*. 5-6 May 2016, Sun City, Southern Africa, S.W. Jacobsz (Ed.). Taylor & Francis Group, London. 87-92.
- Aydin, M.C., and Isik, E., 2015. Evaluation of Ground Snow Loads in the Micro-climate Regions. *Russian Meteorology and Hydrology*. 40(11): 741-748.
- Budetta, P., De Luca, C., and Nappi, M., 2016. Quantitative rockfall risk assessment for an important road by means of the rockfall risk management (RO.MA.) method. *Bull Eng Geol Environ* (2016) 75:1377-1397. DOI 10.1007/s10064-015-0798-6



- Bunce, C.M., Cruden, D.M., and Morgenstern, N.R., 1997. Assessment of the hazard from rock fall on a Highway. *Can. Geotech. J.* 34: 344-356.
- Can, G., 2019. Using geographical information systems and analytical hierarchy method for site selection for wind turbine plants: The case of Çanakkale province, Master Thesis, Graduate School of Natural and Applied Science, Çanakkale Onsekiz Mart University, Turkey.
- Canal, A., and Akin, M., 2016. Assessment of rock slope stability by probabilistic-based slope stability probability classification method along highway cut slopes in Adilcevaz-Bitlis (Turkey). *J. Mt. Sci.* 12(11): 1893-1909. DOI: 10.1007/s11629-016-3954-y
- Climate-Data, 2021. <https://tr.climate-data.org/Access> date: 16.12.2021.
- Copernicus, 2021. Data of land use from Copernicus land Monitoring Service. <https://land.copernicus.eu/Access> date: 16.12.2021.
- Dagdeviren, M., Akay, D., and Kurt, M., 2004. Analytical Hierarchy Process for Job Evaluation and Application. *J. Fac. Eng. Arch. Gazi Univ.* 19(2): 131-138.
- Deparis, J., Garambois, S., and Hantz, D., 2007. On the potential of Ground Penetrating Radar to help rock fall hazard assessment: A case study of a limestone slab, Gorges de la Bourne (French Alps) *Engineering Geology* 94 89-102.
- Ekinci, R., Büyüksaraç, A., Ekinci, Y.L., and Isik, E., 2020. Bitlis İlinin Doğal Afet Çesitliliğinin Değerlendirilmesi. *Journal of Natural Hazards and Environment*, 6(1): 1-11.
- Ekmekcioglu, O., Koc, K., and Özger, M., 2021. District based flood risk assessment in Istanbul using fuzzy analytical hierarchy process. *Stochastic Environmental Research and Risk Assessment* (2021) 35:617-637. <https://doi.org/10.1007/s00477-020-01924-8>
- Geofabrik, 2021. Maps and Data, <https://www.geofabrik.de/data/> Access date: 16.12.2021.
- Giani, G.P., Giacomini, A., Migliazza, M., and Segalini, A., 2004 Experimental and Theoretical Studies to Improve Rock Fall Analysis and Protection Work Design, *Rock Mech. Rock Eng.* 37 (5): 369-389. DOI 10.1007/s00603-004-0027-2
- Gökçe, O., Özden, Ş., and Demir, A., 2008. Spatial and statistical distribution of disasters in Turkey, disaster information inventory (in Turkish). Ministry of Public Works and Settlement General Directorate of Disaster Affairs. Ankara, Turkey.
- Goksu, A.E., 2017. Rock Fall Sensitivity Analysis Report, T.R. Bitlis Governorship Provincial Disaster and Emergency Directorate. Bitlis Turkey.
- Goksu, A.E., and Leventeli, Y., 2018. GIS-Based assessment of the rockfall hazard zones for Bitlis Province, 9th International Symposium on Eastern Mediterranean Geology, 07-11th May 2018, Antalya, Turkey
- Guzzetti, F., Crosta, G., Detti, R., and Agliardi, F., 2002. STONE: a computer program for the three-dimensional simulation of rock-falls. *Computers & Geosciences* 28: 1079-1093.
- Hajkowicz, S., and Collins, K., 2007. A review of multiple criteria analysis for water resource planning and management. *Water Resour Manag* 21:1553-1566. <https://doi.org/10.1007/s11269-006-9112-5>
- HGM, 2021. Republic of Türkiye Ministry of National Defense General Directorate of Mapping. Turkish administrative borders data. <https://www.harita.gov.tr/> Access date: 16.12.2021.
- Isik, E., Aydin, M.C., Bakis, A., Ozluk, M.H., 2012. The Faults near Bitlis and Seismicity of the Region (in Turkish). *BEU Journal of Science* 1(2):153-169.
- Katz, O., Reichenbach, P., and Guzzetti, F., 2011. Rock fall hazard along the railway corridor to Jerusalem, Israel, in the Soreq and Refaim valleys. *Nat Hazards*, 56:649-665. DOI 10.1007/s11069-010-9580-z
- Li, L., and Lan, H., 2015. Probabilistic modeling of rockfall trajectories: a review. *Bull Eng Geol Environ*, 74:1163-1176. DOI 10.1007/s10064-015-0718-9
- Marzorati, S., Luzi, L., and De Amicis, M., 2002. Rock falls induced by earthquakes: a statistical approach. *Soil Dynamics and Earthquake Engineering* 22: 565-577.
- MGM, 2021. Precipitation Data, Climate-Data, Turkish State Meteorological Service, <https://www.mgm.gov.tr/>, Access date 16.12.2021.
- MTA, 2021. Data of geological structure from GeoScience Mab Viewer and Drawing Editor, General Directorate of Mineral Research and Expolaration of Türkiye, <http://yerbilimleri.mta.gov.tr/anasayfa.aspx>, Access date: 16.12.2021.
- Myers, J.H., and Alpert, M.I., 1968. Determinant Buying Attitudes: Meaning and Measurement. *Journal of Marketing*, 32(4): 13-20.
- Saaty, T. L. 1980. The analytic hierarchy process. New York: McGraw-Hill, New York, pp 20-25.
- Saaty, T. L. 1990. How to make a decision: The analytic hierarchy process. *European Journal of Operational Research*, 48(1): 9-26.
- Sevgi Birincioglu, E., 2021. Disaster risk analysis of Bitlis province using geographical information systems and analytical hierarchy method. Master Thesis, Bitlis Eren University Graduate Education Institute, Department of Emergency and Disaster Management, Türkiye.
- Shirzadi, A., Chapi, K., Shahabi, H., Solaimani, K., Kavian, A., and Bin Ahmad, B., 2017. Rock fall susceptibility assessment along a mountainous road: an evaluation of bivariate statistic, analytical hierarchy process and frequency ratio. *Environ Earth Sci* 76(152): 1-17. DOI 10.1007/s12665-017-6471-6
- Subramanian, N., and Ramanathan, R., 2012. A review of applications of Analytic Hierarchy Process in operations management. *Int. J Production Economics*. 138: 215-241.
- TAD, 2021. Agricultural Land Evaluation Portal (TAD Portal), Republic of Turkey Ministry of Agriculture and Forestry General Directorate of Agricultural Reform. <https://www.tarimorman.gov.tr/> Access date: 16.12.2021.
- TUIK, 2021. Population data from Data Portal for Statistical, Turkish Statistical Institute, <https://data.tuik.gov.tr/> Access date: 16.12.2021.
- USGS, 2021. EarthData and Digital Elevation Model (DEM) for Bitlis province, United States Geological Survey (USGS). <https://www.usgs.gov/> Access date: 16.12.2021.
- Wang, Y., Liu, J., and Elhag, T., 2008. An Integrated AHP-DEA Methodology for Bridge Risk Assessment, *Computers & Industrial Engineering*, 54(3): 513-525.

Available online at [www.dergipark.gov.tr/beuscitech](http://www.dergipark.gov.tr/beuscitech)

Journal of Science and Technology

E-ISSN 2146-7706



## New Soliton Solutions Arising in Some NLEEs

Ugur BAYRAKCI <sup>a,\*</sup> , Seyma TULUCE DEMIRAY <sup>a</sup> , Vehpi YILDIRIM <sup>b</sup> 

<sup>a</sup> Osmaniye Korkut Ata University, Department of Mathematics, TR-80000, Osmaniye, Türkiye

<sup>b</sup> Erzurum Technical University, Department of Mathematics, TR-25000, Erzurum, Türkiye

### ARTICLE INFO

#### Article history:

Received 11 May 2022

Received in revised form 25 June 2022

Accepted 27 June 2022

#### Keywords:

Generalized Kudryashov method

(2+1)-dimensional dissipative long wave system

(2+1)-dimensional Date-Jimbo-Kashiwara-

Miwa equation

Soliton solutions

### ABSTRACT

We have worked on (2+1)-dimensional dissipative long wave system (DLWS) and (2+1)-dimensional Date-Jimbo-Kashiwara-Miwa (DJKM) equation. We have applied GKM, which has been obtained by generalizing the Kudryashov method, to the (2+1)-dimensional DLWS and (2+1)-dimensional DJKM equation. Thus, we have got some new soliton solutions of handled system and equation. We have plotted 2D and 3D surfaces of these acquired results by using Wolfram Mathematica 12. Then, we have shown the validity of the acquired solutions.

© 2020. Turkish Journal Park Academic. All rights reserved.

## 1. Introduction

Nonlinear evolution equations (NLEEs) have very significant applications in areas such as mathematical physics, biology, economy, mathematical chemistry, hydrodynamics, fluid dynamics, geochemistry, control theory, meteorology, optics, mechanics, chemical kinematics, biophysics, biogenetics, and so on. Particularly nonlinear partial differential equations, researching chemical reactions occurring in various scientific environments, changes in living populations, heat dissipation on metals, determination of charge and current in electrical circuits, plate and wire vibrations; It is widely used in the study and interpretation of important physical phenomena such as sea, lake, stream and tidal waves, decay of a radioactive object. Various studies are carried out by many scientists to find the solutions of equations, which have such extremely important and widespread areas of use (Ali et al., 2021; Yokus et al., 2020;

Gao et al., 2020; Cinar et al., 2021; Rani et al., 2021; Manafian et al., 2020; Yaslan and Girgin, 2019; Ghanbari and Inc, 2018; Dusunceli et al., 2021; Kumar and Kaplan, 2018; Mirzazadeh et al., 2021). (2+1)-dimensional DLWS is a famous system of equations used in physical applications, nonlinear science and nonlinear wave theory (Chang et al., 2020). (2+1)-dimensional DLWS is given as (Yang and Feng, 2021):

$$\begin{aligned} u_t - u_{xx} - 2u_x v - 2uv_x &= 0, \\ v_{ty} + v_{xy} - 2u_{xx} - 2v_x v_y - 2vv_{xy} &= 0. \end{aligned} \quad (1)$$

Chang et al. used Lie symmetry analysis and dynamical system method for system (Chang et al., 2020). Yang and Feng obtained the solutions of this system by applying the variable separation method and  $\exp(-\Phi(\xi))$ -expansion method (Yang and Feng, 2021).

(2+1)-dimensional DJKM equation is given as (Yuan et al.,

\* Corresponding author. Tel.: +0 328 827 1000; fax: +0 000 000 0000

E-mail address: [ubayrakci42@gmail.com](mailto:ubayrakci42@gmail.com)

ORCID : 0000-0002-1765-2318 (U..Bayrakci), 0000-0002-8027-7290 (S..Tuluçe Demiray), 0000-0003-3837-4756 (V. Yildirim)

2017; Pu and Hu, 2019; Ismael et al., 2020):

$$u_{xxxx} + 4u_{xy}u_x + 2u_{xx}u_y + 6u_{xy}u_{xx} + u_{yyy} - 2u_{xxt} = 0, \tag{2}$$

Pu and Hu examined solitary wave solutions of the equation with the sine-Gordon expansion method (Pu and Hu, 2019). Ismael et al. applied Hirota bilinear method to the equation (Ismael et al., 2020). Yuan et al. obtained solutions of the equation with Hirota method and auxiliary variable (Yuan et al., 2017). Adem et al. performed extended transformed rational function algorithm to the equation (Adem et al., 2019). Singh and Gupta applied the Pickering’s algorithm to the equation (Singh and Gupta, 2018). Guo and Lin used the direct ansatz method for the equation (Guo and Lin, 2019).

In this study, GKM, which is one of the solution methods of NLEEs, is discussed (Tuluçe Demiray, 2020; Tuluçe Demiray and Bayrakci, 2021; Pandir and Eren, 2021; Kaplan and Akbulut, 2021; Gurefe, 2020; Islam et al. 2019). Firstly, the structure of the method is introduced. Afterwards, some soliton solutions of (2+1)-dimensional DJKM and (2+1)-dimensional DLWS were obtained by applying GKM.

## 2. Structure of GKM

We take into account a general nonlinear partial differential equation (NLPDE) for a function  $v$  of three different variables in the following form:

$$R(v, v_t, v_y, v_x, v_{xx}, \dots) = 0. \tag{3}$$

Step1: Firstly, we regard the travelling wave transform as following form;

$$v(x, y, t) = v(\eta), \quad \eta = x + y - mt. \tag{4}$$

Eq. (3) is turned into ordinary differential equation by Eq. (4):

$$L(t, y, x, v, v', v'', \dots) = 0, \tag{5}$$

where superscripts demonstrate ordinary derivatives according  $\eta$ .

Step2: Suppose that we consider the solutions of Eq. (5) as:

$$v(\eta) = \frac{\sum_{i=0}^k a_i Q^i(\eta)}{\sum_{j=0}^l b_j Q^j(\eta)} = \frac{P[Q(\eta)]}{S[Q(\eta)]}, \tag{6}$$

where  $Q$  is  $\frac{1}{1 \pm e^\eta}$ . We should point out that  $Q$  is the solution to the following equation.

$$Q_\eta = Q^2 - Q. \tag{7}$$

Step3: The solution of the nonlinear ordinary differential equation given by Eq. (5) is sought according to the GKM as follows:

$$v(\eta) = \frac{a_0 + a_1 Q + a_2 Q^2 + \dots + a_k Q^k}{b_0 + b_1 Q + b_2 Q^2 + \dots + b_l Q^l}. \tag{8}$$

If we can ascertain values of  $k$  and  $l$  in Eq. (6) through the homogeneous balance principle. Therefore we balance between the highest order derivative and highest order nonlinear term in Eq. (5).

Step4: We embed Eq. (6) into Eq. (5). Thus we get a polynomial  $R(Q)$  of  $Q$ . Thereafter equalizing all coefficients of  $R(Q)$  to zero, we find an algebraic equation system. By solving obtained system, we determine  $c$  and coefficients of  $a_0, a_1, a_2, \dots, a_k, b_0, b_1, b_2, \dots, b_l$ . Finally, we can obtain the soliton solutions of Eq. (5).

## 3. Application of GKM to the equations

Example 1:

For the find the soliton solutions of system (1) we consider the following transformation:

$$u(x, y, t) = u(\eta), v(x, y, t) = v(\eta), \eta = x + y - mt. \tag{9}$$

Putting the Eq. (9) into the system (1), we get the equation

$$u(x, y, t) = \frac{v'}{2} - \frac{mv}{2} - \frac{v^2}{2}. \text{ By performing the necessary}$$

mathematical operations, system (1) is converted to the following ordinary differential equation. Replace Eq. (9) into system (1) and we get the following equation,

$$-m^2 v - v'' + 3mv^2 + 2v^3 = 0. \tag{10}$$

By using balance principle in Eq. (9), we obtain,

$$k = l + 1, \tag{11}$$

If we give  $l = 1$  then  $k = 2$  we find,

$$u(\eta) = \frac{a_0 + a_1 Q + a_2 Q^2}{b_0 + b_1 Q}, \tag{12}$$

$$u'(\eta) = (Q^2 - Q) \times \left[ \frac{(a_1 + 2a_2 Q)(b_0 + b_1 Q) - b_1(a_0 + a_1 Q + a_2 Q^2)}{(b_0 + b_1 Q)^2} \right], \tag{13}$$

$$\begin{aligned}
 u''(\eta) &= \frac{Q^2 - Q}{(b_0 + b_1 Q)^2} (2Q - 1) \times \\
 &\left[ (a_1 + 2a_2 Q)(b_0 + b_1 Q) - b_1 (a_0 + a_1 Q + a_2 Q^2) \right] \\
 &+ \frac{(Q^2 - Q)^2}{(b_0 + b_1 Q)^3} \times \\
 &\left[ 2a_2 (b_0 + b_1 Q)^2 - 2b_1 (a_1 + 2a_2 Q)(b_0 + b_1 Q) \right. \\
 &\left. + 2b_1^2 (a_0 + a_1 Q + a_2 Q^2) \right].
 \end{aligned}
 \tag{14}$$

We obtain the soliton solutions of system (1) in the following different cases;

Case1:

$$a_0 = 0, a_1 = -b_0, a_2 = -b_1, m = 1. \tag{15}$$

Substituting the above values in Eq. (12), we acquire the dark soliton solutions of system (1).

$$\begin{aligned}
 u_1(x, y, t) &= -\frac{1}{4} \left( -1 + \tanh \left[ \frac{x + y - t}{2} \right] \right) \\
 &\times \left( m + \tanh \left[ \frac{x + y - t}{2} \right] \right),
 \end{aligned}
 \tag{16}$$

$$v_1(x, y, t) = -\frac{1}{2} \left( 1 - \tanh \left[ \frac{x + y - t}{2} \right] \right). \tag{17}$$

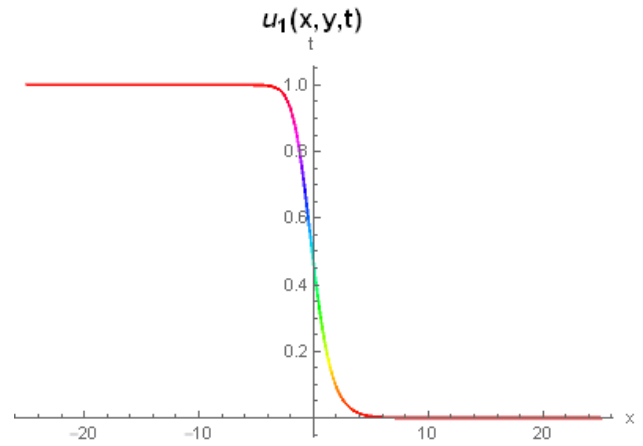
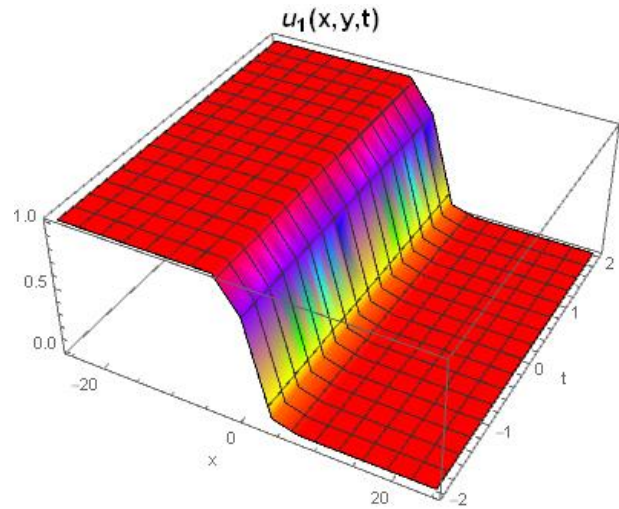


**Figure 1.** 3D of solution (16) for  $y = 2, -25 \leq x \leq 25$  values with  $-2 \leq t \leq 2$  range and 2D plot of solution for  $t = 1$  with these values.

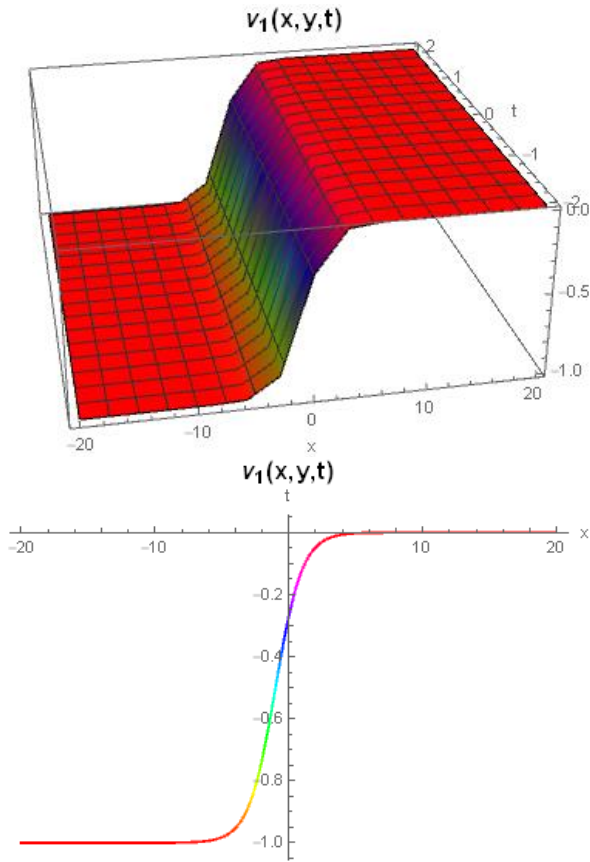


**Figure 2.** 3D of solution (17) for  $y = 2, -20 \leq x \leq 20$  values with  $-2 \leq t \leq 2$  range and 2D plot of solution for  $t = 1$  with these values.

Case2:

$$a_0 = b_1, a_1 = -2b_1, a_2 = b_1, b_0 = -\frac{b_1}{2}, m = 2. \quad (18)$$

Substituting the above values in Eq. (12), we acquire the dark-bright and dark soliton solutions of system (1).

$$u_2(x, y, t) = \frac{1}{4} (1 + \coth[x + y - 2t]) \times (4 + 4 \coth[x + y - 2t] + \operatorname{csch}[x + y - 2t]), \quad (19)$$

$$v_2(x, y, t) = -\frac{1}{2} \left( 1 + \coth \left[ \frac{x + y - 2t}{2} \right] \right)^2 \times \tanh \left[ \frac{x + y - 2t}{2} \right]. \quad (20)$$

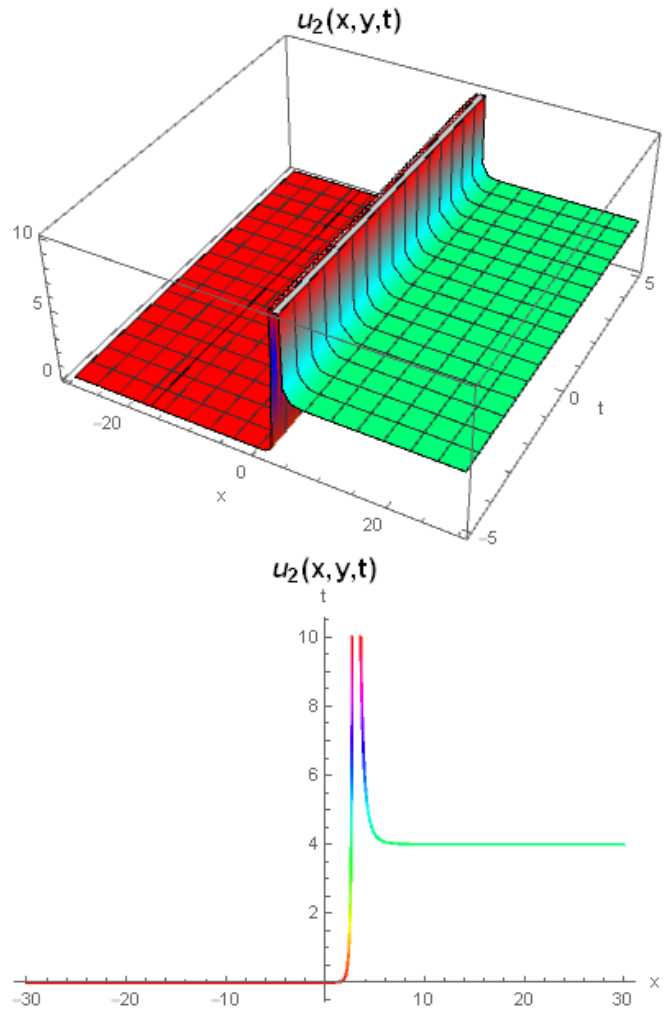


**Figure 3.** 3D of solution (19) for  $y = 2, -30 \leq x \leq 30$  values with  $-5 \leq t \leq 5$  range and 2D plot of solution for  $t = 4$  with these values.

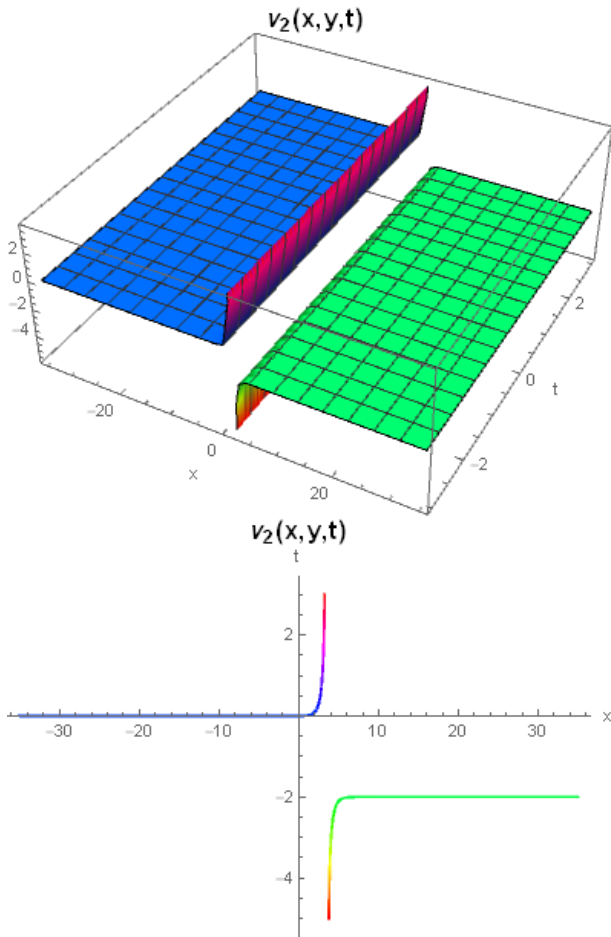


**Figure 4.** 3D of solution (20) for  $y = 0.5, -35 \leq x \leq 35$  values with  $-3 \leq t \leq 3$  range and 2D plot of solution for  $t = 2$  with these values.

Case3:

$$a_0 = \frac{ib_1}{2\sqrt{2}}, a_1 = \left(1 - \frac{i}{\sqrt{2}}\right)b_1, \tag{21}$$

$$a_2 = -b_1, b_0 = -\frac{b_1}{2}, m = i\sqrt{2}.$$

Substituting the above values in Eq. (12), we acquire the bright soliton solutions of system (1).

$$u_3(x, y, t) = \frac{-1}{4} + \frac{i}{2} \operatorname{csc}[ix + iy + \sqrt{2}t] \times \tanh\left[\frac{x + y - i\sqrt{2}t}{2}\right], \tag{22}$$

$$v_3(x, y, t) = -\frac{i}{\sqrt{2}} - i \operatorname{csc}[ix + iy + \sqrt{2}t]. \tag{23}$$

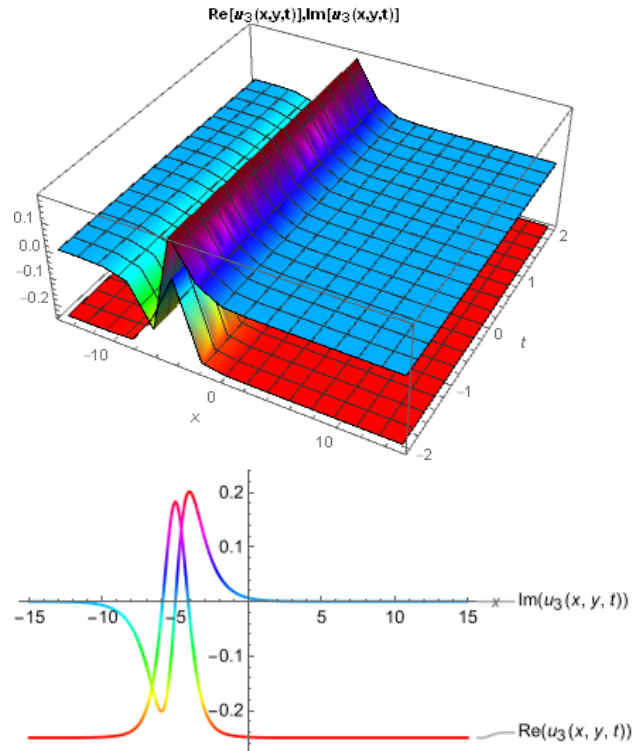


**Figure 5.** 3D of solution (22) for  $y = 5, -15 \leq x \leq 15$  values with  $-2 \leq t \leq 2$  range and 2D plot of solution for  $t = 1$  with these values.

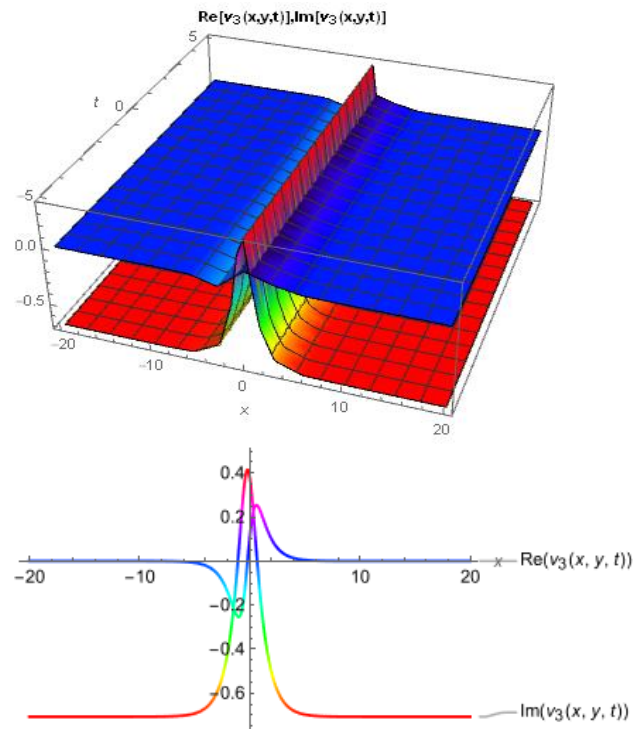


**Figure 6.** 3D of solution (23) for  $y = 0.2, -20 \leq x \leq 20$  values with  $-5 \leq t \leq 5$  range and 2D plot of solution for  $t = 3$  with these values.

Example 2:

For the find the soliton solutions of Eq. (2) we consider following equalities:

$$u(x, y, t) = u(\eta), \eta = n(x + ay - ht). \quad (24)$$

Replace Eq. (24) into Eq. (2) and we get the following equation,

$$an^2u''' + 3an(u')^2 + (a^3 + 2h)u' = 0. \quad (25)$$

By making the  $u' = g$ , transformation in Eq. (25), we find the following equation,

$$an^2g'' + 3ang'^2 + (a^3 + 2h)g = 0. \quad (26)$$

By using balance principle in Eq. (26), we obtain

$$k = l + 2. \quad (27)$$

If we give  $l = 1$  then  $k = 3$  we find the following equations,

$$u(\eta) = \frac{a_0 + a_1Q + a_2Q^2 + a_3Q^3}{b_0 + b_1Q}, \quad (28)$$

$$u'(\eta) = (Q^2 - Q) \times \left[ \frac{(a_1 + 2a_2Q + 3a_3Q^2)(b_0 + b_1Q) - b_1(a_0 + a_1Q + a_2Q^2 + a_3Q^3)}{(b_0 + b_1Q)^2} \right], \quad (29)$$

$$u''(\eta) = \frac{Q^2 - Q}{(b_0 + b_1Q)^2} (2Q - 1) \times \left[ \frac{(a_1 + 2a_2Q + 3a_3Q^2)(b_0 + b_1Q) - b_1(a_0 + a_1Q + a_2Q^2 + a_3Q^3)}{(b_0 + b_1Q)^2} \right] + \frac{(Q^2 - Q)^2}{(b_0 + b_1Q)^3} \left[ \frac{(b_0 + b_1Q)^2 (2a_2 + 6a_3Q) - 2b_1(b_0 + b_1Q)(a_1 + 2a_2Q + 3a_3Q^2) + 2b_1^2(a_0 + a_1Q + a_2Q^2 + a_3Q^3)}{(b_0 + b_1Q)^3} \right]. \quad (30)$$

We get soliton solutions of Eq. (2) in the following different cases;

Case1:

$$a_0 = -\frac{nb_0}{6}, a_1 = nb_0 - \frac{nb_1}{6}, a_2 = n(-b_0 + b_1), a_3 = -nb_1, \quad (31)$$

$$a = \frac{3^{1/3}n^2 + (-9h + \sqrt{81h^2 - 3n^6})^{2/3}}{3^{2/3}(-9h + \sqrt{81h^2 - 3n^6})^{1/3}}.$$

Substituting the above values in Eq. (28), we acquire dark soliton solution of Eq. (2).

$$u_1(x, y, t) = \frac{-n^2}{6}(x + ay - ht) + \frac{n}{2} \tanh \left[ \frac{n(x + ay - ht)}{2} \right], \quad (32)$$

$$\text{where } a = \frac{3^{1/3}n^2 + (-9h + \sqrt{81h^2 - 3n^6})^{2/3}}{3^{2/3}(-9h + \sqrt{81h^2 - 3n^6})^{1/3}}.$$



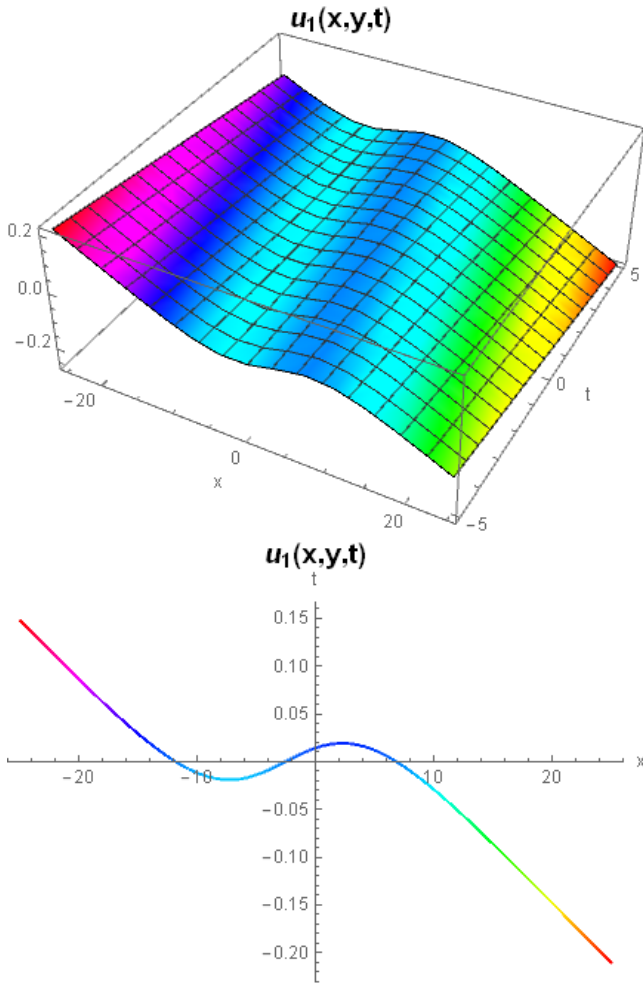


**Figure 7.** 3D of solution (32) for  $n = 0.2755, a = 4, y = 0.5, k = -1, -25 \leq x \leq 25$  values with  $-5 \leq t \leq 5$  range and 2D plot of solution for  $t = 0.5$  with these values.

Case2:

$$\begin{aligned}
 a_0 &= \frac{\sqrt{a^3 + 2hb_0}}{6\sqrt{a}}, a_1 = \frac{\sqrt{a^3 + 2h}(-6b_0 + b_1)}{6\sqrt{a}}, \\
 a_2 &= \frac{\sqrt{a^3 + 2h}(b_0 - b_1)}{\sqrt{a}}, \\
 a_3 &= \frac{\sqrt{a^3 + 2hb_1}}{\sqrt{a}}, n = -\frac{\sqrt{a^3 + 2h}}{\sqrt{a}}.
 \end{aligned}
 \tag{33}$$

Substituting the above values in Eq. (28), we acquire dark soliton solution of Eq. (2).

$$\begin{aligned}
 u_2(x, y, t) &= \frac{\sqrt{a^3 + 2h}}{6\sqrt{a}}(nx + nay - nht) \\
 &\quad - \frac{\sqrt{a^3 + 2h}}{2\sqrt{a}} \tanh\left[\frac{(nx + nay - nht)}{2}\right],
 \end{aligned}
 \tag{34}$$

where  $n = -\frac{\sqrt{a^3 + 2h}}{\sqrt{a}}$ .

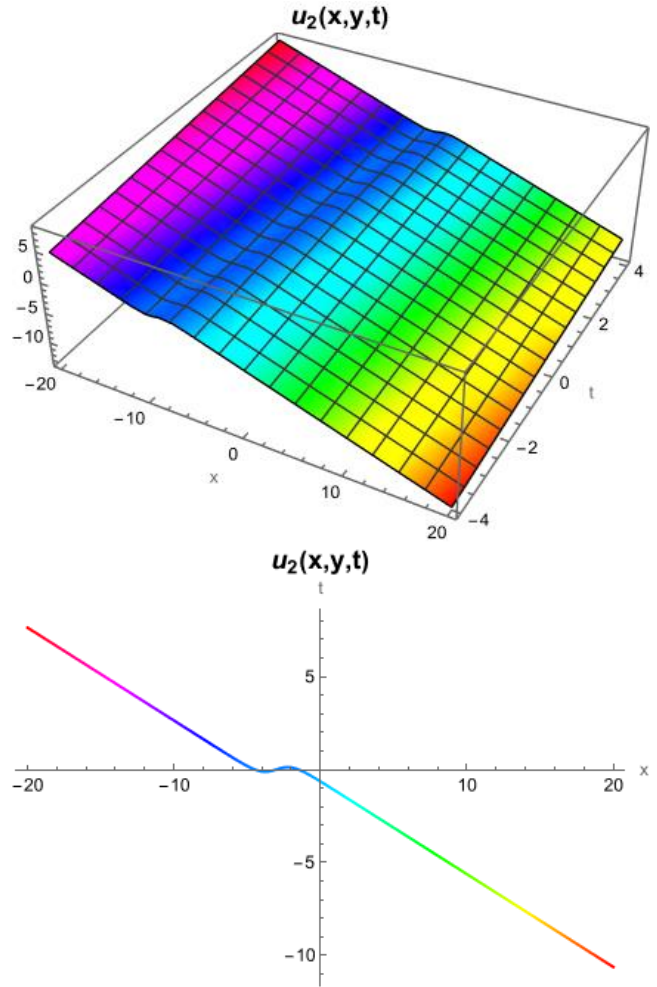


**Figure 8.** 3D of solution (34) for  $n = -\sqrt{3}, a = 1, y = 5, k = 1, -20 \leq x \leq 20$  values with  $-4 \leq t \leq 4$  range and 2D plot of solution for  $t = 2$  with these values.

Case3:

$$\begin{aligned}
 a_0 &= 0, a_1 = 0, a_2 = -\frac{i\sqrt{a^3 + 2hb_1}}{\sqrt{a}}, \\
 a_3 &= \frac{i\sqrt{a^3 + 2hb_1}}{\sqrt{a}}, b_0 = 0, n = -\frac{i\sqrt{a^3 + 2h}}{\sqrt{a}}.
 \end{aligned}
 \tag{35}$$

Substituting the above values in Eq. (28), we acquire trigonometric function solution of Eq. (2).

$$u_3(x, y, t) = -\frac{\sqrt{a^3 + 2h}}{2\sqrt{a}} \times \tan \left[ \frac{\sqrt{a^3 + 2h}(x + ay - ht)}{2\sqrt{a}} \right], \quad (36)$$

where  $n = -\frac{i\sqrt{a^3 + 2h}}{\sqrt{a}}$ .

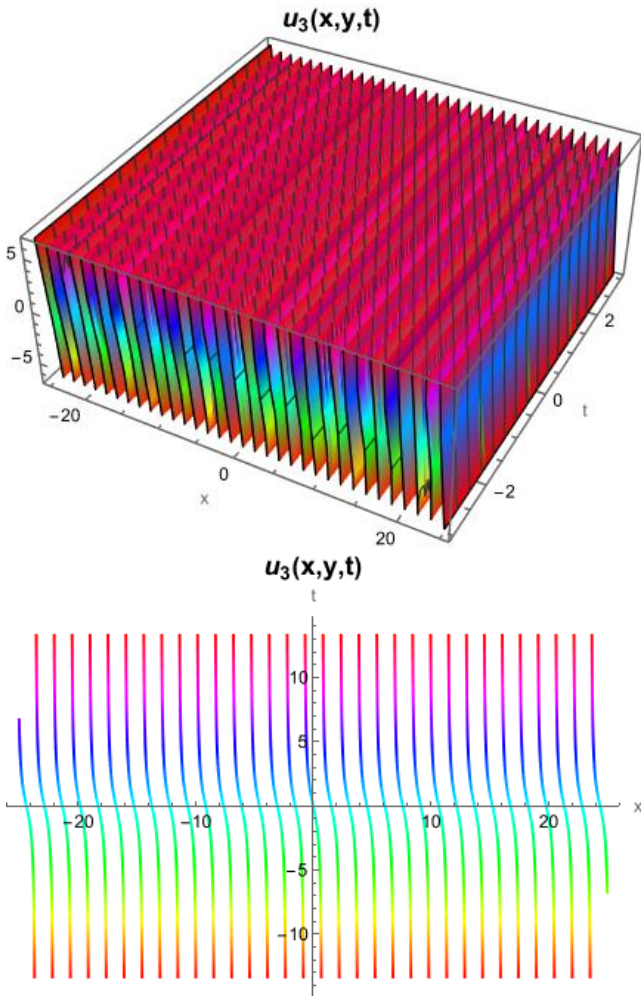


**Figure 9.** 3D of solution (36) for  $a = 4, k = 2, y = 0.5$ ,  $-25 \leq x \leq 25$  values with  $-3 \leq t \leq 3$  range and 2D plot of solution for  $t = 1$  with these values.

Case4:

$$a_0 = -\frac{\sqrt{a^3 + 2hb_0}}{6\sqrt{a}}, a_3 = -a_2 - \frac{\sqrt{a^3 + 2hb_0}}{\sqrt{a}}, \quad (37)$$

$$a_1 = \frac{1}{6} \left( -a_2 + \frac{5\sqrt{a^3 + 2hb_0}}{\sqrt{a}} \right),$$

$$b_1 = \frac{\sqrt{aa_2}}{\sqrt{a^3 + 2h}} + b_0, n = \frac{\sqrt{a^3 + 2h}}{\sqrt{a}}.$$

Substituting the above values in Eq. (28), we acquire dark soliton solution of Eq. (2).

$$u_4(x, y, t) = \frac{i\sqrt{17}\sqrt{a^3 + 2h}(x + ay - ht)}{6\sqrt{a}} - \frac{i\sqrt{17}}{2} \tanh \left[ \frac{\sqrt{a^3 + 2h}(x + ay - ht)}{2\sqrt{a}} \right], \quad (38)$$

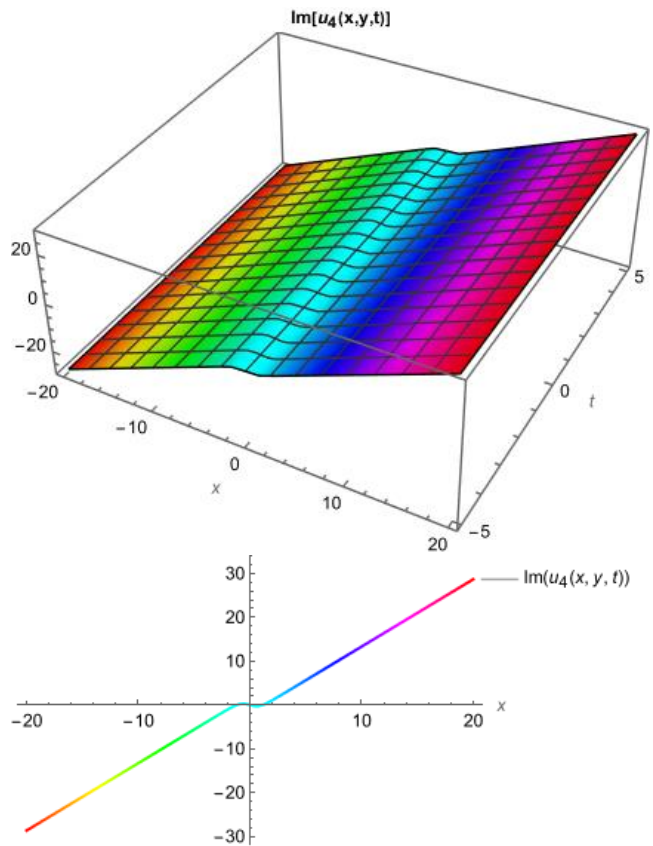


**Figure 10.** 3D of solution (38) for  $a = 2, k = 1, y = 1$ ,  $-20 \leq x \leq 20$  values with  $-5 \leq t \leq 5$  range and 2D plot of solution for  $t = 2$  with these values.

#### 4. Conclusion

In this made study, we discussed GKM, which is one of the NLEEs solution methods. We applied this discussed method to the (2+1)-dimensional DJKM equation and the (2+1)-dimensional DLWS and so we got some soliton solutions of equation and system being studied. At the same time, we drew the drawings of the 2D and 3D graphics of the found soliton solutions by giving certain values. Thus, it has been seen that GKM is a reliable and exact solution method in obtaining NLEEs solutions. In future studies, GKM can be used in research of other NLEEs.

#### References

- Adem, A.R., Yıldırım, Y. and Yaşar, E. 2019. Complexiton solutions and soliton solutions: (2+1)-dimensional Date-Jimbo-Kashiwara-Miwa equation. *Pramana Journal Physics*, 92 (36), 1-12.
- Ali, K. K., Zahibi, A., Rezazadeh, H., Ansari, R., and Inc, M. 2021. Optical soliton with Kudryashov's equation via sine-Gordon expansion and Kudryashov methods. *Optical and Quantum Electronics*, 53 (362), 1-15.
- Chang, L., Liu, H. and Xin, X. 2020. Lie symmetry analysis, bifurcations and exact solutions for the (2+1)-dimensional dissipative long wave system. *Journal of Applied Mathematics and Computing*, 64, 807-823.
- Cinar, M., Onder, I., Secer, A., Yusuf, A., Sulaiman, T. A., Bayram, M. and Aydin, H. 2021. Soliton Solutions of (2 + 1) Dimensional Heisenberg Ferromagnetic Spin Equation by the Extended Rational sine-cosine and sinh-cosh Method. *International Journal of Applied and Computational Mathematics*, 7 (135), 1-17.
- Dusunceli, F., Celik, E., Askin, M. and Bulut, H. 2021. New exact solutions for the doubly dispersive equation using the improved Bernoulli sub-equation function method. *Indian Journal of Physics*, 95 (2), 309-314.
- Gao, W., Ismael, H. F., Bulut, H. and Baskonus, H. M. 2020. Instability modulation for the (2+1)-dimension paraxial wave equation and its new optical soliton solutions in Kerr media. *Physica Scripta*, 95 (3), 1-17.
- Ghanbari, B. and Inc, M. 2018. A new generalized exponential rational function method to find exact special solutions for the resonance nonlinear Schrödinger equation. *The European Physical Journal Plus*, 133 (142), 1-18.
- Guo, F. and Lin, J. 2019. Interaction solutions between lump and stripe soliton to the (2+1)-dimensional Date-Jimbo-Kashiwara-Miwa equation. *Nonlinear Dynamics*, 96, 1233-1241.
- Gurefe, Y. 2020. The generalized Kudryashov method for the nonlinear fractional partial differential equations with the beta-derivative. *Revista Mexicana de Fisica*, 66 (6), 771-781.
- Islam, N., Khan, K. and Islam, M. H. 2019. Travelling wave solution of Dodd-Bullough-Mikhailov equation: a comparative study between Generalized Kudryashov and improved F-expansion methods. *Journal of Physics Communications*, 3 (5), 055004.
- Ismael, H. F., Bulut, H., Park, C. and Osman, M. S. 2020. M-lump, N-soliton solutions, and the collision phenomena for the (2 + 1)-dimensional Date-Jimbo-Kashiwara-Miwa equation. *Results in Physics*, 19, 103329.
- Kaplan, M. and Akbulut, A. 2021. The analysis of the soliton-type solutions of conformable equations by using generalized Kudryashov method. *Optical and Quantum Electronics*, 53 (498), 1-21.
- Kumar, D. and Kaplan, M. 2018. Application of the modified Kudryashov method to the generalized Schrödinger–Boussinesq equations. *Optical and Quantum Electronics*, 50 (329), 1-14.
- Manafian, J., Ivatloo, B. M. and Abapour M. 2020. Breather wave, periodic, and cross-kink solutions to the generalized Bogoyavlensky-Konopelchenko equation. *Mathematical Methods in the Applied Sciences*, 43 (4), 1753-1774.
- Mirzazadeh, M., Akinyemi, L., Şenol, M. and Hosseini K. 2021. A variety of solitons to the sixth-order dispersive (3+1)-dimensional nonlinear time-fractional Schrödinger equation with cubic-quintic-septic nonlinearities. *Optik-International Journal for Light and Electron Optics*, 241, 166318.
- Pandır, Y. and Eren, S. 2021. Exact Solutions of the Two-Dimensional KdV-Burger Equation by Generalized Kudryashov Method. *Journal of the Institute of Science and Technology*, 11 (1), 617-624.
- Pu, J. C. and Hu, H. C. 2019. Exact solitary wave solutions for two nonlinear systems. *Indian Journal of Physics*, 93 (2), 229-234.
- Rani, A., Zulfıqar, A., Ahmad, J. and Hassan, Q. M. U. 2021. New soliton wave structures of fractional Gilson-Pickering equation using tanh-coth method and their applications. *Result in Physics*, 29, 104724.
- Singh, M. and Gupta, R. K. 2018. On Painlevé analysis, symmetry group and conservation laws of Date-Jimbo-Kashiwara-Miwa equation. *Int J Appl Comput Math*, 4 (88), 1-15.
- Tuluçe Demiray, S. 2020. New solutions of Biswas-Arshed equation with beta time derivative. *Optik-International Journal for Light and Electron Optics*, 222, 165405.
- Tuluçe Demiray, S. and Bayrakci, U. 2021. Soliton Solutions for space-time fractional Heisenberg ferromagnetic spin chain equation by generalized Kudryashov method and modified  $\exp(-\Omega(\eta))$  - expansion function method. *Revista Mexicana de Fisica*, 67 (3), 393-402.
- Yang, J. and Feng, Q. 2021. The soliton solutions and evolution of the (2+1)-dimensional dissipative long wave equation. *Results in Physics*, 21, 103974.
- Yaslan, H. Ç. and Girgin, A. 2019. Exp-function method for the conformable space-time fractional STO, ZKBBM and coupled Boussinesq equations. *Arab Journal of Basic and Applied Sciences*, 26 (1), 163-170.
- Yokus, A., Durur, H., Ahmad, H. and Yao, S.W. 2020. Construction of Different Types Analytic Solutions for the Zhiber-Shabat Equation. *Mathematics*, 8 (6), 1-16.
- Yuan, Y. Q., Tian, B., Sun, W. R., Chai, J. and Liu, L. 2017. Wronskian and Grammian solutions for a (2+1)-dimensional Date-Jimbo-Kashiwara-Miwa equation. *Computers and Mathematics with Applications*, 74 (4), 873-879.